DURBAN UNIVERSITY OF TECHNOLOGY

FRACTURE PROPERTIES OF FIBRE AND NANO REINFORCED COMPOSITE STRUCTURES

AVINASH RAMSAROOP

FRACTURE PROPERTIES OF FIBRE AND NANO REINFORCED COMPOSITE STRUCTURES

A THESIS SUBMITTED TO THE

DURBAN UNIVERSITY OF TECHNOLOGY

FOR THE MASTER OF TECHNOLOGY DEGREE

(MECHANICAL ENGINEERING)

BY

AVINASH RAMSAROOP

DEPARTMENT OF MECHANICAL ENGINEERING

FACULTY OF ENGINEERING, SCIENCE

AND THE BUILT ENVIRONMENT

DURBAN 4000, SOUTH AFRICA

SUPERVISOR: PROF K KANNY

2007

DECLARATION

This thesis is being submitted to the Durban University of Technology for the degree of Master of Technology (Mechanical Engineering). I declare that this work is my own and has not been submitted before for any degree or examination to any other university or institution.

_____

AVINASH RAMSAROOP

Student No: 20429589

June 2007

FINAL APPROVED SUBMISSION

_____ _____

Prof K Kanny Date

ACKNOWLEDGEMENTS

This thesis was a combination of long research hours and perseverance which would not have been possible without the assistance and understanding of key figures in both academic and personal capacities. I am indebted to my supervisor, Professor Krishnan Kanny, whose help, encouragement and guidance was unsurpassable. He was always there to offer advice and guide my research to the final point. When difficulties were experienced, he offered encouragement and inspiration.

I thank Dr Selvum Pillay for his guidance and assistance. Although the period of our meeting was short, the knowledge he bestowed was invaluable. I am grateful to the staff of the Department of Mechanical Engineering for their help and support in my study. In particular, I thank Dr Jawahar Paulraj, Vishnu Moodley and Santhesh Hiraman for their assistance and inspiration brought upon by their research work. My research would have proved extremely difficult had it not been for the financial support of KENTRON through the HYSTOU 4 program.

TABLE OF CONTENT

Reference Declaration in Respect of a Master's Dissertation III

Acknowledgements IV

List of Figures IX

List of Tables XIV

Abstract XV

1. Introduction 1

    1.1. Advantages of Composite Materials 1

    1.2. Definition of a Composite Material 2

    1.3. History of Composites 4

    1.4. Fibre Reinforced Plastics 5

    1.5. Thermosetting Matrix 9

        1.5.1. Epoxy Resin 9

    1.6. Thermoplastic Matrix 11

        1.6.1. Polypropylene 11

    1.7. Fibre Reinforcement 12

    1.8. Particulate Reinforcement 16

    1.9. Hybrid Composite Structures 18

    1.10. Composite Materials used in Present Study 19

2. Literature Review 21

    2.1. Delamination of Composite Structures 21

    2.2. Delamination Tests 23

2.2.1. The Double Cantilever Beam (DCB) test 23
2.2.2. The End-Notched Flexure (ENF) test 24
2.2.3. Mixed Mode Testing 26
2.2.4. The Mixed Mode Bending (MMB) test 27
2.3. Fracture Toughness of Fibre-Reinforced Composites 28
2.4. Research of Hybrid Composite Structures 30
2.5. Motivation and Scope of Research 31
3. Manufacturing and Testing Procedures 33
3.1. Manufacturing of Composite Structures 33
3.1.1. Nano-infused Thermoplastic Composites 34
3.1.2. Fibre-reinforced Thermoplastic Composites 35
3.1.3. Fibre-reinforced Thermosetting Composites 36
3.1.4. Hybrid Thermosetting Composites 38
3.2. Testing Procedures 39
3.2.1. X-Ray Diffraction 39
3.2.2. Transmission Electron Microscopy 39
3.2.3. Scanning Electron Microscopy 40
3.2.4. Tensile 40
3.2.5. Single Edge Notched Bend (SENB) 41
3.2.6. Mixed Mode Bending Test 42
4. Experimental Results and Discussion Part 1: Nano-infused Thermoplastic Composites 46
4.1. Single Edge Notched Bend (SENB) Test 47
4.2. X-ray and TEM Characterization 50

4.3. Summary 53

5. Experimental Results and Discussion Part 2: Fibre-reinforced Thermoplastic Composites 54

5.1. Tensile Test 54

5.2. Single Edge Notched Bend (SENB) Test 60

5.3. Mixed Mode Bending (MMB) Test 63

5.4. Summary 66

6. Experimental Results and Discussion Part 3: Fibre-reinforced Thermoset Composites 67

6.1. Tensile Test 67

6.2. Single Edge Notched Bend (SENB) Test 71

6.3. Mixed Mode Bending (MMB) Test 77

6.4. Failure Envelopes 85

6.5. Summary 89

7. Experimental Results and Discussion Part 4: Comparison of Nano and Fibre-reinforced Structures 91

7.1. Comparison of Tensile Properties 91

7.2. Comparison of Stress Intensity Factors 94

7.3. Comparison of Strain Energy Release Rates 96

7.4. Summary 97

8. Experimental Results and Discussion Part 5: Fibre-reinforced Nano-infused Thermoset Composite (Hybrid) 99

8.1. Tensile Test 99

8.2. Mixed Mode Bending (MMB) Test 100

8.3. Summary 104

9. Conclusion 105

10. References 109

List of journal and conference papers 122

LIST OF FIGURES

Figure 1.1: Common composite material systems 3

Figure 1.2: Electron Micrograph cross-section of FRP composite 5

Figure 1.3: Composite bus built by North American Bus Industries 6

Figure 1.4: Bridge in Wotton, Quebec that utilised FRP rods as reinforcement; (a) shows the installation of the rods; and (b) shows a close up of the installed rods 7

Figure 1.5: FRP applications: (a) S-band transmitter for satellite component, (b) flexible ducting, and (c) rigid ducting 8

Figure 1.6: Polypropylene lid of a Tic Tacs box, with a living hinge 12

Figure 1.7: Classification of plant fibres 13

Figure 1.8: Natural fibre composites in the Mercedes Benz E-Class series 13

Figure 1.9: Bundle of glass fibres 15

Figure 1.10: Types of clay-polymer nanocomposites 17

Figure 2.1: Delamination sources at geometric and material discontinuities 21

Figure 2.2: The three basic fracture modes 22

Figure 2.3: DCB specimen in (a) unloaded condition, and (b) loaded condition 24

Figure 2.4: ENF specimen in (a) unloaded condition, and (b) loaded condition 25

Figure 2.5: MMB test shown as the superposition of the DCB and ENF tests 27

Figure 2.6: Schematic of MMB test coupon in testing fixture 27

Figure 3.1: Schematic showing position of delamination insert 33

Figure 3.2: Schematic diagram of compression fixture and moulding process 36

Figure 3.3: Schematic diagram of VARIM technique 37

Figure 3.4: VARIM technique being used to manufacture a thermosetting panel 38

Figure 3.5: Photograph of a test coupon setup in the in-house MMB fixture 42

Figure 4.1: Critical Stress Intensity Factor versus Clay Content for 0 % to 5 % nano-infused polypropylene 47

Figure 4.2: Tensile results of Polypropylene / Cloisite 15A 48

Figure 4.3: X-ray diffraction pattern of (a) CL15A, and PP with (b) 0.5 wt % CL15A, (c) 1 wt % CL15A, (d) 2 wt % CL15A, (e) 3 wt % CL15A, and (f) 5 wt % CL15A. 51

Figure 4.4: TEM images of polypropylene infused with (a) 1 %, and (b) 5 % Cloisite 15A 52

Figure 5.1: Stress versus Strain plots for Polypropylene / Chopped S2 Glass and Polypropylene / Woven S2 Glass 55

Figure 5.2: SEM image of PP / Woven S2 Glass showing insufficient wetting of the fibres 56

Figure 5.3: Polypropylene / Chopped S2 Glass test coupon after tensile test showing (a) front view and (b) side view 57

Figure 5.4: Polypropylene / Woven S2 Glass test coupon after tensile test showing (a) front view and (b) side view 58

Figure 5.5: Secondary cracking observed in the Polypropylene / Woven S2 Glass coupon on the (a) front face and (b) back face 59

Figure 5.6: Load versus Stress Intensity Factor responses for Polypropylene / Chopped S2 Glass and Polypropylene / Woven S2 Glass 60

Figure 5.7: Photographs of Polypropylene / Woven S2 Glass specimen after SENB test showing “kinking” phenomenon on (a) top edge and (b) front surface. 61

Figure 5.8: Crack length versus Time responses for Polypropylene / Chopped S2 Glass and Polypropylene / Woven S2 Glass 63

Figure 5.9: Load versus Strain Energy Release Rate for Polypropylene / Woven S2 Glass 64

Figure 5.10: Delamination Length versus Time for Polypropylene / Woven S2 Glass under Mixed Mode conditions 65

Figure 6.1: Stress versus Strain for Epoxy / Chopped S2 Glass and Epoxy / Woven S2 Glass 68

Figure 6.2: Fracture surfaces of thermoset tensile test coupons; (a) front of chopped fibre specimen; (b) rear of chopped fibre specimen; (c) side of chopped fibre specimen; (d) inside of chopped fibre specimen; (e) front of woven fibre specimen; (f) rear of woven fibre specimen; (g) side of woven fibre specimen; (h) inside of woven fibre specimen 69

Figure 6.3: Load versus Stress Intensity Factor for Epoxy / Chopped S2 Glass 71

Figure 6.4: Load versus Stress Intensity Factor for Epoxy / Woven S2 Glass 72

Figure 6.5: Crack Length versus Time for Epoxy / Chopped S2 Glass and Epoxy / Woven S2 Glass 74

Figure 6.6: Fracture surfaces of Epoxy / Chopped S2 Glass SENB test coupons showing (a) front of specimen, and (b) rear of specimen. 75

Figure 6.7: Fracture surfaces of Epoxy / Woven S2 Glass SENB test coupons showing (a) front of specimen, and (b) rear of specimen 76

Figure 6.8: Load versus Displacement responses for Epoxy / Woven S2 Glass specimens for mode mixtures of G_I/G_{II} = 4/1, 1/1, and ¼ 78

Figure 6.9: Delamination Length versus Time responses for Epoxy / Woven S2 Glass specimens for mode mixtures of G_I/G_{II} = 4/1, 1/1, and ¼ 81

Figure 6.10: Load versus Strain Energy Release Rate responses for Epoxy / Woven S2 Glass specimens for mode mixtures of G_I/G_{II} = 4/1, 1/1, and ¼ 83

Figure 6.11: Photographs of Epoxy / Woven S2 Glass MMB test coupon showing (a) delamination area, and (b) edge view 84

Figure 6.12: Mode I Component versus Mode II Component Epoxy / 24 layers S2 Woven Glass specimens for mode mixtures of G_I/G_{II} = 4/1, 1/1, and ¼ 85

Figure 6.13: Mode I Component versus Mode II Component Epoxy / 24 layers S2 Woven Glass specimens for mode mixtures of G_I/G_{II} = 4/1, 2/1, 1/1, ½ and ¼ 87

Figure 6.14: Mode-Mix Ratio versus Load for Epoxy / Woven S2 Glass 88

Figure 7.1: Stress versus Strain plots of nano-infused and fibre-reinforced polypropylene 92

Figure 7.2: Tensile response of Epoxy / Chopped S2 Glass, Epoxy / Woven S2 Glass, PP / Woven S2 Glass, PP / 5 % Cloisite 15A, and un-reinforced PP 93

Figure 7.3: Comparison of Load versus Stress Intensity Factor for 5 % nano-infused and woven fibre-reinforced polypropylene 94

Figure 7.4: Load versus Strain Energy Release Rate for Epoxy / Woven S2 Glass and Polypropylene / 5 % Cloisite 15A 97

Figure 8.1: Stress versus Strain for hybrid and conventional woven fibre-reinforced epoxy composites 100

Figure 8.2: Load versus Displacement responses for mode-mix ratios of G_I/G_{II} = 4/1, 1/1, and ¼ of Epoxy / Woven S2 Glass and Cloisite 30B / Epoxy / Woven S2 Glass 101

Figure 8.3: Load versus Strain Energy Release Rate for mode-mix ratios of G_I/G_{II} = 4/1, 1/1, and ¼ of Epoxy / Woven S2 Glass and Cloisite 30B / Epoxy / Woven S2 Glass 102

Figure 8.4: Delamination Length versus Time for mode-mix ratios of G_I/G_{II} = 4/1, 1/1, and ¼ of Epoxy / Woven S2 Glass and Cloisite 30B / Epoxy / Woven S2 Glass 103

LIST OF TABLES

Table 1.1: Comparative Properties of Fibre Reinforcements 14

Table 3.1: List of materials and their suppliers 34

ABSTRACT

Interlaminar cracking or delamination is an inherent disadvantage of composite materials. In this study the fracture properties of nano and fibre-reinforced polypropylene and epoxy composite structures are examined. These structures were subjected to various tests including Single Edge Notched Bend (SENB) and Mixed Mode Bending (MMB) tests. Polypropylene nanocomposites infused with 0.5, 1, 2, 3 and 5 weight % nanoclays showed correspondingly increasing fracture properties. The 5 weight % specimen exhibited 161 % improvement in critical stress intensity factor (K_{IC}) over virgin polypropylene. XRD and TEM studies show an increase in the intercalated morphology and the presence of agglomerated clay sites with an increase in clay loading. The improvement in K_{IC} values may be attributed to the change in structure.

Tests on the fibre-reinforced polypropylene composites reveal that the woven fibre structure carries 100 % greater load and exhibits 275 % lower crack propagation rate than the chopped fibre specimen. Under MMB conditions, the woven fibre structure exhibited a delamination propagation rate of 1.5 mm/min which suggests delamination growth propagates slower under Mode I dominant conditions. The woven fibre / epoxy structure shows 147 % greater tensile modulus, 63 % greater critical stress intensity factor (K_{IC}), and 184 % lower crack propagation rate than the chopped fibre-reinforced epoxy composite. MMB tests reveal that the load carrying capability of the specimens increased as the mode-mix ratio decreased, corresponding to an increase in the Mode II component. Delamination was through fibre–matrix interface with no penetration of fibre layers. A failure envelope was developed and tested and may be used to determine the critical applied load for any mode-mix ratio.

The 5 weight % nanocomposite specimen exhibited a greater load carrying capability and attained a critical stress intensity factor that was 10 % less than that of the fibre-reinforced polypropylene structure, which had three times the reinforcement weight. Further, the nanocomposite exhibited superior strain energy release rates to a material with ten times the reinforcement weight. The hybrid structure exhibited 27 % increase in tensile modulus over the conventional fibre-reinforced structure. Under MMB conditions, no significant increase in load carrying capability or strain energy release rate over the conventional composite was observed. However, the hybrid structure was able to resist delamination initiation for a longer period, and it also exhibited lower delamination propagation rates.

1. INTRODUCTION

In the technologically advanced era that we currently live in, there is a growing demand for cheaper and more durable materials for a variety of applications. Previously metals and metal alloys were used to manufacture anything and everything from paper clips to skyscrapers. Then plastics were discovered and a revolution began where plastics started replacing metal components, for example, gears, bearings, etc. Plastics are easier to mould into complex parts as well as being lighter than their metal counterparts and just as durable. Initially plastics were expensive, but as their application and demand in everyday life increased, the manufacturing costs of plastic components decreased.

The use of plastic components are limited to low end applications such as food containers and dustbins due to their relatively low strength. High end applications such as automotive, marine and aerospace structures still required the use of metals and their alloys. Thus there was a need for a strong yet lightweight material and composite materials were developed.

1.1. ADVANTAGES OF COMPOSITE MATERIALS

Composites have many advantages over other materials [1]. They are stronger and stiffer than metals on a density basis, or in other words, they have superior stiffness-to-weight ratios. Composites can be custom designed. Metals and metal alloys have isotropic characteristics, that is, the material properties are the same in all directions. Composites, on the other hand, can have very selective directional properties to meet specific application needs. These materials can also be formed into many complex shapes during fabrication, even providing finished, styled surfaces

in the process. Parts that were formerly assembled out of several smaller metallic components can be fabricated into a larger single part, thus reducing manufacturing costs. Composites have inherent characteristics that allow production to be established for a small fraction of the cost that would be required in metallic fabrication. Composite structures also exhibit high corrosion resistance and outstanding durability. They can be designed to resist degradation in extremely harsh and corrosive environments. These materials have exhibited apparent infinite life characteristics. Some other advantages include high continuous operating temperatures, low radar detection, and good electrical properties.

1.2. DEFINITION OF A COMPOSITE MATERIAL

A composite material is formed by the combination of two or more materials that have different properties [2-3]. These different materials work together to give the overall composite material enhanced properties that are better than those of the separate constituent parts. The argument now would be that a composite material is similar to an alloy. This, however, is not the case because in an alloy the different materials or constituents dissolve or blend into each other to form the final material. In the final alloy the different materials are indistinguishable. In a composite, on the other hand, the different materials do not dissolve or blend into each other and can be easily distinguished from one another [3].

A composite material is made up of two basic constituents, namely, a matrix and the reinforcement [2-3]. The reinforcement is usually the constituent that provides the composite with its strength. It can be either in particulate form or fibres. The matrix is the constituent that surrounds and binds the reinforcement as well as serves the protection against damage [3]. It also

aids in the distribution of the applied load to the reinforcement. Figure 1.1 shows the common composite material systems.

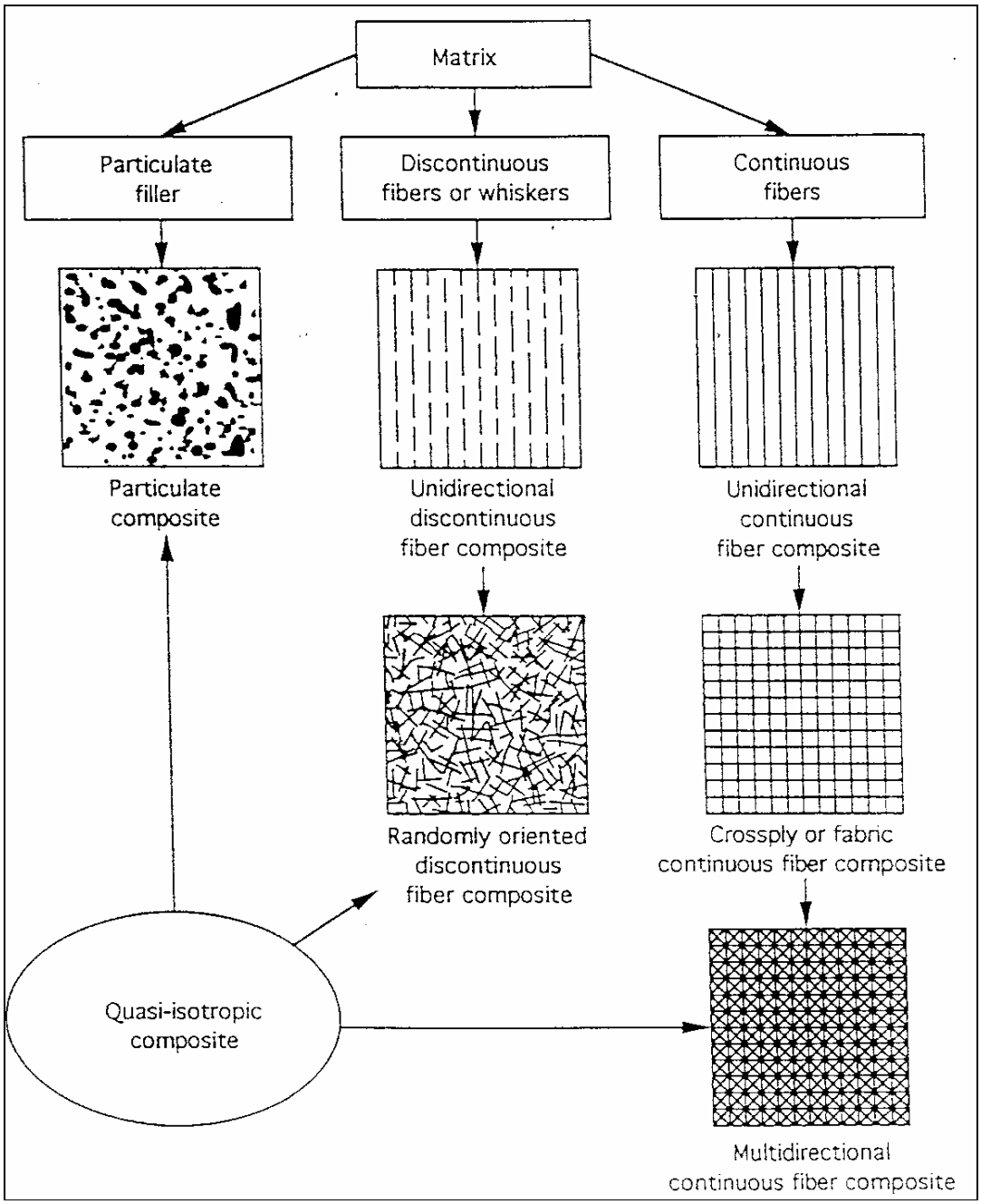

Figure 1.1: Common composite material systems [Course Notes: Mechanics of Composite Materials, University of Kwa-Zulu Natal]

1.3. HISTORY OF COMPOSITES

Although the concept of composite materials is fairly new, they have been in use for millennia. The most primitive application is mud and straw bricks [2-4]. A cake of dried mud is easy to break by applying a tensile force on one edge via bending. However, mud can still make a good strong wall where all the forces are compressive. A piece of straw, on the other hand, has a lot of strength when it is stretched but almost no strength when it is crumpled up. If pieces of straw were embedded in a block of mud and allowed to dry hard, the resulting mud / straw brick resists both squeezing and tearing and makes an excellent building material. Put more technically, it has both good compressive strength and good tensile strength. In terms of matrix / reinforcement constituents, the reinforcement material is the straw, while the mud is the matrix. This is probably the earliest example of a fibre-reinforced composite.

Composites also exist in nature, for example, wood [3-4]. Wood has long fibres of cellulose that are held together by a much weaker substance called lignin. Cellulose is also found in cotton and linen, but it is the binding power of the lignin that makes a piece of timber much stronger than a bundle of cotton fibres.

An example of a particulate-filled composite is concrete [3-4]. The particulate-filler is small stones or gravel, and this is bound together by cement, which acts as the matrix. Concrete has good compression strength but lacks any beneficial tensile properties. To overcome this deficiency, reinforcement in the form of steel rods is added to produce reinforced concrete. The steel rods have excellent tensile properties with low compressive capabilities. However, the combination of steel rods in concrete results in a structure that has both good compressive and tensile properties.

Modern composites consist of more advanced materials than these primitive examples. However the basic concept of a matrix and reinforcement remains unchanged. Of the many types of modern composite materials, the most commonly used is fibre-reinforced plastics (FRP) [1]. An FRP is typically organized as a laminated structure consisting of layers of unidirectional fibre or woven fibre fabric reinforcement that is embedded within a polymer matrix material [1,5-7]. Figure 1.2 shows a cross-section of an FRP composite structure with circles representing the fibres and the surrounding dotted portions represent the matrix.

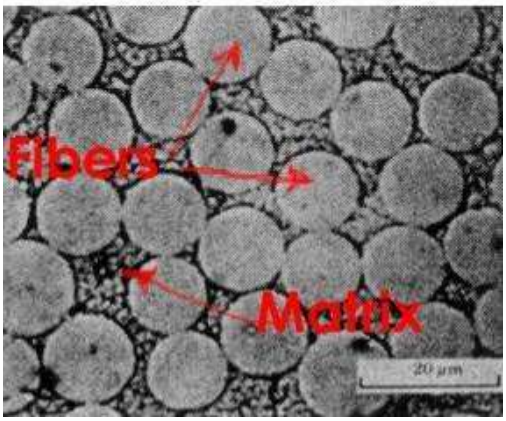

Figure 1.2: Electron Micrograph cross-section of FRP composite [7]

1.4. FIBRE REINFORCED PLASTICS

FRP composites have found applications in the aerospace, automotive and construction industries. In the aerospace industry, applications range from wall and floor panels to the fuselage [8-9]. A recent example would be the Airbus A380, which comprises of approximately 20 – 22 % of composites [4,10]. These include the front fairing, upper fuselage shells, crown and side panels, and the upper sections of the forward and aft upper fuselage. Also the top and bottom skin panels, the front, centre and rear spars, the rear pressure bulkhead, the upper deck floor beams,

and the ailerons, spoilers and outer flaps. The A320 is the first subsonic aircraft to incorporate composite structures in the fuselage [11]. These structures comprise of Aramid Fibre (AFRP), Glass Fibre (GFRP) and Carbon Fibre (CFRP) Reinforced Plastics.

Other applications in the aerospace industry include wall and floor panels, pack boards, instrument panels, dividers and bulkheads, EMI-shielded panels, racks and enclosures, ducting, and, decorative panels and trims [12]. Composites are even used in the space shuttle in the nose cap and wing leading edges where re-entry temperatures exceed 1260 °C [13].

In the aerospace industry, performance demands justify the high costs. However, FRP structures can no longer be considered as exotic materials suitable only for these niche applications [8]. Everyday applications are as diverse as automobile bodies and civil infrastructure. In the automotive industry composites are used in bumpers, rear seats, centre consoles and door panels. Certain body panels are also manufactured from composite materials, for example, Chevrolet uses fibre reinforced composites for the entire body of their Corvettes [14]. North American Bus Industries built a fully composite bus, shown in Figure 1.3, for use in their transit system [15].

Figure 1.3: Composite bus built by North American Bus Industries [15]

In the construction industry, polymer composites have been long in use. Applications range from non-structural gratings and claddings to full structural systems such as framing for industrial supports, buildings, long span roof structures, tanks, bridge components, and complete bridge systems [16].

Bridges represent only one aspect of the construction industry activities, but it is one that has attracted the strongest interest for the utilisation of FRP structures [8]. Composite pedestrian bridges have been constructed and put into use in the United States. A complete FRP composite bridge was erected in Ohio, USA and opened to traffic in 1997 [17]. This bridge is still in service and is performing to expectations and according to mathematical criteria that was established prior to the opening of the bridge. Another bridge design that was implemented in Wotton, Quebec [18] used FRP composite rods to reinforce a new concrete bridge (Figure 1.4).

(a) *(b)*

Figure 1.4: Bridge in Wotton, Quebec that utilised FRP rods as reinforcement; (a) shows the installation of the rods; and (b) shows a close up of the installed rods [18]

Fibre reinforced plastics have benefits of light weight and high strength that make it attractive for strengthening existing concrete bridge structures. FRP can be wrapped like wallpaper around bridge columns and beams to provide additional reinforcement to increase earthquake resistance, durability, and corrosion resistance [19]. This technique has been used by Fibrwrap Construction Inc. of Los Angeles, California, USA for a seismic retrofit of the Arroyo Seco Bridge which is located in Pasadena, California, USA [20]. The bridge's concrete columns were wrapped with glass fibre- and aramid-fibre reinforced epoxy composite. The low-profile composite jackets had a final thickness of less than 19 mm, yet provided strength comparable to that of a full-scale steel jacketing.

Other applications of FRP composites include swimming pools [21], satellite components (Figure 1.5a), flexible ducting (Figure 1.5b) and rigid ducting (Figure 1.5c), covers, shafts on golf clubs, hulls for luxury boats, and many more.

(a) *(b)* *(c)*

Figure 1.5: FRP applications: (a) S-band transmitter for satellite component, (b) flexible ducting, and (c) rigid ducting [22]

The properties of an FRP composite depend on the choice of fibre reinforcement and matrix materials [23]. The matrix is usually a polymer resin or plastic which is either thermosetting or thermoplastic [3].

1.5. THERMOSETTING MATRIX

Thermosetting plastics or thermosets are polymer materials that cure, depending on the chemistry, either at ambient or at elevated temperatures [24-25]. The curing process transforms the resin into a plastic or rubber by a cross-linking process. The cross-linking process forms a molecule with a larger molecular weight, resulting in a material with a higher melting point [24]. Thermoset materials are generally stronger than thermoplastic materials due to the 3-D network of bonds that form during curing. They are also better suited to high-temperature applications up to the decomposition temperature of the material.

Thermosets are in a liquid form when being prepared but harden and become rigid when they are processed into a composite material. They are usually supplied as viscous syrups but are also available in powder or malleable form (prepregs) [24-25]. Unlike thermoplastics, a thermoset material cannot be melted and re-shaped after it is cured. This makes them undesirable in recycling applications. The most common thermosetting matrix systems are polyester and epoxy resins, which account for approximately 85% of the market, with epoxies commanding the majority of usage in high performance aerospace type applications [25].

1.5.1. Epoxy resin

Epoxy resins are relatively low molecular weight pre-polymers capable of being processed under a variety of conditions. These resins can be formulated to give a wide range of properties. There

are two important advantages of epoxy resins. Firstly they can be partially cured and stored in that state, and secondly they exhibit low shrinkage during cure.

When compared with other thermosets, epoxies generally have better resistance to alkalis and solvents but slightly poorer weathering resistance [25]. Their electrical properties, wear resistance and thermal stability are excellent. Epoxy resins are used as structural or engineering adhesives in aircraft, automobiles, bicycles, golf clubs, skis, snow boards, etc. Epoxy adhesives are almost unmatched in heat and chemical resistance [26]. They are also used in paints, for corrosion protection, and coatings, for washers, driers, etc. In electrical applications they are employed in motors, generators, transformers, switchgear, bushings, and insulators. They are also used to encapsulate electronic components.

In order to convert the epoxy resins into a hard and rigid material, it is necessary to cure the resin with hardener. The curing process is an exothermic chemical reaction in which the epoxy resin reacts with a curing agent or hardener to form a highly cross-linked, three-dimensional network. Epoxy resins cure quickly and easily at practically any temperature from 5 ℃ to 150 °C depending on the choice of curing agent.

A wide variety of curing agents for epoxy resins are available. The choice of resin and hardener depends on the application, the process selected, and the properties desired. Curing agents for epoxies include amines, polyamides, phenolic resins, anhydrides, isocyanates and polymercaptans [27]. The amine and phenolic resin based curing agents are widely used for curing of epoxy resins.

1.6. THERMOPLASTIC MATRIX

Thermoplastics are rigid at low temperatures but soften when they are heated. Although they are less commonly used than thermosetting plastics they do have some advantages, such as greater resistance to fracture, long shelf life of the raw material, capacity for recycling and a cleaner, safer workplace because solvents are not needed for the hardening process [28]. Examples of this type of resin system include polypropylene and polyamide.

1.6.1. Polypropylene

Annually the production of thermoplastics is approximately 84 billion kilograms. This is about 50% of the total worldwide polymer industry production. Polypropylene (PP) accounts for approximately 20% of this worldwide production or about 34 billion kilograms per year. Hence polypropylene is one of the most widely used thermoplastics, not only because of its balance of physical and mechanical properties, but also due to its environmental friendliness such as recyclability and low cost [29].

Polypropylene has an excellent combination of low density, high stiffness and toughness, and heat distortion temperature above 100 °C. This provides it with an extraordinary versatility of properties and applications. Furthermore it has good tensile strength, a superior working temperature, excellent resistance to organic solvents, degreasing agents and electrolytic attack. It also has excellent acid and alkali resistance. Polypropylene is light in weight, resistant to staining, and has a low moisture absorption rate. It has very good resistance to fatigue and a melting point of 160 ˚C. PP can be easily fabricated by being hot gas welded, spin welded, fusion and butt welded. It can also be machined with wood or metal working tools, vacuum formed or ultra-sonic sealed.

Polypropylene is used in automotive components, plastic parts, food packaging, textiles, reusable containers, etc. Many plastic items for medical or laboratory use are made from PP because it is autoclavable, that is, it can withstand the heat in an autoclave. Polypropylene is used to manufacture most plastic living hinges [30], such as those on flip-top bottles (Figure 1.6).

Figure 1.6: Polypropylene lid of a Tic Tacs box, with a living hinge [30]

Ceramics, carbon and metals can also be used as the matrix for some highly specialised purposes [3]. For example, ceramics are used when the material is exposed to high temperatures and carbon fibres are used for products that are exposed to friction and wear.

1.7. FIBRE REINFORCEMENT

The other constituent of FRP composites is the fibre reinforcement, and this can be divided into two categories, namely, natural and synthetic. Natural or plant fibres are fibres that are obtained from nature. These fibres undergo a pre-processing technique that allows them to be used in composite structures [31]. Figure 1.7 shows the main categories of plant fibres.

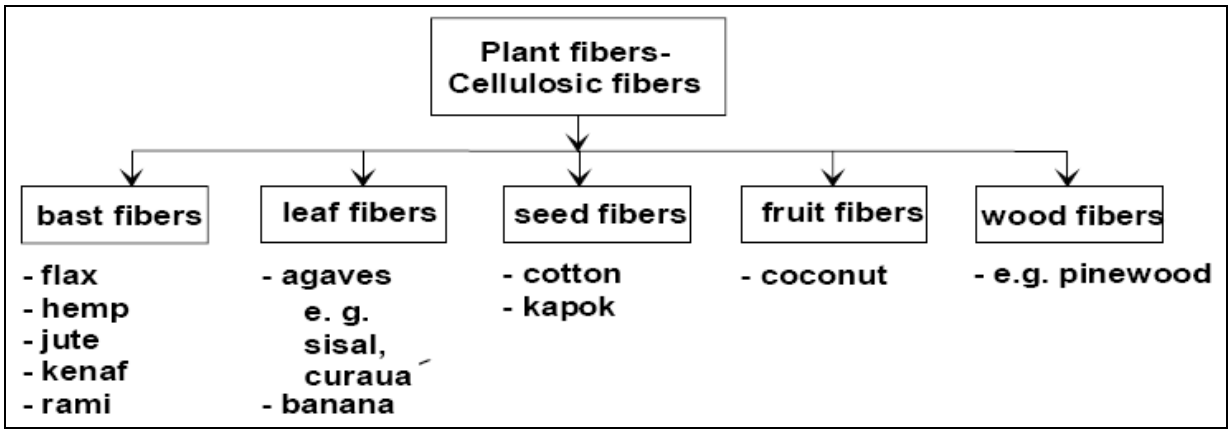

Figure 1.7: Classification of plant fibres [31]

The applications of natural fibre composites are greatly concentrated in the interior of passenger cars and truck cabins. They are used in door panels, cabin linings and for thermo-acoustic insulation. Mercedes Benz utilised natural fibre composites in their E-Class series [31]. The distribution of these composites throughout the vehicle is shown in Figure 1.8.

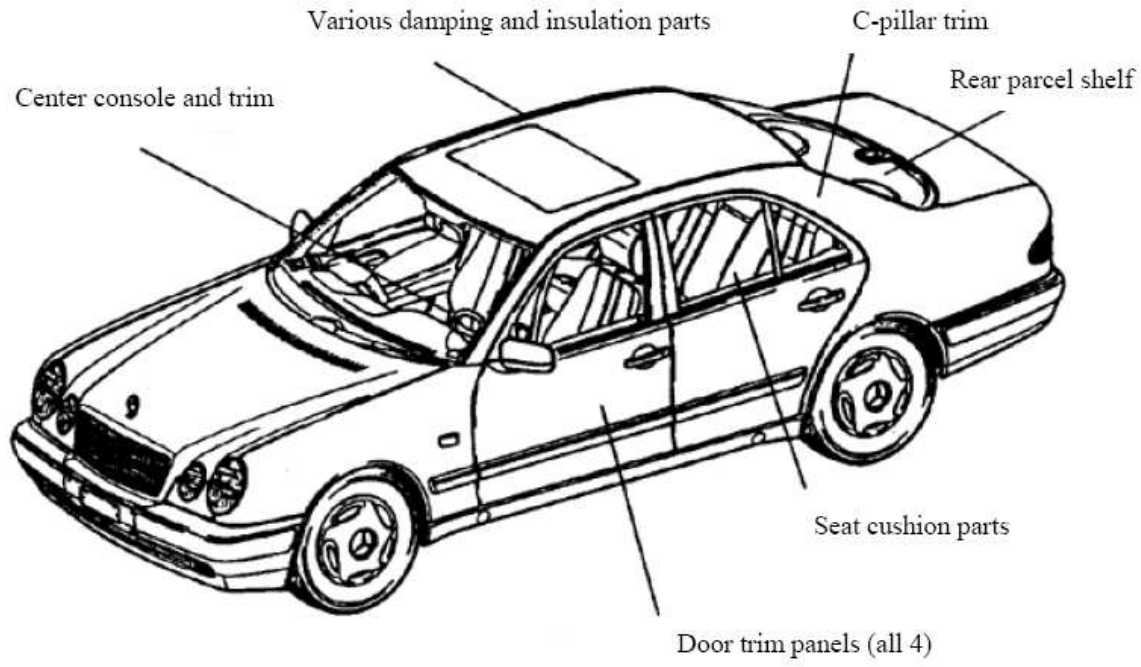

Figure 1.8: Natural fibre composites in the Mercedes Benz E-Class series [31]

A great advantage was achieved both in weight reduction and improvement in mechanical properties. For example, the door panels were previously constructed from wood fibre materials. These were replaced by sisal fibre mat in an epoxy resin matrix. A weight reduction of approximately 20 % was achieved with an improvement in mechanical properties, which is important for passenger safety in the event of an accident.

Synthetic fibres, on the other hand, are man-made components. Common synthetic fibres include Nylon, Olefin, Acrylic, Polyester, etc [32-33]. Specialty synthetic fibres include Spandex, Vinalon, Aramids (also known as Nomex, Kevlar and Twaron), Carbon, Glass, etc. The most popular fibres used in composite materials are carbon, aramid and glass. Table 1.1 compares some properties of these three fibres [34].

Table 1.1: Comparative Properties of Fibre Reinforcements

Property	**Carbon**	**Aramid (Kevlar 49)**	**E-Glass**	**S-Glass**
Tensile strength, MPa	3400 – 5500	3600 – 4100	1400 – 3400	3600 – 4500
Elasticity modulus, GPa	200 – 500	120 – 130	72 – 76	82 – 86
Elongation to break, %	1.4 – 2.2	2.5 – 2.8	3.0 – 4.5	5.0 – 5.7
Density, g/cm^3	1.7 – 2.1	1.44 – 1.48	2.54 – 2.63	2.46 – 2.48
Cost Ratio	45	35	15	15

Carbon fibres are produced from precursor polyacrylonitrile (PAN) in 3 stages [34]. These fibres provide the best combination of high strength, high stiffness (high modulus), and low density, but have lower elongation. Carbon fibres have a tensile strength between 3000 and 6000 MPa and a tensile modulus of elasticity ranging from about 200 to 500 GPa. Its density is between 1.7 and

2.1 g/cm^3 with a fibre diameter of 7 to 10 μm. Applications of carbon fibres include musical instruments, hoods and spoilers of automobiles, sport equipment, and shoes [35].

Aramid fibres are produced by chemical synthesis and have an aromatic (benzene ring type) polyamide linear structure [34]. The name is a shortened form of "aromatic polyamide". Kevlar is a type of aramid fibre and is used for high-performance composite applications where light weight, high strength and stiffness, damage resistance, and resistance to fatigue and stress rupture are important. The major industrial applications for aramid fibres include flame-resistant clothing and helmets, body armour, boat hull material, and speaker woofers [36].

Glass is by far the most widely used reinforcement fibre and is the lowest in cost [37-38]. The glass fibres have a lower strength and modulus but a higher density when compared to carbon and aramid fibres. Glass fibres are produced by drawing monofilaments of glass from a furnace containing molten glass and gathering a large number of these filaments to form a strand of glass fibres. The strands are then used to make glass fibre yarns or rovings, which consist of a collection of bundles of continuous filaments. A single roving is shown in Figure 1.9.

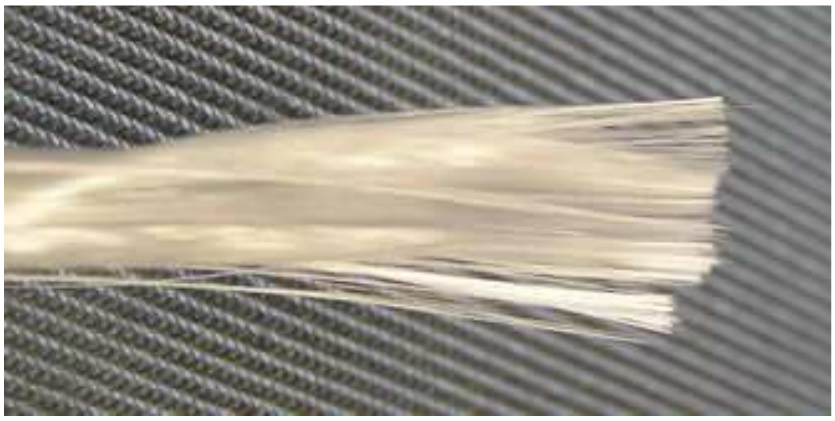

Figure 1.9: Bundle of glass fibres [37]

The rovings may be in continuous strands or woven to make woven roving. Glass-fibre reinforcing mats are made of continuous strands or chopped strands. The strands are usually held together with a resinous binder. Combination mats are made with woven roving chemically bonded to chopped-strand mat.

There are many different types of glass that can be used in composite materials [34]. E-glass is the most commonly used glass for fibre reinforcement. S-glass has an extra high strength-to-weight ratio and is more expensive than E-glass. It is used primarily for military and aerospace applications. S+R-Glass is a very high performance, but high cost glass. It is used almost exclusively in the aerospace industry

1.8. PARTICULATE REINFORCEMENT

A fast developing area in composite research involves the field of nanocomposites. These composite structures contain reinforcement on the nano-scale level. Usually macroscopic reinforcing elements cause imperfections such as voids and inadequate matrix – particle bonding. If the reinforcing elements are smaller then structural imperfections decreases as there are fewer voids and better matrix – particle bonding. Therefore reinforcing elements with dimensions on the nano-scale level would be ideal to give the best improvements in a composite structure.

Clays are considered a fundamental reinforcing element in nanocomposites [39]. Both industry and academia have shown great interest in these composites because of two major findings. First, the Toyota Research Group [40] developed a Nylon-6 (N6) / montmorillonite (MMT) nanocomposite. They discovered that very small amounts of clay loading resulted in pronounced improvements of thermal and mechanical properties. The second finding was made by Vaia et al

[41]. They found that it was possible to melt-mix polymers with clay without the use of organic solvents.

Clay polymer nanocomposites exhibit remarkable improvement in properties when compared to virgin polymer or conventional composites. These improvements include high modulus [42-46], increased strength and heat resistance [47], decreased gas permeability [48-52] and reduced flammability [53-57]. A study conducted by Moodley and Kanny [58] reported 85 % increase in tensile properties and 80 % increase in flexural properties compared to the virgin material. Kojima et al [59], who researched polyamide nanocomposites, showed that the stiffness and strength increased by 100 % and 50 % respectively with nanoclay loadings of less than 4 % weight. Similar findings were reported by Kato et al [60], Kawasumi [61] and Chow [62]. The advantage that these composite structures have over FRPs is that they are lighter and hence have a higher strength to weight ratio. Furthermore, the improvement in mechanical properties can be, in some cases, better than that of FRPs.

There are three types of clay polymer nanocomposites that are thermodynamically achievable [63]. These are shown in Figure 1.10.

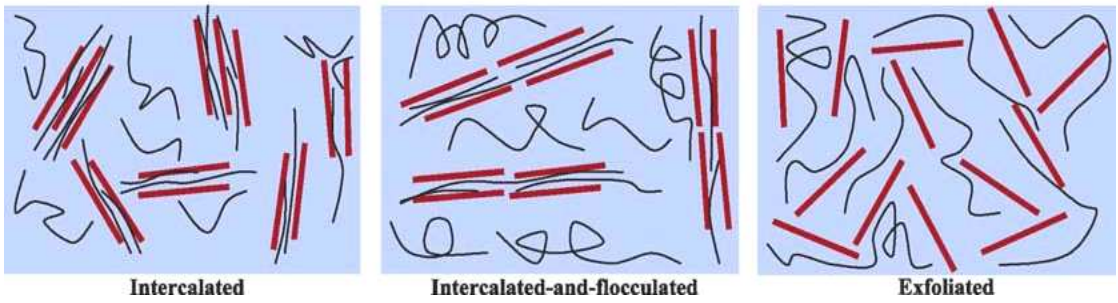

Figure 1.10: Types of clay-polymer nanocomposites [63]

1. *Intercalated*: In intercalated nanocomposites, the insertion of a polymer matrix into the gallery spacing of the clay occurs in a regular crystallographic fashion, regardless of the clay to polymer ratio. Intercalated nanocomposites normally have an interlayer of few molecular layers of polymer in the gallery spacing. Properties of the composites typically resemble those of ceramic materials.
2. *Flocculated*: Conceptually this is similar to intercalated nanocomposites. However, silicate layers of clay are some times flocculated due to hydroxylated edge–edge interaction.
3. *Exfoliated*: The individual clay layers are separated in a continuous polymer matrix, and the average distance depends on clay loading. Usually, the clay content of an exfoliated nanocomposite is much lower than that of an intercalated nanocomposite.

Applications of clay polymer nanocomposites include mirror housings, door handles, engine covers, intake manifolds, and timing belt covers on various vehicle types [64]. GM Motors, Safari and Chevrolet use a clay / polypropylene nanocomposite material for a ‘step-assist’, an optional extra to improve access to the vehicle [65]. Considerable interest is now being shown in clay / polyamide nanocomposites as both fuel tank and fuel line components for cars [66].

Fibre-reinforced and particulate-reinforced composite structures can be combined to form a structure that is superior to either composite system on its own. These are classed as hybrid composites.

1.9. HYBRID COMPOSITE STRUCTURES

A hybrid composite is one where there are two or more reinforcing constituents in a matrix system. Two simple examples would be a fibre-fibre structure and a particulate-fibre structure. A

fibre-fibre hybrid composite would have two different fibre types as the reinforcement, such as glass and aramid, in a polymer matrix. Both these fibre types impart their individual properties to the composite. This results in a structure that is superior to the individual fibre / matrix composites. In a particulate-fibre structure, one would have a conventional fibre-reinforced composite that is further reinforced by particulate fillers, or vice versa. An example mentioned earlier was that of reinforced concrete, where conventional concrete was further reinforced by the addition of steel rods.

1.10. COMPOSITE MATERIALS USED IN PRESENT STUDY

In this study, two types of matrix materials were used. A thermoset, epoxy, and a thermoplastic, polypropylene, were chosen because they are widely used and have good physical and mechanical properties. There were also two types of reinforcing constituents. One was a fibre reinforcement material in the form of S2 glass, and the other was a particulate reinforcement material in the form of nanoclays.

The S2 glass fibre was used in conjunction with the epoxy and polypropylene to produce conventional fibre-reinforced composite panels. These composite structures have good structural capabilities and are very durable. Davalos [67] researched epoxy / glass composites as reinforcements for wood in order to improve the performance and durability of timber structures. Au et al [68] conducted a similar study on concrete beams. Vaidya et al [69] manufactured the floor of a mass transit bus using PP and glass fibres in the form of woven tape.

A hybrid composite structure consisting of S2 glass fibre, epoxy and nanoclays was also studied. Clay / polypropylene nanocomposites, synthesised in a parallel study, were also researched.

Fibre-reinforced composites are extensively used and the demand and applications for these materials is growing. The interest in hybrid fibre-reinforced structures is increasing and they may even become more popular than conventional composite materials. However, these laminated structures have one distinct disadvantage. They are prone to interlaminar cracking or delamination failure [70-72].

2. LITERATURE REVIEW

2.1. DELAMINATION OF COMPOSITE STRUCTURES

Delamination is a phenomenon where the reinforcement in a composite material becomes separated from the matrix, and this may lead to catastrophic failure. The most common sources of delamination are the material and structural discontinuities shown in Figure 2.1. Delamination occurs at stress free edges due to the mismatch in properties of the individual layers (see Figure 2.1a and 2.1c), at ply drops where thickness must be reduced (see Figure 2.1b and 2.1d), and at regions subjected to out-of-plane loading (see Figure 2.1e and 2.1f) such as bending of curved beams [71]. Other sources of delamination include impact damage and manufacturing defects.

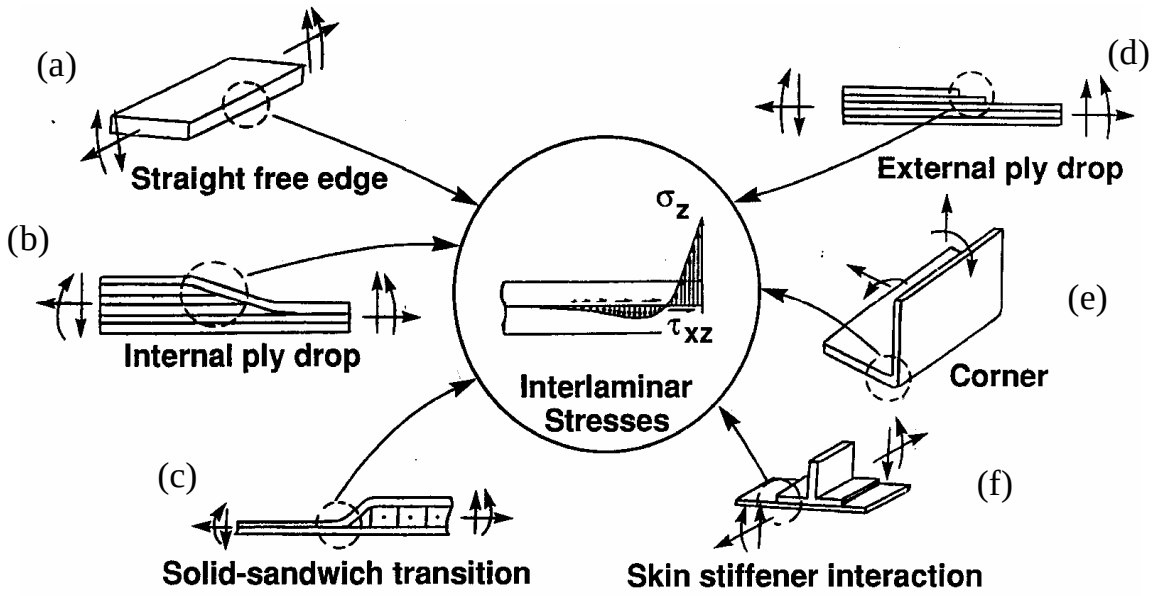

Figure 2.1: Delamination sources at geometric and material discontinuities [71]

Interlaminar cracking or delamination failure in composite structures may occur as a result of the three basic fracture modes shown in Figure 2.2. These include the opening mode (Mode I), the sliding shear mode (Mode II), and the scissoring shear mode (Mode III).

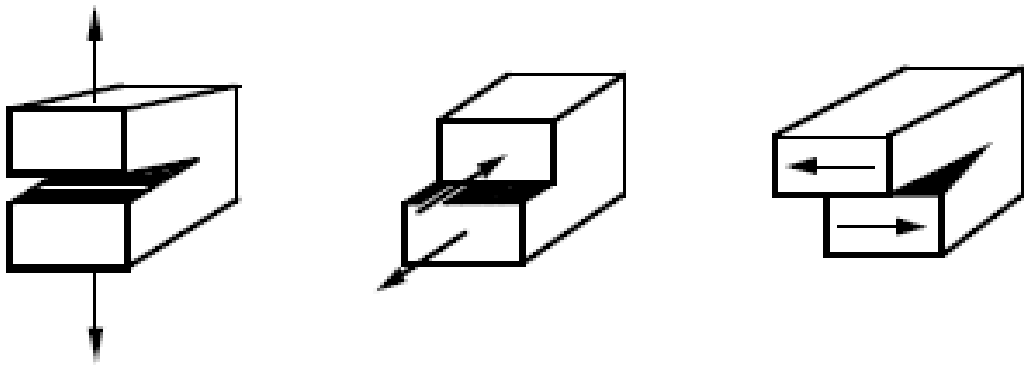

Mode I - Opening Mode | *Mode II - Sliding Shear Mode* | *Mode III - Scissoring Shear Mode*

Figure 2.2: The three basic fracture modes [71]

To enable the safe use of composites in key primary structures, it is important to be able to predict the delamination initiation and propagation. Hence catastrophic failure may be contained, either by arresting or redirecting the delamination path. A major step towards predicting delamination or crack failure is to characterise a material's interlaminar fracture toughness [70] or, in other words, a material's ability to resist delamination or cracking. A more conventional method to determine the fracture toughness is to express it in terms of the stress intensity factor, K_I, K_{II} and K_{III}, or the strain energy release rate, G_I, G_{II} and G_{III}. These correspond to crack growth and delamination for each of the basic fracture modes. In order to evaluate the stress intensity factor and strain energy release rate of a particular composite, it has to be subjected to delamination tests.

2.2. DELAMINATION TESTS

There are various test procedures used to determine the delamination properties of materials under the three basic fracture modes. In traditional isotropic materials, Mode I failure is the most prominent as this mode has the lowest fracture toughness. Hence Mode I testing is the most commonly used. Laminated composite materials, on the other hand, are prone to both Mode I and Mode II fracture modes. Therefore these two modes are the most frequently researched. Delamination due to Mode III conditions is considered inapplicable [73-74], as this mode's fracture toughness is higher when compared to the other two modes [75]. Therefore tests regarding this failure mode will not be discussed.

The various delamination tests for Mode I include Double Torsion (DT), Width-Tapered Double Cantilever Beam (WTDCB), Wedge Insert Fracture (WIF), and Double Cantilever Beam (DCB). For Mode II tests there are End-Loaded Split (ELS), Rail Shear Method, Centre Notched Flexure (CNF), Cantilever Bend End Notched (CBEN), Curvature-Driven Delamination (CCD), and End-Notched Flexure (ENF). The commonly used test for Mode I is the Double Cantilever Beam (DCB), while for Mode II the End-Notched Flexure (ENF) test is common practice.

2.2.1. The Double Cantilever Beam (DCB) test

This test has been used since the 1960's to determine the Mode I interlaminar fracture toughness in composite materials [76]. Figure 2.3a shows the specimen used in the DCB test. The specimen is a beam type with a length L, width b, thickness $2h$, and crack length a. It is manufactured with an even number of fibre layers [77], with a delamination that lies between the central layers, thereby creating two arms of equal fibre content. The specimen is then loaded such that these two

arms are pulled away from each other as illustrated in Figure 2.3b, thereby causing the crack length to increase.

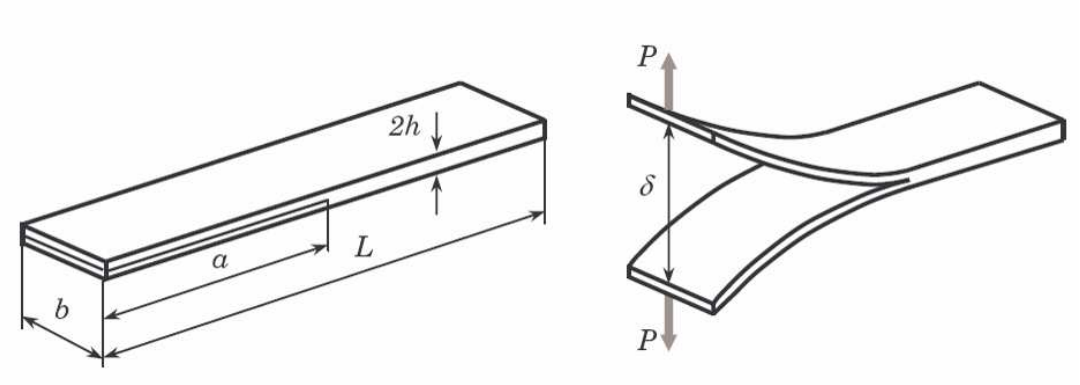

(a) *(b)*

Figure 2.3: DCB specimen in (a) unloaded condition, and (b) loaded condition

The strain energy release rate, which is a function of load and crack length, may be determined by the following equation:

$$G_I = \frac{12P^2a^2}{b^2h^3E_1} \tag{2.1}$$

Where: G_I is the Mode I strain energy release rate, *P* is the applied load, *a* is the crack length, *b* is the width of the coupon, *h* is the height or thickness of the coupon, and E_1 is the elastic modulus in the fibre direction.

2.2.2. The End-Notched Flexure (ENF) test

This test was designed by Carlsson et al [78] and is based on shear deformation beam theory. Figure 2.4a shows the ENF test specimen, which is a beam type with a span *2L*, width *b*, thickness *2h*, and crack length *a*. It is manufactured similarly to the DCB specimen with an even number of fibre layers and an implanted delamination at the mid-plane. The specimen is loaded at

the centre which results in a bending load condition, shown in Figure 2.4b. This in turn causes the crack to propagate through a shear or sliding mechanism.

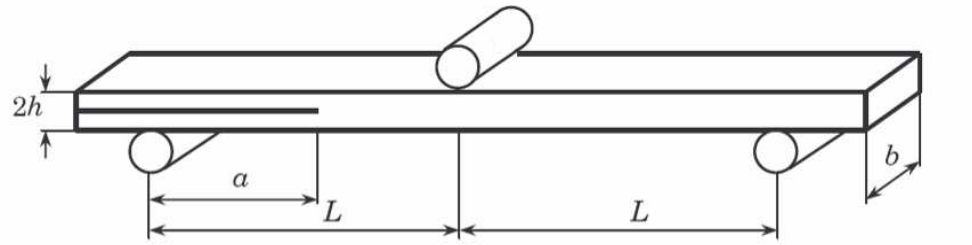

(a)

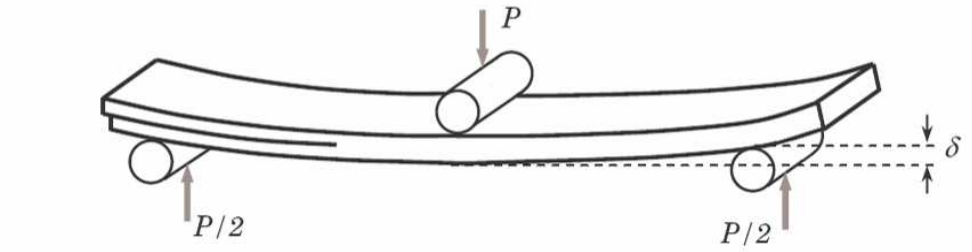

(b)

Figure 2.4: ENF specimen in (a) unloaded condition, and (b) loaded condition

In this case the strain energy release rate is calculated by the following equation:

$$G_{II} = \frac{9P^2a^2}{16b^2h^3E_1} \tag{2.2}$$

Where: G_{II} is the Mode II strain energy release rate, P is the applied load, a is the crack length, b is the width of the coupon, h is the height or thickness of the coupon, and E_1 is the elastic modulus in the fibre direction.

2.2.3. Mixed Mode Testing

Although the DCB and ENF tests are quite popular, they only account for pure Mode I or pure Mode II crack propagation. However, in most engineering applications, delamination initiates and propagates under the combined influence of normal and shear stresses [79-80]. Therefore, tests of delamination resistance should account for the effects of combined stresses.

Tests have been developed that take into account both Mode I and Mode II failure mechanisms. These have been termed mixed mode delamination tests, some of which include Variable Mixed-Mode (VMM), End Notched Cantilever Beam (ENCB), Mixed Mode Flexure (MMF), Arcan, Edge Delamination Tension (EDT), Cracked Lap Shear (CLS), and Mixed Mode End Load Split (MMELS).

The disadvantage of having so many different tests to describe or determine one material property is that various results may be obtained. Also these tests do have their drawbacks, for example, in the MMELS test the mode-mix ratio varies with the crack extent. The CLS test, although simple, requires numerical nonlinear analysis to determine the Mode I / Mode II ratio [80]. In addition, different mode-mix ratios require different lay-ups and only a limited range of ratios is possible. The EDT and Arcan tests also require numerical analysis to determine the mode-mix ratio. In the MMF test, different Mode I / Mode II ratios require different thicknesses of specimens. In an attempt to standardise testing under both Mode I and Mode II conditions, the Mixed Mode Bending (MMB) test was proposed to determine the strain energy release rate under mixed mode conditions.

2.2.4. The Mixed Mode Bending (MMB) test

This test was first proposed by Reeder and Crews [79-80], and it combines the loading effects of both the DCB and ENF tests, as shown in Figure 2.5.

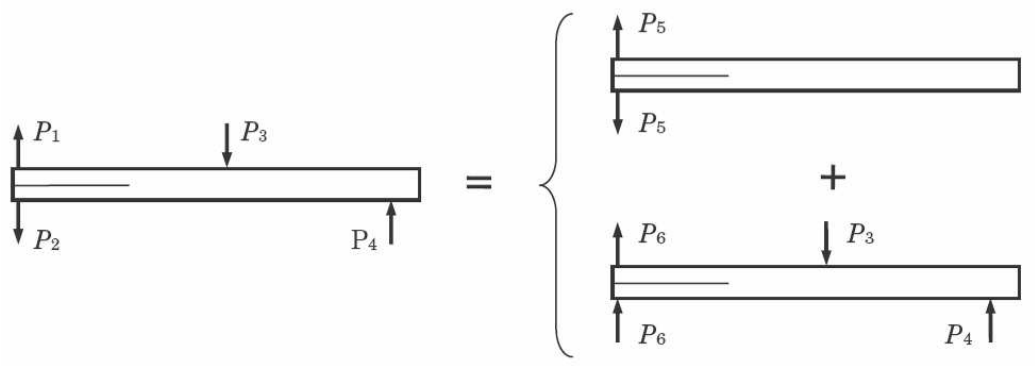

Figure 2.5: MMB test shown as the superposition of the DCB and ENF tests

Upon further investigation of the test fixture, Reeder and Crews determined that there were nonlinear effects present. Therefore they modified the fixture to overcome these nonlinear effects [70,81]. Later the MMB test was standardised by ASTM [82]. A schematic of the MMB test fixture is shown in Figure 2.6.

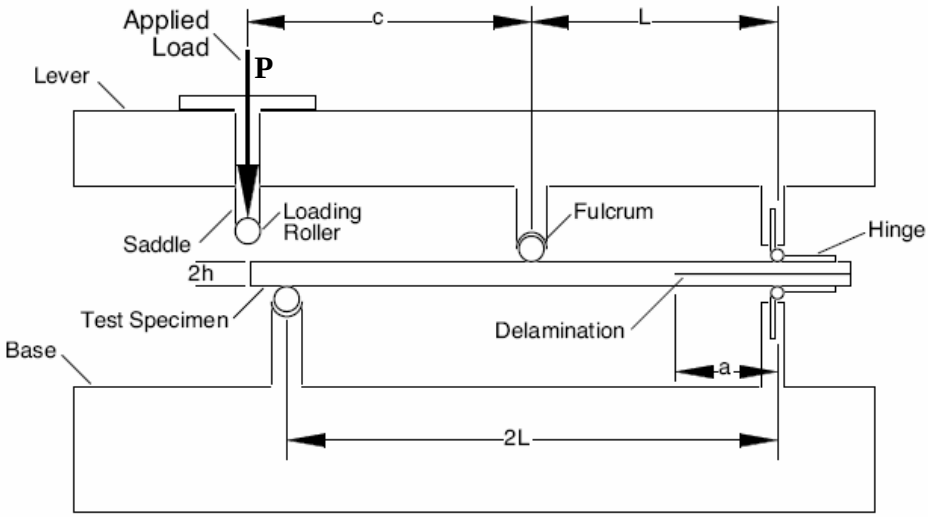

Figure 2.6: Schematic of MMB test coupon in testing fixture [79 – 80]

The test specimen is similar to the type used in the DCB test with a width of *b*. In Figure 2.6 the specimen is shown to have a test span length of *2L*, height of *2h*, and initial delamination length of *a*. The test coupon is attached to the fixture via hinges that are adhesively bonded to the coupon. The fixture itself comprises of a base, a lever and a saddle. The base has a hinge attachment on one end, and, at a distance of *2L*, a roller support on the other, which serves the purpose of the reducing the frictional forces. The lever is similar to the base with the only difference being that the roller support is a distance *L* from the hinge attachment. This roller support is referred to as the fulcrum. The saddle, where the load is applied, is attached to the lever a distance *c* from the fulcrum.

The mechanism of the test is simple. A load, *P*, is applied to the saddle, and this causes the lever to apply a bending load at the centre (fulcrum) and a tearing load at the hinge attachment. By varying the distance *c*, the position of saddle, and consequently that of the applied load, is changed and thus different ratios of the bending to tearing loads can be obtained.

2.3. FRACTURE TOUGHNESS OF FIBRE-REINFORCED COMPOSITES

Alif et al [83] conducted DCB tests on Epoxy / Glass and Epoxy / Carbon composites. These composites consisted of woven fibres with plain, twill and satin weave patterns. It was found that the fracture toughness increased with increased weave index. In the twill and satin weave glass composite structures the crack propagation along the fibres in the 0° direction encountered less resistance than the propagation in the 90° direction. Crack propagation in the satin weave carbon composite was associated with stick-slip behaviour. Fibre bridging also contributed to fracture resistance in the twill and satin weave glass / epoxy composites. Similar results were obtained by Suppakul et al [84].

In a study by El-Hajjar and Haj-Ali [85], a Polyester / E-glass composite was subjected to an eccentrically loaded, single-edge-notch tension (ESET) test. The Mode I fracture toughness of a thick pultruded section was determined and nonlinear material behaviour and stable crack growth was observed. Two data reduction methods were used. Both methods yielded reliable toughness values with one being simpler to use.

Mode I DCB and Mode II ENF fracture toughness tests were conducted on unidirectional and woven E-glass composite structures by Compston and Jar [86]. Standard vinyl ester and an elastomer modified vinyl ester were used as matrices. The G_C results from both modes were consistent with matrix toughness and this was supported by fracture surface examination. Greater deformation was evident in the modified matrix. Similar findings were reported by [87-90].

Furthermore, the G_C initiation values were insignificant in both modes; however, the woven fibres did affected crack growth behaviour. Hence the G_C values for crack propagation were different. It was found during the Mode I testing that the unidirectional specimens showed more stable crack growth. In Mode II, the opposite was true. The woven fibre coupons had more stable crack growth as well as a higher critical strain energy release rate than the unidirectional case.

Prombut et al [91] studied fracture toughness properties of multidirectional carbon fibres in a tough epoxy matrix. Specimens were subjected to asymmetrical double cantilever beam (ADCB) and asymmetrical mixed mode flexure (AMMF) tests. The aim of this study was to establish propagation criteria for delamination between plies of different orientations. The results showed there was no change of delamination plane, an acceptable crack front profile, no initial specimen curvature, and no energy dissipation through global specimen damage.

The study conducted by Rikards et al [92] focused on the mixed mode fracture toughness of glass / epoxy composites. The test method was the compact tension shear (CTS). In the case of the pure Mode II loading conditions, it was shown that there were no significant differences in the results between the ENF and CTS tests. However, under Mode I conditions, differences were noted between the results of the DCB and CTS specimens due to the larger scatter CTS data. A further finding was that the energy required to drive the crack in pure Mode II conditions was about 9 times higher than under pure Mode I conditions. The energy required for mixed mode conditions was in between.

In a study conducted by Kim and Mayer [93], the delamination fracture toughness of carbon / epoxy laminates with mismatched layers was measured using the Mixed-Mode Bending test. The delamination crack did not grow along the mid-plane of the specimen as expected, but propagated to the interface one layer above the mid-plane. Delamination fracture toughness decreased as the mismatch angle increased. As the mismatch angle increased, the flexural modulus of the laminate decreased, and thus fracture energy decreased. The results from this study can be effectively used for analyzing delamination fracture phenomena such as ballistic impact damage. It can also be utilised in designing the alignment of fibre in materials development.

2.4. RESEARCH OF HYBRID COMPOSITE STRUCTURES

Research has been conducted on fibre-reinforced hybrid structures with favourable improvements in properties. Wu et al [94] studied the mechanical properties of glass and carbon fibre-reinforced composite structures with polyamide-6 and 3 weight % nanoclay infused polyamide-6 as matrices. The tensile strength of the nano-infused polyamide-6 with 30 weight % glass fibre was 11 % greater than that of the polyamide-6 with the same fibre content. The increase in tensile

modulus of this hybrid structure was 42 %. An 11 % increase in tensile strength was also noted in the case of the polyamide-6 and nano-infused polyamide-6 reinforced with 20 weight % of carbon fibre. Here the improvement in tensile modulus was 48 %. Increases in flexural strength and modulus were also achieved. The flexural strength and modulus of the hybrid structure with 30 weight % glass fibre increased by 10 % and 81 %, respectively. In the case of the 20 weight % carbon fibre-reinforced structures, there was an improvement of 7 % in flexural strength and 57 % in flexural modulus.

A study conducted by Vlasveld et al [95] showed a 40 % improvement in flexural and compressive strength at elevated temperatures of continuous E-glass fibre-reinforced structures with a nanocomposite matrix. They concluded that these hybrid structures can be used in applications where the temperature is 40 – 50 °C higher.

Wichmann et al [96] conducted a study on glass fibre-reinforced structures with nanoparticle modified epoxy matrix. They reported an increase in interlaminar shear strength but no significant increase in the interlaminar toughness values. They concluded that a significant increase in the fracture toughness of neat nanoparticle modified matrix could not be transferred to the FRP in a comparable manner.

2.5. MOTIVATION AND SCOPE OF RESEARCH

According to Pavan Kumar [97], it has been observed that DCB and ENF specimens have been analysed using both finite element and analytical methods. Studies are available dealing with DCB and ENF tests of unidirectional and multidirectional thermoset composites. Furthermore, few DCB and ENF analytical studies on the analyses of unidirectional, random fibre and

multidirectional thermoplastic structures were conducted. The available literature shows little evidence of MMB tests on thermoset and thermoplastic composites, and in particular glass fibre-reinforced structures. Moreover, there are few studies available on the Mode I and Mode II testing of hybrid composites, but the available literature shows no evidence of any research on MMB testing of these structures.

Materials, in general, may be categorised as being either ductile or brittle [98]. This depends on the characteristics of failure. In the case of polymers, there are two primary deformation mechanisms, namely, crazing and shear band formation [99]. Shear band formation is believed to be the precursor to ductile failure [100]. Brittle failure occurs when crazing is the dominant deformation mechanism [101]. Thermoset polymers exhibit brittle fracture at low temperatures and ductile fracture at high temperatures [102]. The failure mechanism in thermoplastics can be both brittle and ductile. The failure mechanisms for tensile, flexural and other common mechanical testing are well documented. However, literature on failure mechanisms under DCB, ENF and MMB conditions are not extensive.

Therefore this study involves the processing and analysis of random fibre and multidirectional conventional and hybrid composite structures. Specimens were subjected to fracture toughness tests in order to determine the stress intensity factor and the strain energy release rate. The crack initiation, crack propagation and crack paths that were observed during the testing of these composite structures are discussed. The relationships of crack resistance and other properties between the various composite structures are described.

3. MANUFACTURING AND TESTING PROCEDURES

3.1. MANUFACTURING OF COMPOSITE STRUCTURES

The following polymer composites were manufactured:

- Nano-infused thermoplastic
- Fibre-reinforced thermoplastic
- Fibre-reinforced thermoset
- Fibre-reinforced nano-infused thermoset (Hybrid)

The nano-infused thermoplastic structure was manufactured using a melt-blend technique. The Vacuum Assisted Resin Infusion Method (VARIM) was used to manufacture the fibre-reinforced and hybrid thermoset structures. And a modified compression moulding technique [103] was used in the manufacture of the fibre-reinforced thermoplastic composites. These techniques are described later. All composite panels, with the exception of the nano-infused thermoplastic, were manufactured with an implanted Teflon delamination at one end as shown in Figure 3.1. The purpose of the implanted defect was to facilitate delamination initiation and propagation.

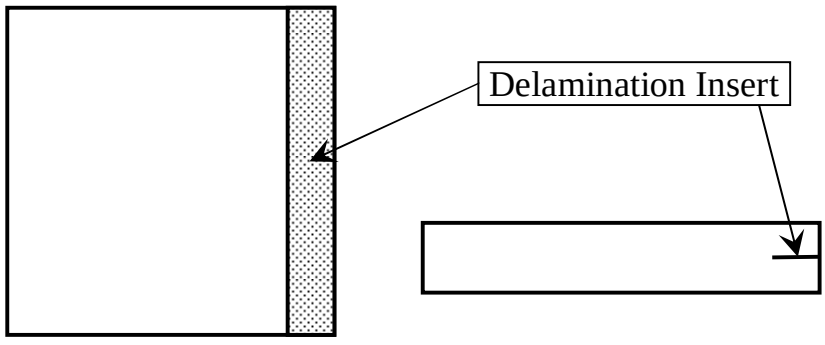

(a) Top View *(b) Edge View*

Figure 3.1: Schematic showing position of delamination insert

The materials used in the manufacture of the above composite structures were obtained from various suppliers. Table 3.1 shows these materials and the company they were obtained from, as well as the supplier location.

Table 3.1: List of materials and their suppliers

Material	Supplier	Location
Cloisite 15A nanoclay	Southern Clays	Texas, USA
Cloisite 30B nanoclay	Southern Clays	Texas, USA
Chopped S2 Glass Fibres	NCS Resins	Durban, South Africa
Woven S2 Glass Fibres	AMT Composites	Durban, South Africa
Polypropylene	Chempro	Durban, South Africa
Epoxy Resin + Hardener	AMT Composites	Durban, South Africa

3.1.1. Nano-infused Thermoplastic Composites

For this structure polypropylene was used as the matrix and Cloisite 15A nanoclay was used as the reinforcement. Panels with 0.5, 1, 2, 3, and 5 weight % loading of nanoclay were manufactured. To simplify the reading of this text a name convention was adopted for the nano-infused polypropylene structures. The name spells out the matrix, the nanoclay infused, and the weight percentage of the nanoclay used. For example, the polypropylene specimen with 2 % weight loading of Cloisite 15A would be referred to as PP02CL15A. These nano-infused structures were manufactured using a melt-blend technique. In this technique, the polypropylene pellets and the nanoclay were combined in REIFFENHAEUSER screw extruder. The extruder has a 40 mm single rotating screw with a length / diameter ratio (L/D) of 24 and driven by a 7.5 kW motor. The heating banks along the length of the screw were set up to gradually heat the

pellet / clay mixture. This temperature gradient setup was executed to avoid thermal shock. The polypropylene pellets and Cloisite 15A nanoclay was blended at approximately 180 °C before being extruded into a mould.

3.1.2. Fibre-reinforced Thermoplastic Composites

Polypropylene and S2 Glass fibres were used to produce two types of conventional thermoplastic panels, namely:

- Polypropylene / Chopped S2 Glass
- Polypropylene / Woven S2 Glass

The woven S2 Glass fibres had a fibre orientation of 0º and 90º. These panels were manufactured using a modified compression moulding technique, for which an in-house fixture was designed and constructed. Figure 3.2 shows a schematic of the fixture and the moulding process. The manufacturing process is quite simple. Polypropylene pellets were placed on an aluminium plate that was gradually heated to 170 ºC. Upon complete transition of the pellets into the liquid phase, the S2 Glass mat was placed on top of the melted polypropylene. The glass mat was then evened out to ensure no wrinkling as well as to allow the plastic to penetrate through the fibre mat. Thereafter, another layer of plastic pellets were placed on the now wetted S2 Glass mat. Once this layer of pellets was melted, the process was repeated until the required number of glass layers was achieved. A second heated aluminium plate, also at 170 ºC, was used to compress the composite via a hydraulic press. The compression ensured proper wetting of the fibres and an even distribution of plastic. Both types of panels consisted of 4 layers of glass fibre with a final thickness of 6 mm. The fibre weight fraction for these composite structures was 30 %.

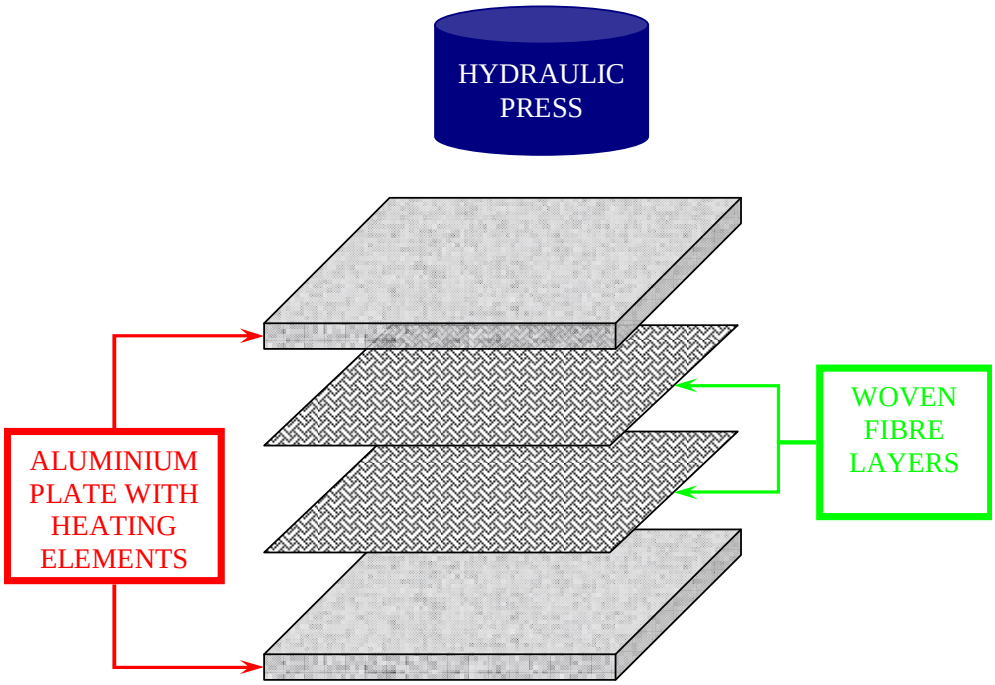

Figure 3.2: Schematic diagram of compression fixture and moulding process

3.1.3. Fibre-reinforced Thermosetting Composites

These polymer structures were produced from LR20 Epoxy resin and S2 Glass fibres. Two types of panels were manufactured:

- Epoxy / Chopped S2 Glass
- Epoxy / Woven S2 Glass

As in the case of the thermoplastic structures, the S2 Glass fibres had an orientation of 0º and 90º. The manufacturing method used in this case was the VARIM technique. In this technique vacuum was utilised to impregnate the glass fibres with epoxy resin. Figure 3.3 shows a schematic of this process. A mould was painted with a release agent, which served in preventing the composite panel from adhering to the mould surface. The fibres were then laid out on the now painted mould, and a peel ply and distribution mesh were placed on top of these. The peel ply

was used to prevent the adhesion of the fibres and distribution mesh. The distribution mesh assisted the resin flow process. Infusion and vacuum pipes were laid and the entire setup was covered with a vacuum bag, which was sealed with vacuum sealing tape. The infusion pipe was initially closed off, and the vacuum pipe was connected to a vacuum pump. The pump was turned on and all the air inside the vacuum bag was removed. The infusion pipe was then inserted into the resin mixture and opened up. Once all the fibres were wetted, the infusion pipe was closed off and the vacuum pump was left running until the resin cured.

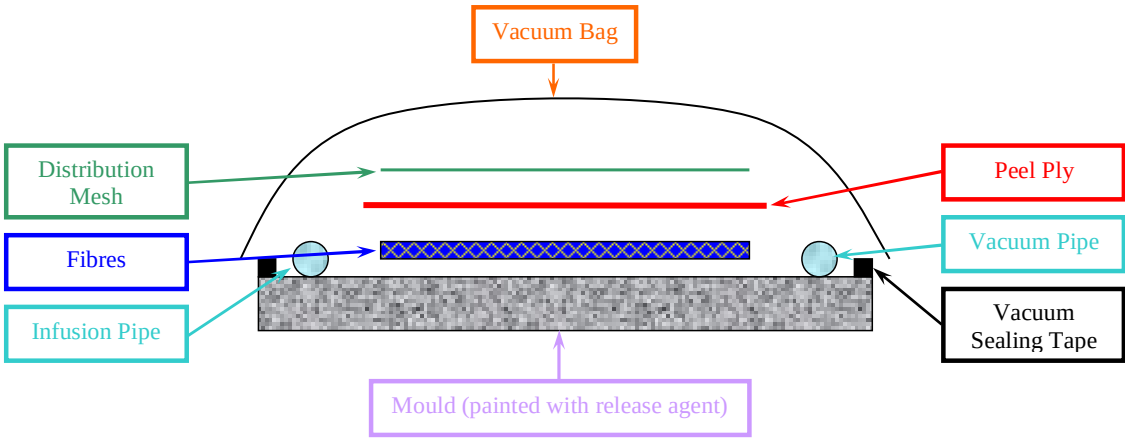

Figure 3.3: Schematic diagram of VARIM technique

Both types of composite panels consisted of 24 layers of fibres. The final thickness of these thermosetting composites was 9.7 mm and 7.5 mm for the chopped and woven fibre panels, respectively. The fibre weight fraction achieved for the woven panel was 66 %, while 63 % was achieved for the chopped case. Figure 3.4 shows a thermosetting panel being processed with the VARIM technique.

Figure 3.4: VARIM technique being used to manufacture a thermosetting panel

3.1.4. Hybrid Thermosetting Composites

This type of polymer composite consisted of 24 layers of Woven S2 Glass fibres and a nano-infused epoxy matrix. The nano reinforcement used was Cloisite 30B nanoclay with a weight loading of 2 %. This nanoclay was combined with the epoxy resin prior to the infusion process by means of a magnetic stirrer (with a heating plate). The resin was poured into a beaker and placed on the stirrer at an initial mixing speed of 300 rpm. The resin was then gradually heated to approximately 70 ˚C, and, simultaneously, the speed was also steadily increased to 1100 rpm. The Cloisite 30B nanoclay was then added to the resin and allowed to disperse completely. Thereafter the resin / nanoclay mixture was gradually cooled to room temperature with the mixing speed also steadily decreasing to the initial speed of 300 rpm. At this point the hardener was added to the resin / nanoclay mixture and the normal procedure for the VARIM technique was followed. The resulting hybrid structure was the nano-infused Epoxy / Woven S2 Glass

composite, or Cloisite 30 B / Epoxy / Woven S2 Glass structure. This composite panel had a final thickness of 7.5 mm with a fibre volume fraction of 45 % and a nanoclay volume fraction of 5 %.

3.2. TESTING PROCEDURES

The polypropylene nanocomposites were characterised using X-ray Diffraction (XRD) and Transmission Electron Microscopy (TEM). Scanning Electron Microscopy (SEM) analysis was conducted to determine fibre wetting of the fibre-reinforced polypropylene composites. Thereafter these structures were subjected to Single Edge Notched Bend (SENB) tests to ascertain their fracture toughness properties. The other composite panels were cut into test coupons according to ASTM testing standards. These were then subjected to Tensile, Single Edge Notched Bend (SENB), and Mixed Mode Bending (MMB) tests. All tests were conducted on a Lloyds Tensile Tester, with a 20 kN load cell.

3.2.1. X-Ray Diffraction

X–Ray diffraction patterns were obtained using a Philips PW1050 diffractometer using monochromated Co-Kά radiation. (λ = 0.1788965 nm, 40 kV, 120 mA) at room temperature. The diffractrograms were scanned from 2.5˚ to 10° (2θ) in steps of 0.02˚ using a scanning rate of 0.5˚/min. X-ray diffractrograms were taken on Cloisite 15A clay and polypropylene composites containing 0.5, 1, 2, 3 and 5 wt.% Cloisite 15A nanoclay to confirm the formation of nanocomposites on addition of organo clay.

3.2.2. Transmission Electron Microscopy

Microscopic investigation of selected nanocomposite specimens at the various weight compositions were conducted using a Philips CM120 BioTWIN transmission electron

microscope with a 20 to 120 kV operating voltage. The cryo and low dose imaging TEM has BioTWIN objective lens that gives high contrast and a resolution of 0.34 nm. The microscope is equipped with an energy filter imaging system (Gatan GIF 100) and digital multi-scan CCD cameras (Gatan 791). The specimens were prepared using a LKB / Wallac Type 8801 Ultramicrotome with Ultratome III 8802A Control Unit. Ultra thin transverse sections, approximately 80-100 nm in thickness were sliced at room temperature using a diamond knife. The sections were supported by 100 copper mesh grids sputter-coated with 3 nm thick carbon layer.

3.2.3. Scanning Electron Microscopy

Fibre wetting studies on the fibre-reinforced polypropylene structures were conducted using a Philips XL30 Environmental SEM with accelerating voltage 0.2 to 30 kV and magnification 15 to 500 000. The microscope is equipped with a conventional filament emission gun giving a beam spot size of 20 nm and image resolution of 2 nm. Thin transverse sections, approximately 2 to 7 mm in thickness were cut from selected specimens.

3.2.4. Tensile

Tensile tests were carried out, in accordance with the ASTM D 3039 / D 3039M – 93 testing standard [104], in order to determine the elastic modulii that were required to evaluate the mixed mode strain energy release rates. The test coupons were 200 mm in length and 13 mm in width. The results from the tensile test were used to plot a Stress versus Strain curve, and an equation best describing the plot was determined. This equation was differentiated, and was then used to determine the slope (elastic modulus) of the plotted curve at each data point. The slope values were then averaged to determine the average elastic modulus of the specimen.

3.2.5. Single Edge Notched Bend (SENB)

The ASTM D 5045 – 93 testing standard [105] was used as the guideline for the SENB test coupons. The dimensions of the test coupons were obtained from the testing standard, and were different for each composite type. Each specimen had an initial crack length of 5 mm. Specimens were subjected to this test using a three-point-bend fixture. This test was performed to determine the Mode I fracture toughness (K_I) of the manufactured composite structures. K_I was evaluated via the following equation:

$$K_I = \frac{P}{B\sqrt{W}} f\left(\frac{a}{W}\right) \tag{3.1}$$

Where,

K_I = stress intensity factor (MPa√m)

P = critical load (N)

B = thickness of specimen (m)

W = height of specimen (m)

f(a/W) = correction factor

$$f\left(\frac{a}{W}\right) = \frac{3\frac{S}{W}\sqrt{\frac{a}{W}}}{2\left(1+2\frac{a}{W}\right)\left(1-\frac{a}{W}\right)^{\frac{3}{2}}}\left[1.99-\frac{a}{W}\left(1-\frac{a}{W}\right)\left\{2.15-3.93\left(\frac{a}{W}\right)+2.7\left(\frac{a}{W}\right)^2\right\}\right] \tag{3.2}$$

Where,

S = span length of the specimen (m)

a = crack length (m)

W = height of the specimen (m)

The Mode I strain energy release rates, G_I, for the SENB specimens was determined as follows,

$$G_I = \frac{K_I^{\ 2}}{\mathrm{E}} \tag{3.3}$$

Where,

G_I = Mode I strain energy release rate (J/m^2)

E = Youngs Modulus (GPa)

3.2.6. Mixed Mode Bending Test

A fixture for this test was designed and manufactured in-house in accordance with the original and redesigned apparatus by Reeder and Crews [70,79-81], as well as research carried out by Adams et al [106]. The test coupons were prepared as stipulated in the ASTM D 6671 / D 6671M – 04 [82] testing standard, and were 130 mm in length and 25 mm in width. The initial delamination length was 25 mm.

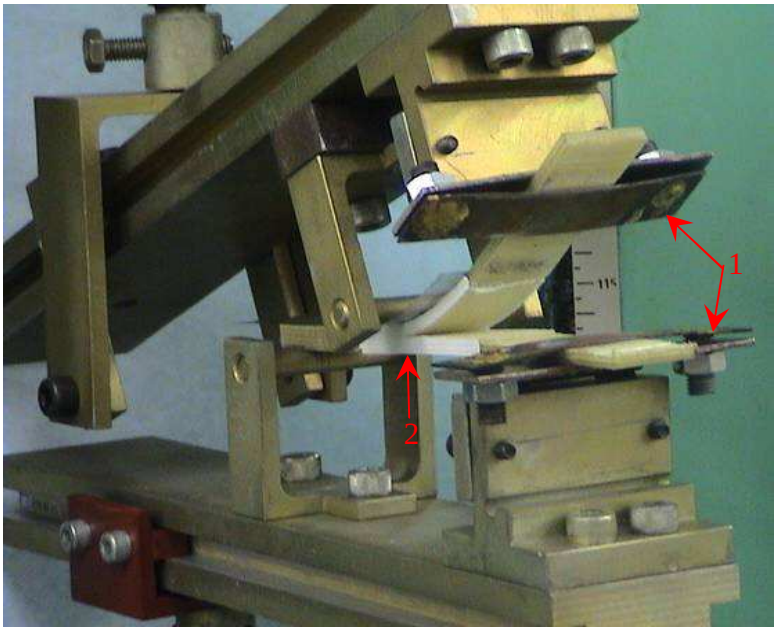

Figure 3.5: Photograph of a test coupon setup in the in-house MMB fixture

Figure 3.5 shows a photograph of the in-house test fixture with a test coupon set up in it. The apparatus on the opening side of the coupon, labelled as 1, is a re-useable hinge. Conventional methods use hinges that are bonded to the specimen using high strength adhesive. A shortcoming of this is that some of the force applied to the test coupon goes into the adhesive bond. If this bond is weak, then the hinge becomes separated from the specimen and testing has to restart. The re-useable hinge eliminates this problem by gripping the specimen directly, and this ensures that the applied force is only directed into the specimen. The side labelled 2 in was painted with white correction fluid to assist in the detection of the crack tip.

During the testing procedure the load, displacement, crack length and time were recorded. This data was used to determine the strain energy release rate (G) using the equations proposed by Crews and Reeder [70,79-81] and Adams et al [106]. They are as follows:

$$G = G_I + G_{II} \tag{3.4}$$

G_I and G_{II} are the strain energy release rates for the Mode I and Mode II components, respectively, and are given by:

$$G_I = \frac{12 P_I^2 (a + xh)^2}{b^2 h^3 E_1} \tag{3.5}$$

$$G_{II} = \frac{9 P_{II}^2 (a + 0.42xh)^2}{16 b^2 h^3 E_1} \tag{3.6}$$

In equations (3.5) and (3.6) a is the crack length, b is the width of the coupon, and h is half the thickness of the coupon. P_I and P_{II} are the opening and shearing components of the applied load, and are given by:

$$P_I = P\left(\frac{3c - L}{4L}\right) \tag{3.7}$$

$$P_{II} = P\left(\frac{c + L}{L}\right) \tag{3.8}$$

P is the applied load, L is the length of the specimen, and c is the distance from the midpoint of the coupon to the loading point, and is shown in Figure 2.6. The value x in equations (3.5) and (3.6) is a correction factor and is calculated by:

$$x = \left[\frac{E_1}{11G_{13}}\left(3 - 2\left(\frac{\Gamma}{\Gamma + 1}\right)^2\right)\right]^{1/2} \tag{3.9}$$

Where:

$$\Gamma = 1.18\frac{\sqrt{E_1 E_2}}{G_{13}} \tag{3.10}$$

Equations (3.9) and (3.10) contain the term G_{13}, which is the shear modulus in fibre plane 1-3, and this is approximately equal to G_{12}, and is given by:

$$\frac{1}{G_{12}} = \frac{V_f}{G_f} + \frac{V_m}{G_m} \tag{3.11}$$

V is the volume fraction, *G* is the shear modulus, and subscript *f* is for fibre and *m* is for matrix. The mode-mix ratio may be determined by using the following equation:

$$\frac{G_I}{G_{II}} = \frac{4}{3}\left[\frac{3c - L}{c + L}\right]^2 \quad , \quad c \geq \frac{L}{3} \tag{3.12}$$

Equation (3.12) has a limitation for the value of c in that it must be greater than or equal to *L/3*. If $c = L/3$ then, in equation (3.5), $P_I = 0$, and hence $G_I = 0$ in equation (3.5). In equation (3.4), $G = G_{II}$ and the loading becomes pure Mode II. Equation (3.12) becomes invalid for values of $c < L/3$, as this model did not account for contact between the two arms of the specimen.

The value of *c*, the distance from the specimen midpoint to the applied load, can be determined for a given mode-mix ratio from equation (3.12). As stated in Section 2.8.4, by varying this distance *c*, various mode-mix ratios can be obtained, and this results in a change of the bending and shear stresses. For instance, the bending stress experienced would be greater when *c* is smaller, that is, when the applied load is closer to the midpoint, than when *c* is large. A larger bending stress would correspond to a greater Mode II component.

4. EXPERIMENTAL RESULTS AND DISCUSSION PART 1: NANO-INFUSED THERMOPLASTIC COMPOSITES

In Chapters 4 to 8 the experimental results obtained from various tests conducted on four different material systems are discussed. These material systems include nano-infused thermoplastics, fibre-reinforced thermoplastics, fibre-reinforced thermosets and hybrid thermosets. Chapters 4, 5, 6 and 8 each discuss a different material system with regards to either the tensile, SENB, MMB, or a combination of these test results. Further, the damage or fracture paths observed in each test case are discussed where appropriate. Comparisons between the various structures regarding their tensile and fracture toughness properties are discussed in Chapter 7.

This chapter deals with nano-infused thermoplastics. Here, molten polypropylene was infused with Cloisite 15A nanoclay as described in Section 3.1.1. The clay particles were thoroughly dispersed in the matrix creating a homogeneous mix. Hence it may be expected that the structure exhibits the same properties in all directions and is isotropic. The most prominent failure mode of isotropic materials is Mode I. Hence only SENB tests were performed on the nano-infused polypropylene composites. These structures were infused with 0.5, 1, 2, 3 and 5 weight % loadings of Cloisite 15A. XRD and TEM analyses were performed. The fracture mechanism is described.

4.1. SINGLE EDGE NOTCHED BEND (SENB) TEST

Three specimens from each of the clay loading cases were tested. The length, width and thickness of the test coupons were 126 mm, 25 mm and 5 mm, respectively. The specimens were tested at a cross-head speed of 1 mm/min. The critical stress intensity factor (K_{IC}) and other related properties for each nanocomposite structure was determined. The critical stress intensity factor obtained for each clay loading case is shown in Figure 4.1.

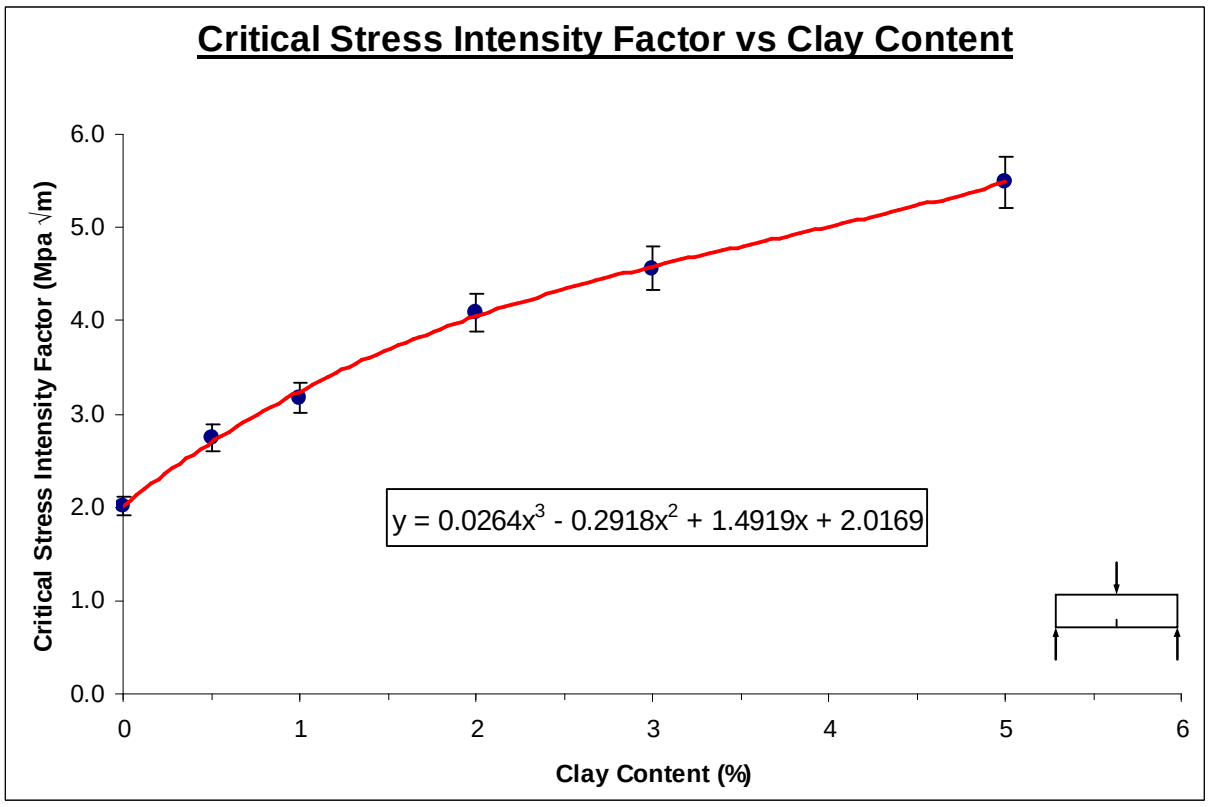

Figure 4.1: Critical Stress Intensity Factor versus Clay Content for 0 % to 5 % nano-infused polypropylene

In Figure 4.1, the specimen with 5 weight % clay loading exhibits the most improvement in fracture properties. Here the critical stress intensity factor was found to be 5.24 MPa√m. This

infers that the load bearing capability of this specimen has increased. This result was not expected as other studies conducted on the same material showed a decrease in load bearing capacity for clay loadings greater than 2 weight %. In a parallel study, Moodley et al [58] characterised the mechanical properties of polypropylene infused with 0.5, 1, 2, 3 and 5 weight % loadings of Cloisite 15A nanoclay. (These nanocomposites were manufactured using the melt-blend technique. Details of this process are available in Chapter 3.) Their findings revealed an 85 % increase in tensile properties and an 80 % increase in flexural properties when compared to virgin polypropylene. The tensile results obtained by Moodley et al [58] are shown in Figure 4.2.

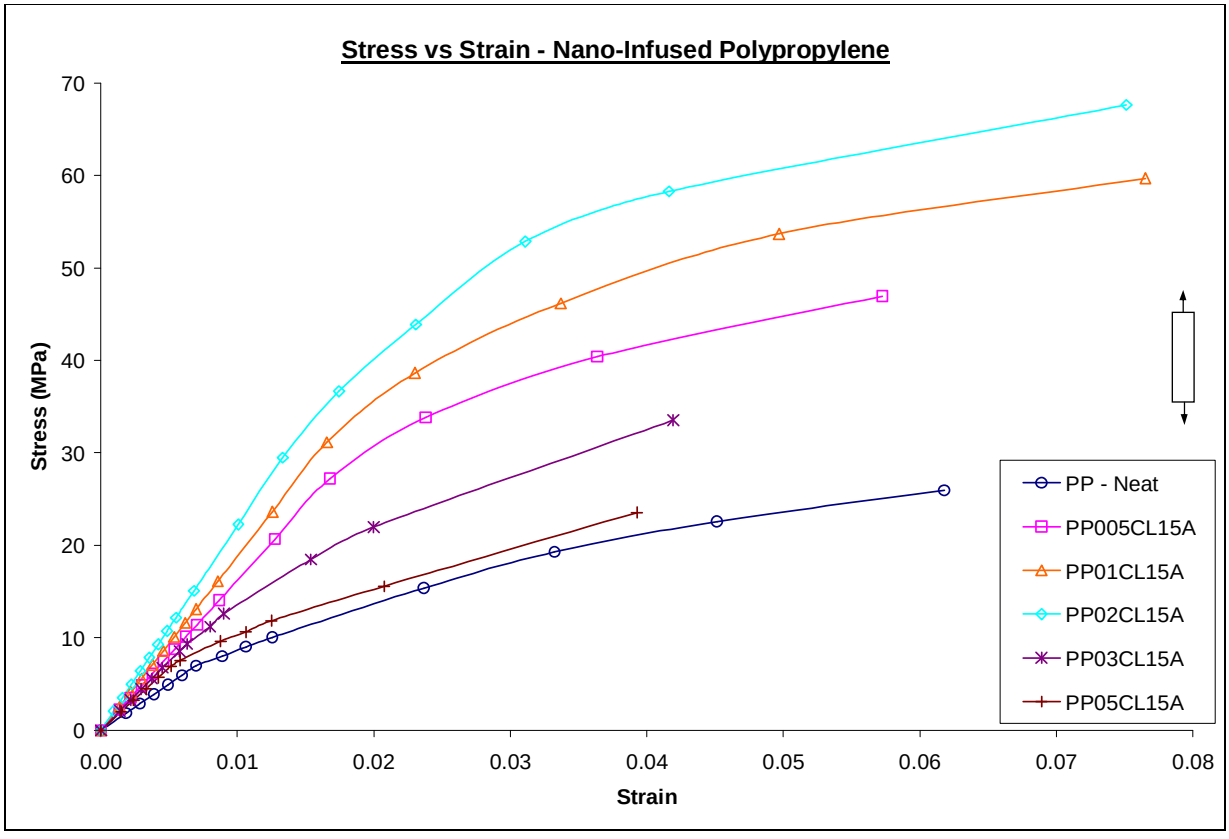

Figure 4.2: Tensile results of Polypropylene / Cloisite 15A [58]

The stress – strain responses in Figure 4.2 shows that the material stiffness (gradient) and hence load bearing capacity increased with increasing clay content up to 2 weight %. This was consistent with the findings of this study. Then with the addition of more clay the stiffness decreases (Figure 4.2) as seen with the responses for 3 and 5 weight %. This is inconsistent with the results from the current research as there was a further increase in properties after the 2 weight % threshold. The inconsistency in these results may be attributed to different modes of loading. The improvement of tensile properties at low concentrations of clay loadings (2 weight % and less) may be accounted for by the uniformly dispersed clay tactoid and intercalated structures [107]. However, at clay loadings greater than 2 weight %, agglomerated clay sites are formed and these act as high stress concentration areas. Bharadwaj et al [108] suggested that the degradation in tensile properties may be attributed to the cross-linked bonds decreasing with increasing clay content. This results in the nanocomposite structure becoming more brittle.

Hence it was expected that the 2 weight % nanocomposite would have the best improvement in critical stress intensity factor as it showed the most improvement in tensile response. A study conducted by Bharadwaj et al [108] showed that the elastic modulus for polyester nanocomposites were at maximum for clay concentrations of 2 weight %. However, in the fracture toughness test, the load bearing capacity of the specimens increased from 0 to 5 weight % and consequently the 5 weight % specimen showed the most improvement in K_{IC}. This increase in fracture toughness properties beyond the 2 weight % threshold may be linked to an increase in hardness properties. The improvement in hardness and fracture toughness may be due to the presence of intercalated and agglomerated structures. This phenomenon is verified in the study by Moodley et al [58] where the increase in hardness up to 5 weight % was attributed to the agglomeration of clay sites.

Returning to Figure 4.1, the curve shown represents the best fit curve that incorporates all data points from 0.5 to 5 weight % clay loadings. This curve is based on a third order polynomial function for which the equation is:

$$K_{IC} = 0.0264C_C^{\ 3} - 0.2918C_C^{\ 2} + 1.4919C_C + 2.0169 \qquad (4.1)$$

Where: C_C = clay concentration (%)

Using equation (4.1), the critical stress intensity factor for other clay loadings between 0 and 5 weight % may be calculated. For example, K_{IC} for a clay loading of 4 weight % is 5.01 MPa√m. Equation (4.1) may not be valid for clay loadings greater than 5 weight %, however the curve does have a positive gradient between 3 and 5 weight % and this suggests an increase in K_{IC} values after 5 weight %.

The increase in K_{IC} values of these nanocomposites seen here suggests that the material may be undergoing a structure change. In order to verify this hypothesis an in-depth X-ray diffraction (XRD) and transmission electron microscopy (TEM) studies were conducted.

4.2. X-RAY AND TEM CHARACTERIZATION

XRD patterns of Cloisite 15A (CL15A) clays and of clay-polypropylene nanocomposites are shown in Figure 4.3. The Cloisite 15A shows a distinct peak at the 2θ value of 3.3° and the corresponding initial intergallery spacing is 31.09 Å. No distinct peaks were found in the polypropylene nanocomposites containing different weight fractions of Cloisite 15A. During

mixing the polymer infuses and intercalates between the intergallery spacing of layered silicates and separates the clay layers gradually. The disappearance of peak indicates the separation of clay layers and the formation of intercalated or exfoliated nanocomposite. The final confirmation can be achieved only by analyzing transmission electron micrographs pictures.

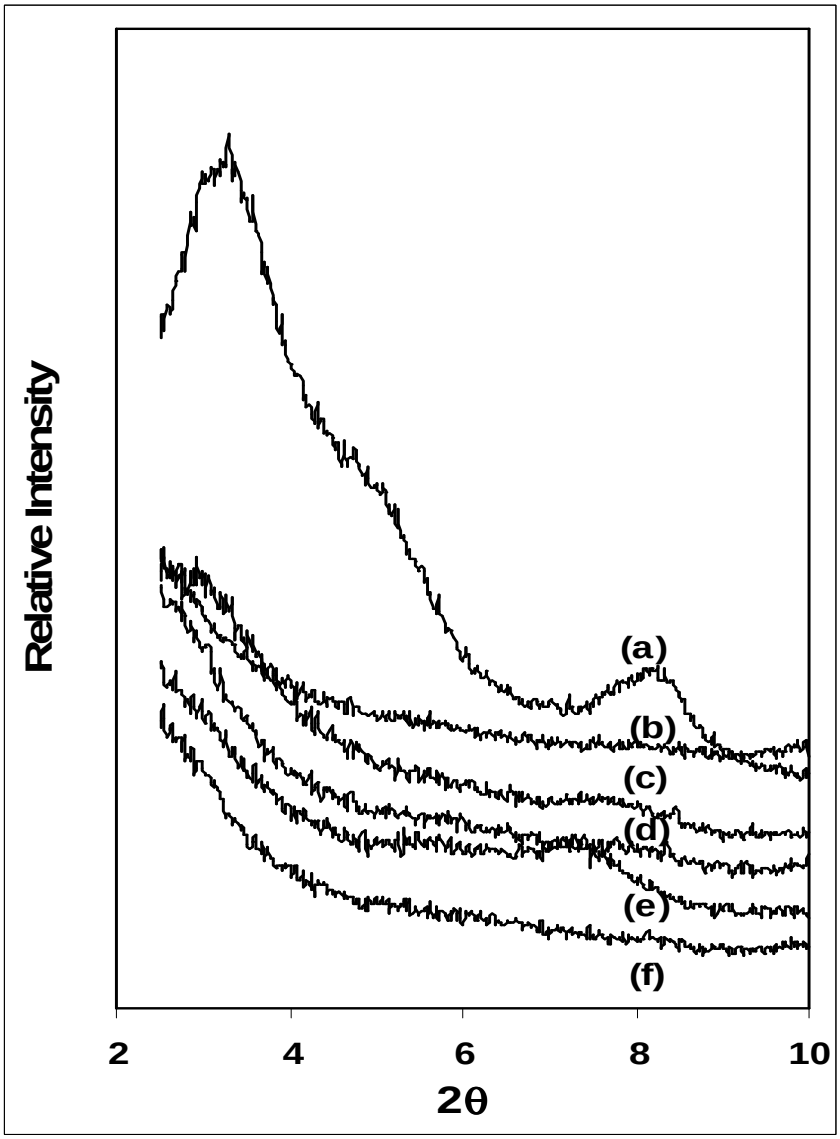

Figure 4.3: X-ray diffraction pattern of (a) CL15A, and PP with (b) 0.5 wt % CL15A, (c) 1 wt % CL15A, (d) 2 wt % CL15A, (e) 3 wt % CL15A, and (f) 5 wt % CL15A [58]

Transmission electron microscope pictures (Figure 4.4) were taken on nanocomposite samples with 1 and 5 weight % nanoclay to compare with the XRD pattern. In the analysis of PP with 1 weight % nanoclay the TEM images shows that the nanoclay dispersed well and the clay platelets were regularly intercalated and exfoliated (Figure 4.4a). This confirms that the PP with 1 weight % nanoclay has exfoliated and intercalated as represented by the XRD figures (Figure 4.3). The PP with 5 weight % nanoclay displays a different behaviour (Figure 4.4b). The clay platelets are closely packed compared to the PP nanocomposites with 1 weight % nanoclay. It resembles an intercalated structure. This confirms that incorporation of nanoclays to the polypropylene matrix leads to the formation of intercalated and exfoliated nanocomposites for lower clay concentration (1 weight %), and intercalated nanocomposites for higher clay concentration (5 weight %).

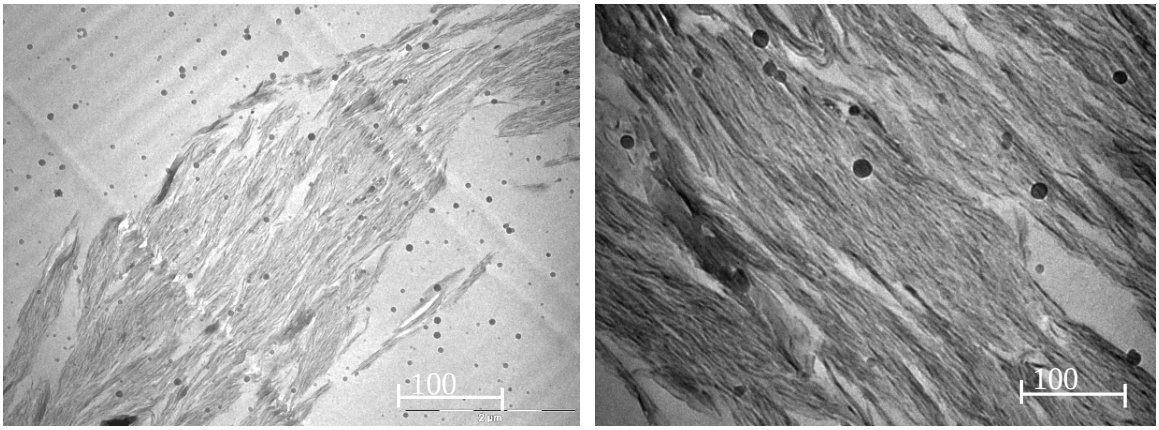

(a) *(b)*

Figure 4.4: TEM images of polypropylene infused with (a) 1 %, and (b) 5 % Cloisite 15A [58]

These intercalated and agglomerated structures act as load bearing agents, and also double as crack arrestors. The dispersion of the clay platelets forces the crack to propagate through complex

pathways on the microscopic level, while the agglomerated clay sites reduces crack propagation by either arresting the crack or forcing it to propagate around the agglomeration. The increase in the critical stress intensity factor of the nano-infused polypropylene structures were due to the presence of these intercalated and agglomerated morphologies. Thus the nanocomposite's resistance to crack initiation and propagation was increased.

These polypropylene nanocomposites exhibited catastrophic fracture. Upon reaching the maximum load bearing capability, the specimens immediately fractured. This is characteristic of a brittle material. The fractured surface was clean with little fragmentation.

4.3. SUMMARY

The 5 weight % specimen showed the most improvement in critical stress intensity factor (K_{IC}). It had an increase of approximately 161 % in K_{IC} over virgin polypropylene. XRD and TEM analyses showed there was an increase in intercalated and agglomerated morphologies with increasing clay content. These morphologies were responsible for the improvement in K_{IC}.

5. EXPERIMENTAL RESULTS AND DISCUSSION PART 2: FIBRE-REINFORCED THERMOPLASTIC COMPOSITES

This chapter discusses the two types of fibre-reinforced thermoplastic composites that were manufactured, namely, polypropylene reinforced with 4 layers of chopped S2 glass and polypropylene reinforced with 4 layers of woven S2 glass. Specimens from these panels were subjected to tensile, SENB and MMB tests as described in Chapter 3. For each test, the damage and fracture paths observed are discussed. The tensile and SENB results of the chopped fibre and woven fibre structures are compared to each other.

5.1. TENSILE TEST

Five specimens from each composite type were tested. The dimensions of the test coupons were 200 mm in length, 13 mm in width, and, 9.7 mm and 7.5 mm in thickness for the chopped and woven fibres respectively. The specimens were tested at a cross-head speed of 1 mm / min. Stress versus Strain responses were plotted and are shown in Figure 5.1.

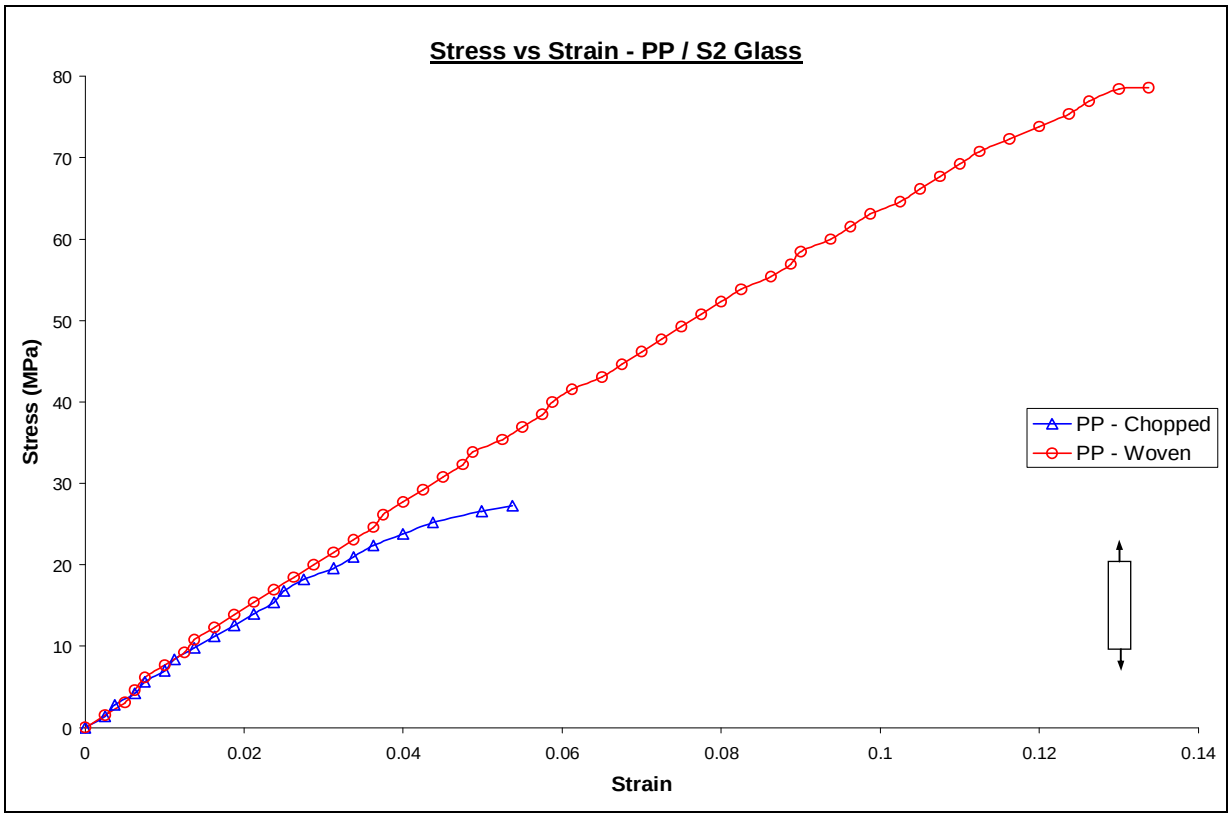

Figure 5.1: Stress versus Strain plots for Polypropylene / Chopped S2 Glass and Polypropylene / Woven S2 Glass

The initial tensile response is typical for visco-elastic materials, in that they are initially linear and later become nonlinear. The elastic modulus for each composite structure was calculated using the gradient and is further described in Chapter 3. The average modulus for the Polypropylene / Chopped S2 Glass was found to be 697 MPa, and for the Polypropylene / Woven S2 Glass an average value of 710 MPa was calculated. These values are low for these types of composite structures especially for the woven fibre case. This may be the result of insufficient wetting encountered during the manufacturing process. A Scanning Electron Microscope (SEM) analysis was conducted in order to verify this hypothesis. The resulting SEM image is shown in Figure 5.2.

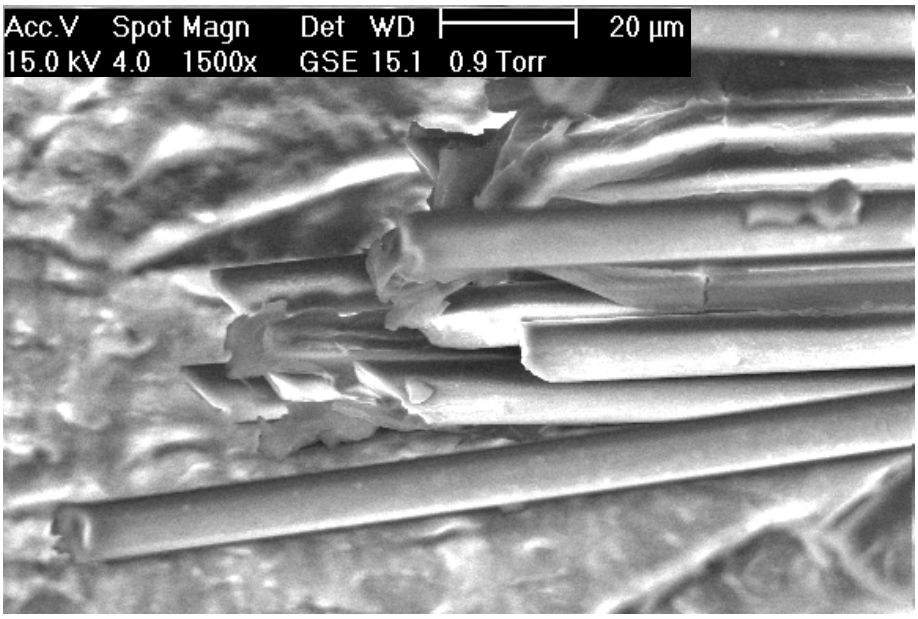

Figure 5.2: SEM image of PP / Woven S2 Glass showing insufficient wetting of the fibres

Figure 5.2 shows the SEM image of Woven S2 Glass in the polypropylene matrix. It can be seen that the individual fibres are not properly wetted by the matrix in that they are not coated by the polypropylene. The polypropylene was able to wet the individual rovings but was unable to penetrate the fibre mat at the filament level. Hence there was insufficient load transfer from the matrix to the fibres and this resulted in the low modulus values achieved.

Although the woven fibre coupon achieved a low modulus, it still carried 100 % greater load than the chopped fibre case. The reason for this is that more of the applied load was transferred to the woven fibres, even though there was insufficient wetting. Due to the structured orientation of the woven fibres, the applied load was evenly distributed throughout the specimen. Hence the load carrying capability was greater than the chopped fibre specimen. The stress distribution in the chopped fibre coupon was uneven which can be attributed to the random orientation of the fibres.

Therefore high stress concentration areas were formed, and this led to the failure of the coupon. These areas of high stress concentration can be seen when examining the fractured area of the chopped fibre specimen which is shown in Figure 5.3.

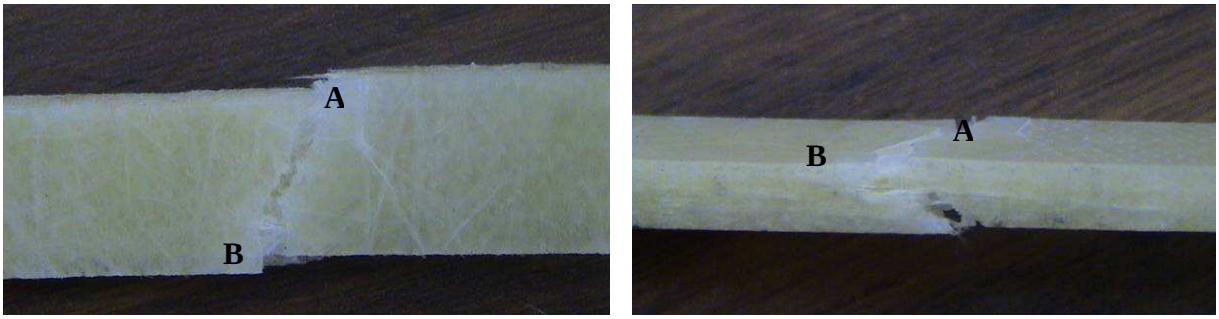

(a) *(b)*

Figure 5.3: Polypropylene / Chopped S2 Glass test coupon after tensile test showing (a) front view and (b) side view.

The fracture of the Polypropylene / Chopped S2 Glass test coupon, shown in the above figure, began at points A and B. At these points an accumulation of stresses occurred and this is shown by the crazing (white area) on the coupon. This stress concentration was greater than the threshold of the material and failure occurred at points A and B. Thereafter there was catastrophic failure along the width of the specimen as the load bearing area decreased.

The test coupon shown in Figure 5.3 exhibits a fracture path that is angled. This angle was determined to be approximately 20º to the vertical in Figure 5.3a. In Figure 5.3b the fracture path is angled at 45º to the vertical, and this is typical of a shear crack. When the load was applied to the specimen, stresses were transversely induced along the fibre edges. Due to the random nature of the fibres, high stress concentration areas were created. The induced stresses in these areas

were not greater than the allowable stress but they were sufficient to rupture the matrix. The angled fracture shown in Figure 5.3a is actually the path taken by these stresses, along the fibre edges, through the width of the coupon. The fracture path in the case of the woven fibre specimens, shown in Figure 5.4, was different.

(a) *(b)*

Figure 5.4: Polypropylene / Woven S2 Glass test coupon after tensile test showing (a) front view and (b) side view.

Unlike the chopped fibre case, the fracture path across the width of the woven fibre coupon, shown in Figure 5.4a, was perpendicular to the edge of the specimen. Here as well, the applied load induced transverse stresses along the fibre edges. However, due to the more structured layout of the woven fibres, the stresses were more evenly distributed. Hence, high stress concentration areas were not formed, and the entire width of the specimen experienced the same stress. This resulted in a straighter fracture path. Figure 5.4b shows the fracture path through the thickness of the coupon. Compared to the chopped fibre case, the woven fibre specimen exhibited a gentler fracture path that was approximately 30º to the horizontal. The fracture path in the woven fibre coupon originated in all matrix layers, and then propagated along the fibre-matrix

interface, before penetrating the fibre mat. This may be substantiated by a more rigorous inspection of the Polypropylene / Woven S2 Glass coupons.

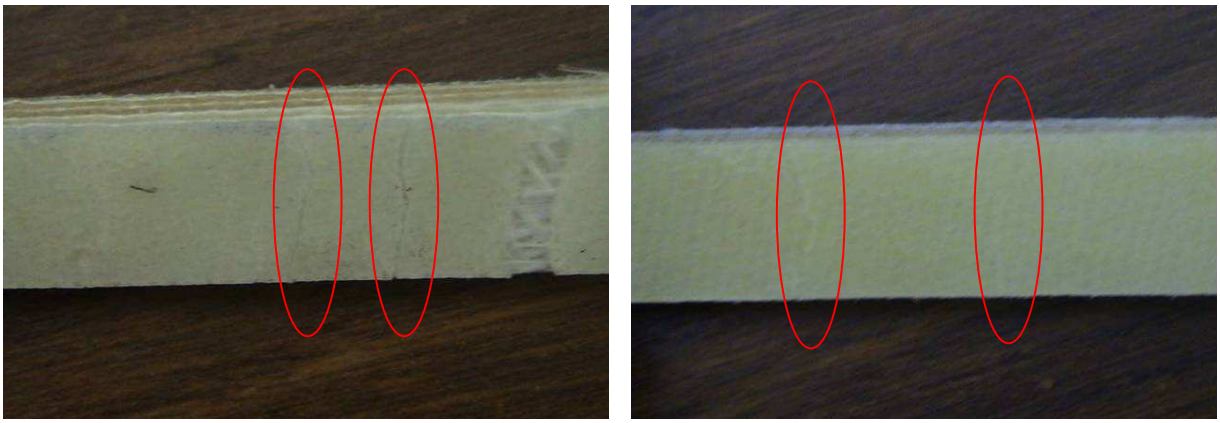

(a) *(b)*

Figure 5.5: Secondary cracking observed in the Polypropylene / Woven S2 Glass coupon on the (a) front face and (b) back face.

Closer examination of the surface of the woven fibre coupons revealed secondary cracks as shown by the ringed areas in Figure 5.5. These cracks were formed during the increased application of the load and there was no apparent pattern to their locations, that is, the distance between the cracks on all test coupons were not regular. As the loading increased, many of these smaller cracks coalesced into a primary crack and failure occurred in the matrix layer. Cracks were also evident on the matrix sub-layers of the test coupon, and here as well, developed into primary cracks. These primary cracks coalesced and lead to the overall failure of the specimen. This accounts for the fracture path seen in Figure 5.4b.

5.2. SINGLE EDGE NOTCHED BEND (SENB) TEST

Three specimens from each of the two fibre-reinforced polypropylene composite types were tested. Each specimen was 150 mm in length, 25 mm in width and 6 mm in thickness, and had an initial crack length of 5 mm. These composite structures were tested at a cross-head speed of 1 mm / min under Mode I conditions. The stress intensity factors (K_I) were determined using equations (3.1) and (3.2), and are shown in Figure 5.6.

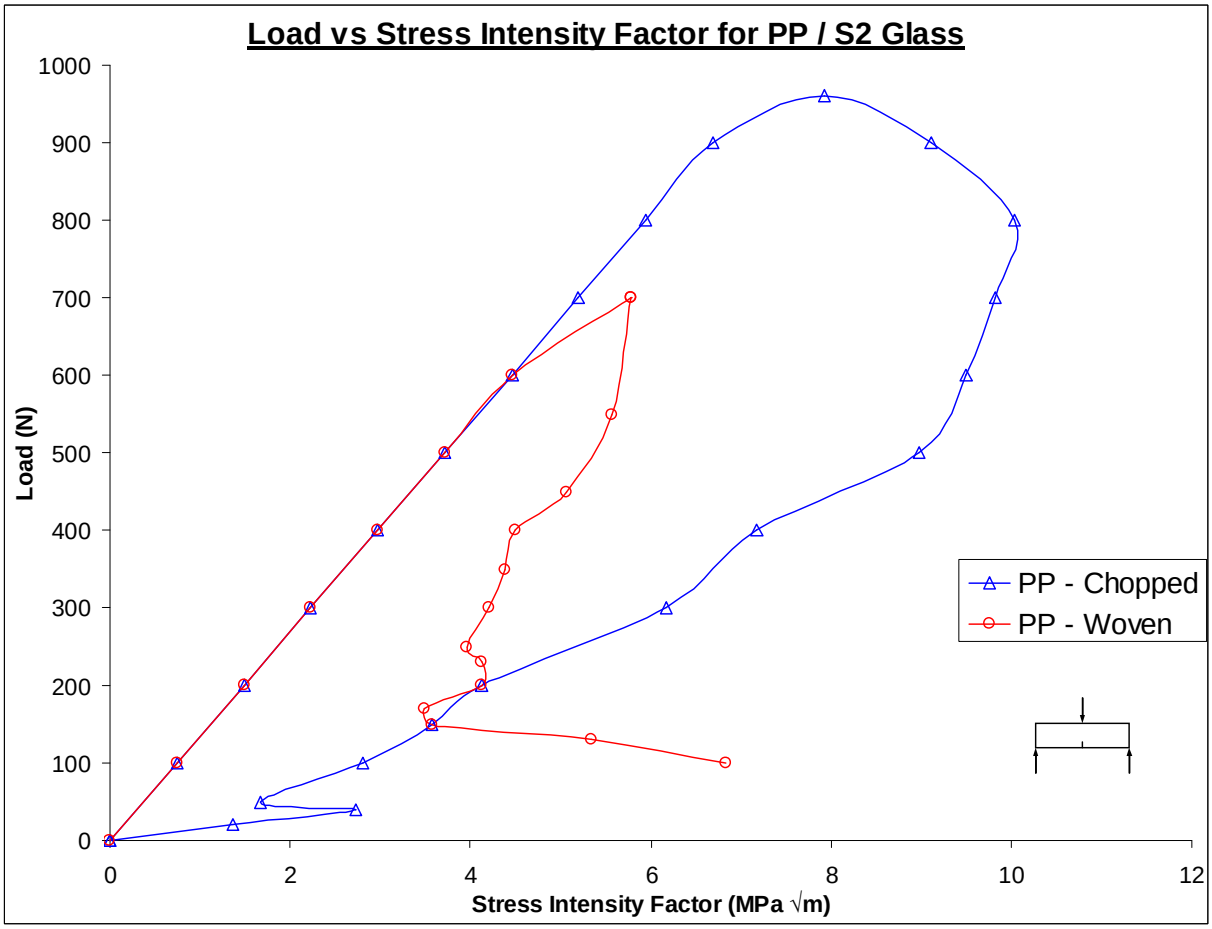

Figure 5.6: Load versus Stress Intensity Factor responses for Polypropylene / Chopped S2 Glass and Polypropylene / Woven S2 Glass

In figure 5.6, the chopped fibre specimen exhibited a superior Load versus Stress Intensity Factor response than the woven fibre specimen. The chopped fibre coupon achieved a critical stress intensity factor of 7.92 MPa√m at a load of 960 N, while a critical stress intensity factor of 5.78 MPa√m at a load of 700 N was obtained in the woven fibre case. The poor performance of the woven fibre structure was due to a "kinking" phenomenon that occurred. This is shown in Figure 5.7.

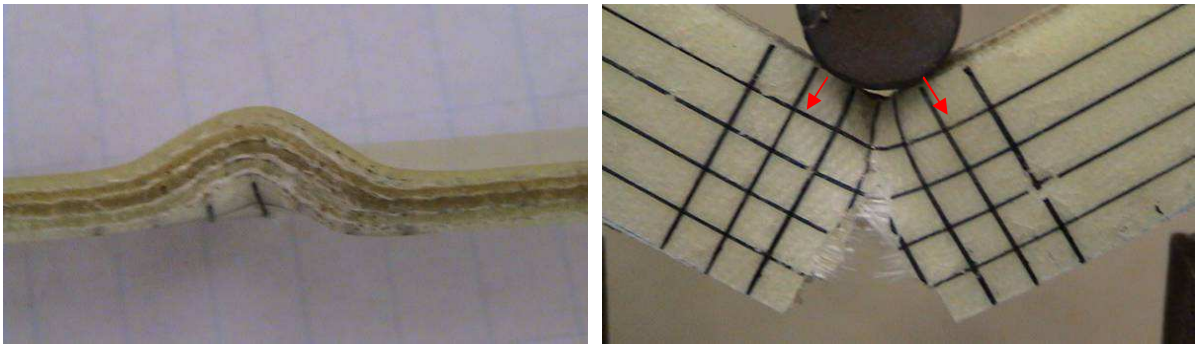

(a) (b)

Figure 5.7: Photographs of Polypropylene / Woven S2 Glass specimen after SENB test showing "kinking" phenomenon on (a) top edge and (b) front surface.

The "kinking" observed on the top edge of the test coupon in Figure 5.7a occurred directly beneath the loading point and directly above the crack front, as shown in Figure 5.7b. This occurrence was unnoticeable in the chopped fibre structure. In the case of the random fibre coupon, the applied load caused a stress concentration at the crack front. Upon further loading, this stress concentration increased and became larger than the matrix threshold. Crack growth was initiated because the random orientation of the fibres could not contain the accumulated stress. Therefore cracking occurred easily with no significant local stresses at the loading point.

The woven fibre structure experienced a similar occurrence. The applied load induced a stress concentration at the crack front, which increased with increasing load. However, once the matrix threshold was reached, crack initiation did not occur. This was because the structured fibre layout of these coupons was able to contain the accumulated stress at the crack front. These stresses were redirected to the next vulnerable point which was the area in contact with the test fixture, and this caused significant local stresses to be induced at the loading point. Although these stresses were not greater than the breaking stress of the fibres, it was greater than the matrix threshold. Thus the matrix succumbed to the induced localised stresses and was compressed by the test fixture, with no evidence of fibre damage. Upon further loading the stress concentration at the crack front increased to the point where it was large enough to initiate crack growth. Due to the test fixture compression of the coupon, the applied load was not directly above the crack front anymore but applied to adjacent areas as depicted by the arrows in Figure 5.7b. This phenomenon was observed in all woven fibre test coupons.

Although the woven fibre specimen experienced this “kinking” phenomenon, it still exhibited superior crack containment properties to the chopped fibre case. Figure 5.8 shows the relationship between Crack Length versus Time for the chopped and woven fibre-reinforced polypropylene specimens. For polypropylene composite structures, the crack initiated directly beneath the loading point, which is typical of a Mode I crack. The chopped fibre coupon experienced rapid crack growth compared to the slow crack growth of the woven fibre case. The crack propagation rate for the chopped fibre was 3.41 mm/min, while the woven fibre had a crack propagation rate of 0.91 mm/min. This crack containment may be attributed to the structured fibre layout of the Polypropylene / Woven S2 Glass.

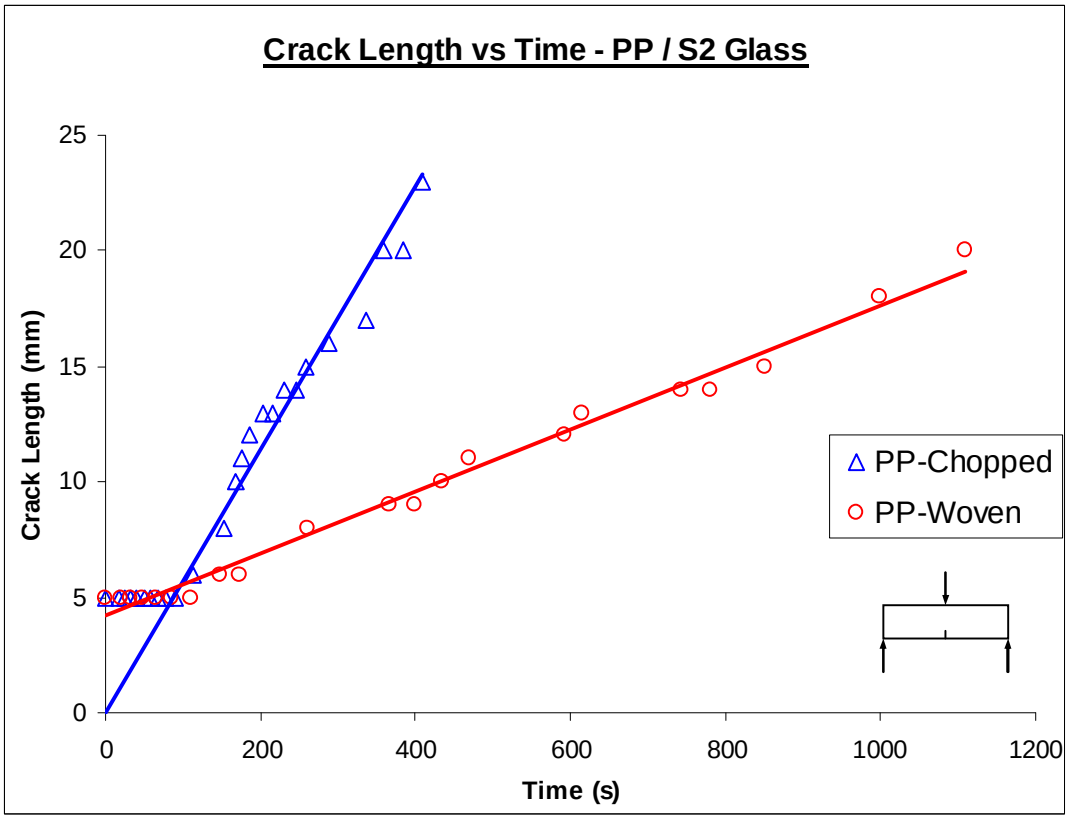

Figure 5.8: Crack length versus Time responses for Polypropylene / Chopped S2 Glass and Polypropylene / Woven S2 Glass

5.3. MIXED MODE BENDING (MMB) TEST

Of the two types of fibre-reinforced polypropylene composites manufactured, only the woven fibre structure was subjected to the mixed mode bending test. This is because equations (3.4) – (3.12) are only valid for directional fibres. Three specimens from this composite were tested at a cross-head speed of 1 mm / min under the mode-mix ratio of $G_I/G_{II} = 4$. For this ratio, the tearing stress is greater than the bending stress. Each specimen had an overall length of 200 mm, a width of 25 mm and an overall thickness of 8 mm. The initial delamination length was 25 mm. Figure 5.9 shows the Load versus Strain Energy Release Rate response.

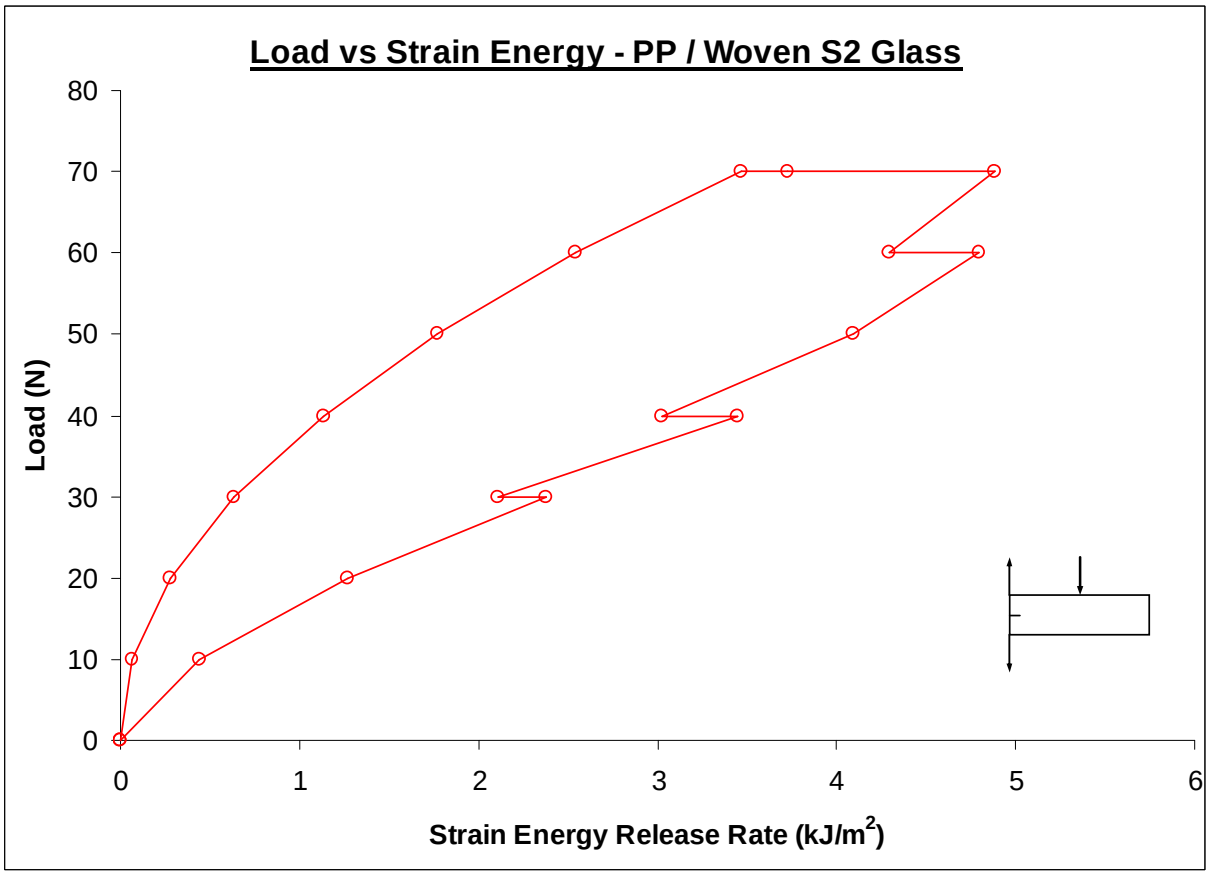

Figure 5.9: Load versus Strain Energy Release Rate for Polypropylene / Woven S2 Glass

For Polypropylene / Woven S2 Glass, the strain energy increases from zero to its critical value of 3.47 kJ/m^2 at an applied load of 70 N. Delamination growth initiated at this point, and thereafter the applied load remained steady at 70 N while the strain energy release rate continued to increase. This increase was due to the ongoing delamination growth. When the strain energy release rate of 4.88 kJ/m^2 was reached, the load bearing capability of the specimen began to decrease, and the response in Figure 5.9 eventually returned to the origin.

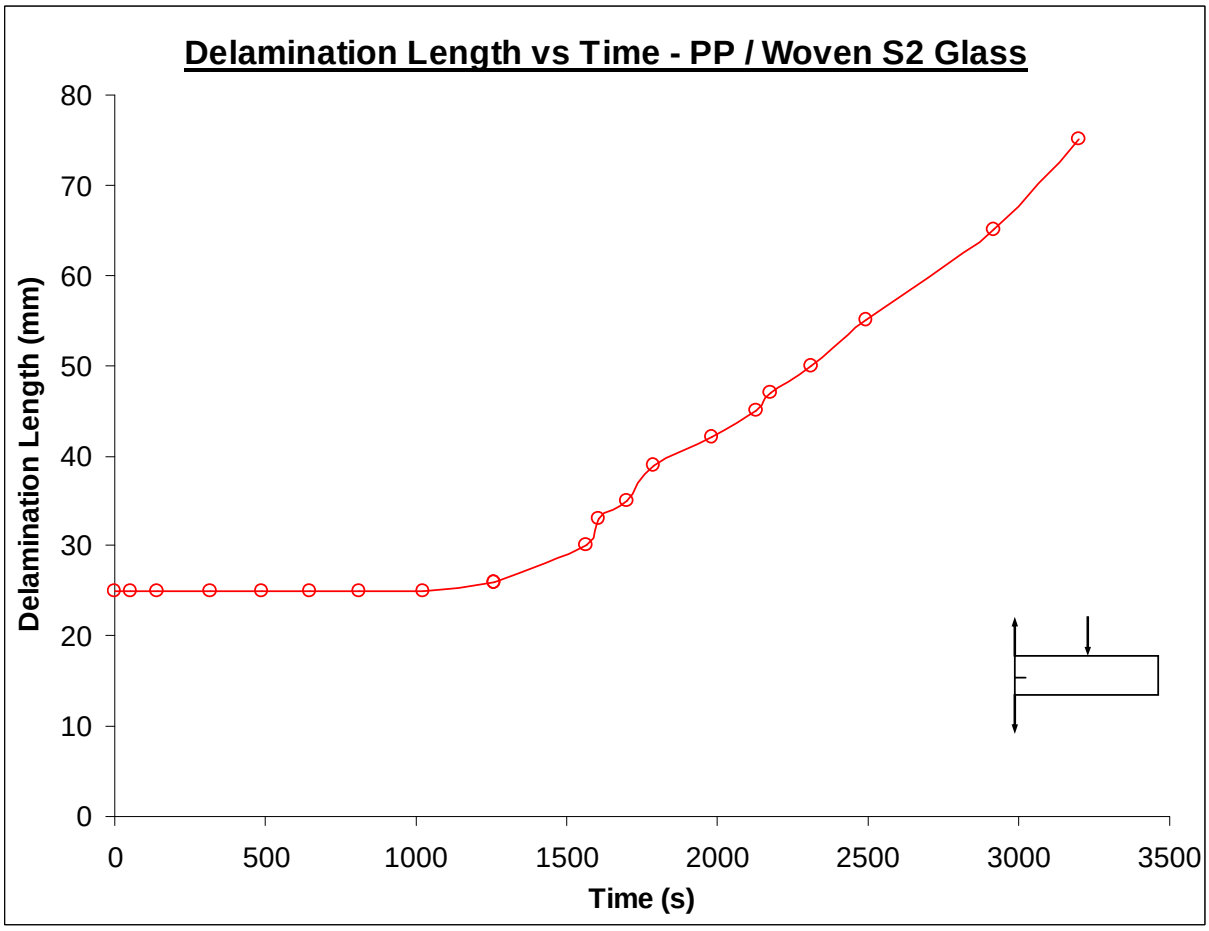

Figure 5.10: Delamination Length versus Time for Polypropylene / Woven S2 Glass under Mixed Mode conditions

The delamination growth rate response, shown in Figure 5.10, is initially linear until t = 1256 s. Delamination growth initiated here and thereafter the response remains approximately linear as delamination propagation continues. The delamination propagation rate was determined to be 1.5 mm/min. For this mode-mix ratio, the tearing load was greater than the bending load. This, together with the slow propagation rate, indicates that delamination growth propagates slower under Mode I dominant conditions.

5.4. SUMMARY

The woven fibre specimen achieved a low modulus value which was attributed to insufficient wetting of the fibres at the filament level. However, due to its structured fibre layout, it carried 100 % greater load than the chopped fibre specimen. In contrast to the woven fibres, the chopped fibres were unable to effectively contain the induced shear stresses and hence the fracture path, and exhibited shear cracking. Secondary cracks were observed in the woven fibre case and these cracks coalesced to form primary cracks which lead to the failure of the specimen. In the SENB test, the woven fibre structure showed a lower critical stress intensity factor, and this was due to the "kinking" observed. Nevertheless, it exhibited superior crack containment properties to the chopped fibre case. The crack propagation rates in the woven fibre and chopped fibre specimens were 0.91 mm/min and 3.41 mm/min, respectively. The critical strain energy release rate for the woven fibre structure was 3.47 kJ/m^2, and the delamination propagation rate was 1.5 mm/min. Delamination propagation rate is slower under Mode I dominant conditions.

6. EXPERIMENTAL RESULTS AND DISCUSSION PART 3: FIBRE-REINFORCED THERMOSET COMPOSITES

The fibre-reinforced thermoset composites manufactured for this study were epoxy reinforced with chopped S2 glass and epoxy reinforced with woven S2 glass. Each composite type consisted of 24 layers of glass fibres with a fibre volume fraction of 50 %. Specimens prepared from these panels were subjected to tensile, SENB and MMB tests as described in Chapter 3. The tensile and SENB results of the chopped fibre and woven fibre structures are compared to each other and the damage and fracture paths observed are discussed.

6.1. TENSILE TEST

Three specimens of each type were tested from the two thermoset composite types. The test coupon sizes were 200 mm in length, 13 mm in width, and, 9.7 mm and 7.5 mm in thickness for the chopped and woven fibres respectively. The specimens were tested at a cross-head speed of 1 mm / min.

Stress – Strain responses were plotted and these are shown in Figure 6.1. The curves in the figure represent the typical tensile responses for Epoxy / Chopped S2 Glass and Epoxy / Woven S2 Glass. The elastic modulus of all specimens was determined as described in Chapter 3. As expected, the woven fibre specimen was superior to the chopped fibre case. An elastic modulus of 15.76 GPa was obtained for the woven fibre coupon and the chopped fibre specimen had a modulus of 6.39 GPa. Due to the random orientation of fibres, the chopped fibre structure had a lower load carrying capacity than the woven fibre structure.

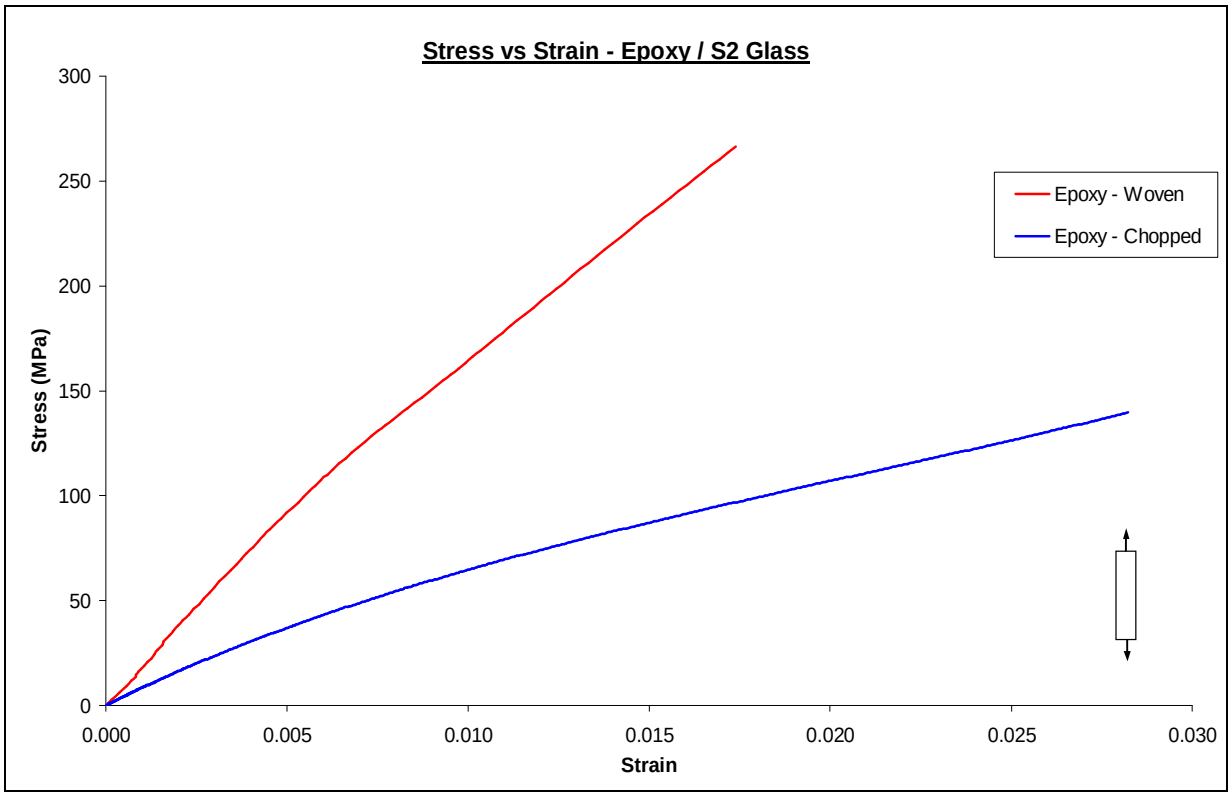

Figure 6.1: Stress versus Strain for Epoxy / Chopped S2 Glass and Epoxy / Woven S2 Glass

Photographs of the fracture surfaces of the fibre-reinforced epoxy structures are shown in Figure 6.2. These are the typical fracture surfaces obtained for the thermoset chopped and woven fibre specimens during the tensile test. The front and rear faces of the chopped fibre specimen (Figures 6.2a and 6.2b) and woven fibre specimen (Figures 6.2e and 6.2f) appear similar with the fracture path being more or less directly across the width of the specimen. However, the examination of the side view of the specimens (Figures 6.2c and 6.2g) show a different scenario. Here the fracture path did not travel directly through the thickness of the coupon but propagated at an angle of approximately 10° to the horizontal in the chopped fibre coupon, and along the length in the woven fibre case.

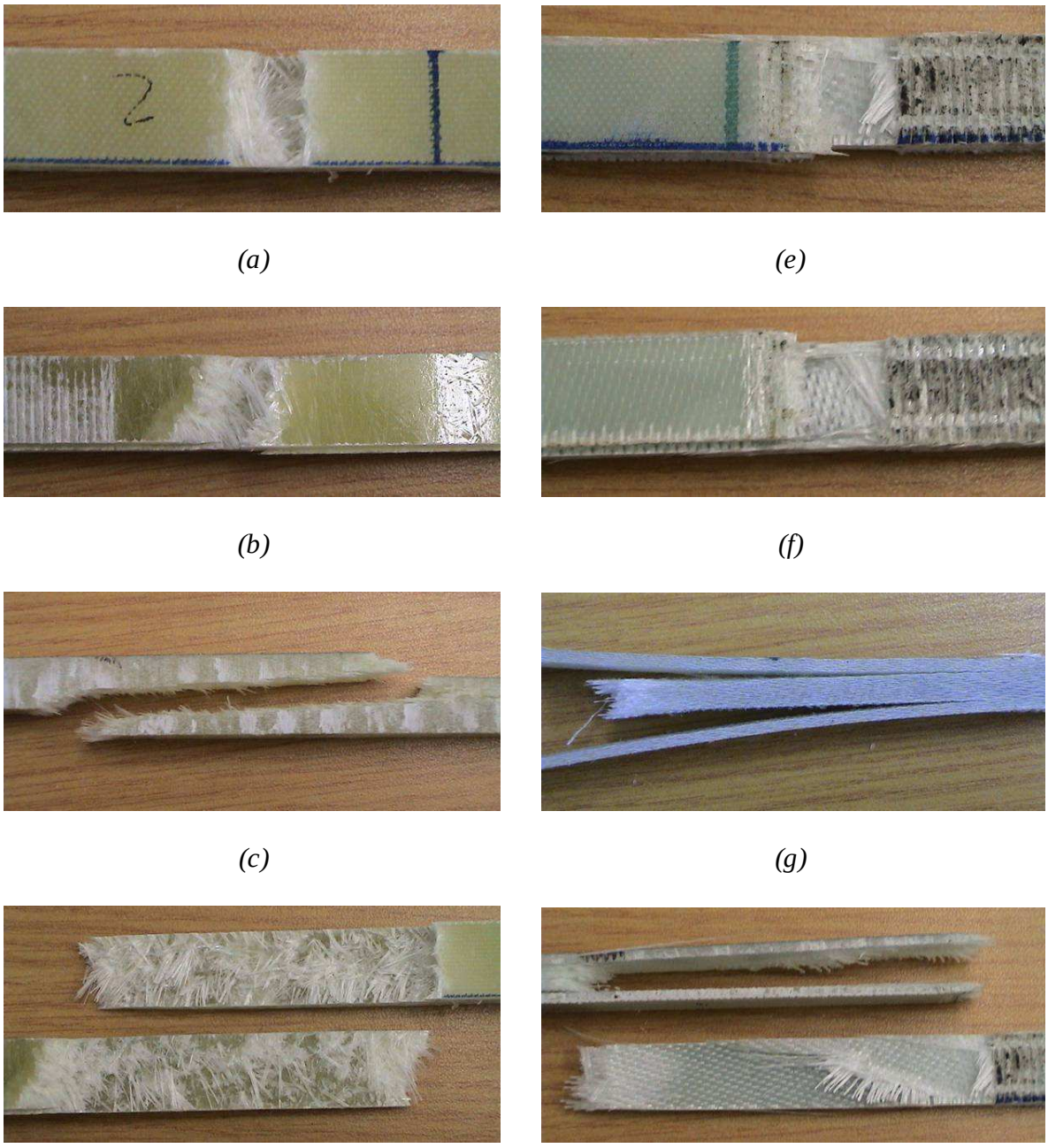

(a) *(e)*

(b) *(f)*

(c) *(g)*

(d) *(h)*

Figure 6.2: Fracture surfaces of thermoset tensile test coupons; (a) front of chopped fibre specimen; (b) rear of chopped fibre specimen; (c) side of chopped fibre specimen; (d) inside of chopped fibre specimen; (e) front of woven fibre specimen; (f) rear of woven fibre specimen; (g) side of woven fibre specimen; (h) inside of woven fibre specimen.

Due to the random orientation of the chopped fibre mat, fibres from one layer were allowed to co-exist and become integrated in the fibre layer above and below. When the load was applied, it induced shear stresses along the fibre edges. The random nature of the fibres caused certain areas of the coupon to accumulate more shear stresses than others. This is evident by the crazing seen in Figure 6.2d that indicate high stress zones. The intermingling fibres made it possible for the shear stresses to travel through the thickness of the coupon. This resulted in some of the high stress zones increasing in magnitude. These higher stress concentration areas coalesced and resulted in the angled fracture path shown in Figure 6.2c. The conclusion that may be drawn from this is that the fracture path through the thickness of a chopped fibre specimen would be random. However, all three specimens displayed angled fracture paths, with the only difference being the angle of the path. Similar angled fracture paths were also observed in the Polypropylene / Chopped S2 Glass structure discussed earlier.

The fibre layout in the woven fibre specimen was structured and hence there was no intermingling of fibres between the layers. As a result, the shear stresses induced along the fibre edges by the applied load were evenly distributed and did not travel through the thickness of the coupon. Therefore there were fewer areas of high stress concentration and the woven fibre coupon was able to carry a greater load than the chopped fibre specimen. Figure 6.2g shows signs of delamination failure, in that, the fracture path propagates along the length of the coupon and then through the thickness. When the load was applied, delamination occurred between the outer layers on both sides of the coupon and the inner layers. These outer layers carried the applied load as they did not experience fracture at this point. Upon further loading, the delamination reached a critical phase where the outer layers reached load bearing threshold. Fracture occurred at these outer layers and thereafter there was complete failure as the inner layers could not sustain

the applied load. Figure 6.2h shows crazing at the fracture point of the inner portion of the woven fibre test coupon. This suggests that the inner layers experienced higher stresses than the outer layers.

6.2. SINGLE EDGE NOTCHED BEND (SENB) TEST

Five specimens from each of the two fibre-reinforced epoxy composite types were tested. The chopped fibre test coupons had a length, width and thickness of 200 mm, 26 mm, and 9.7 mm, respectively. The woven fibre specimens were 140 mm in length, 26 mm in width, and 7.5 mm in thickness. The specimens were tested at a cross-head speed of 1 mm / min. The stress intensity factors (K_I) were determined using equations (3.1) and (3.2). The typical Load versus Stress Intensity Factor response for the chopped fibre / epoxy structure is shown below.

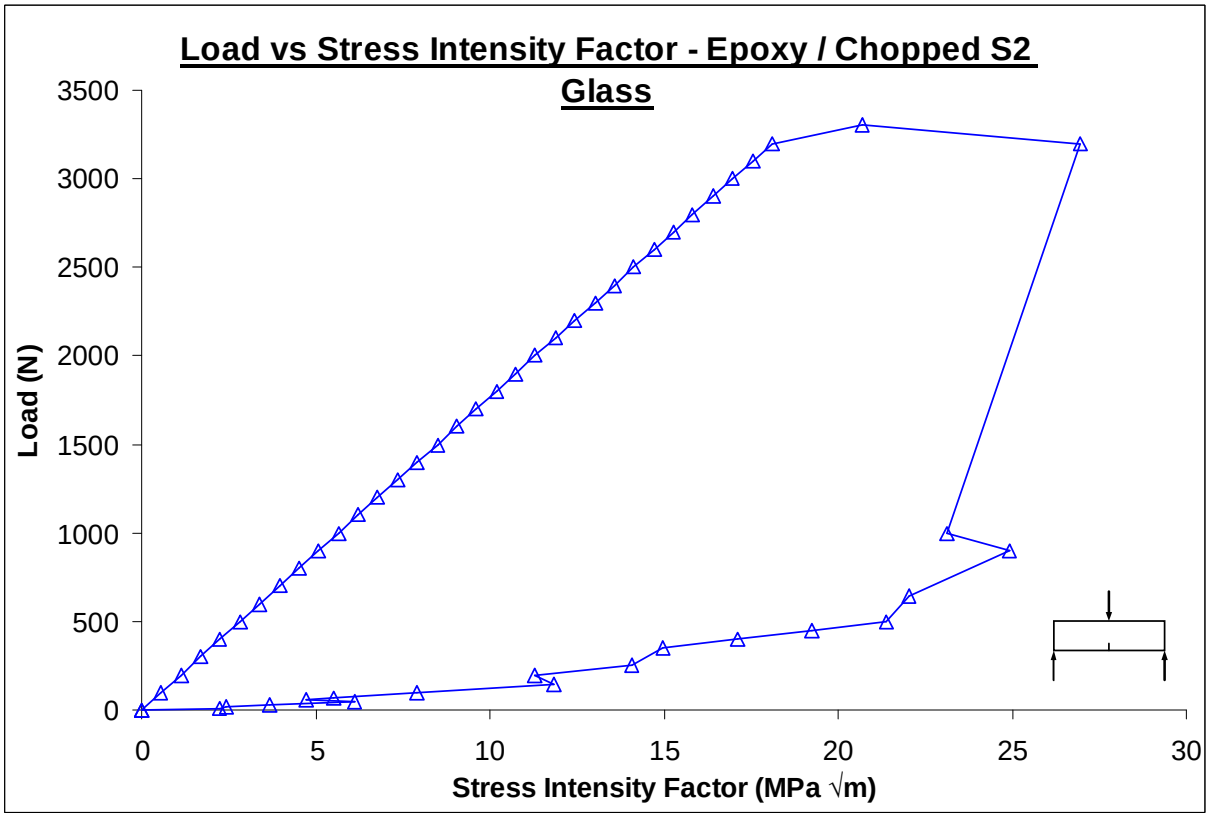

Figure 6.3: Load versus Stress Intensity Factor for Epoxy / Chopped S2 Glass

The initial linear portion of the response in Figure 6.3 was due to zero crack growth. The chopped fibre specimen achieved its critical stress intensity factor (K_{IC}) of 20.68 MPa√m at the maximum applied load of 3300 N. After crack initiation, there was a very rapid decrease in load with a minimal decrease in the stress intensity factor. This was due to the low resistance offered by the chopped fibres in containing the crack front, owing to their unstructured orientation. The stress intensity factor drops to zero since the crack had propagated through the width of the coupon and the specimen became completely unloaded. The woven fibre SENB response is shown below.

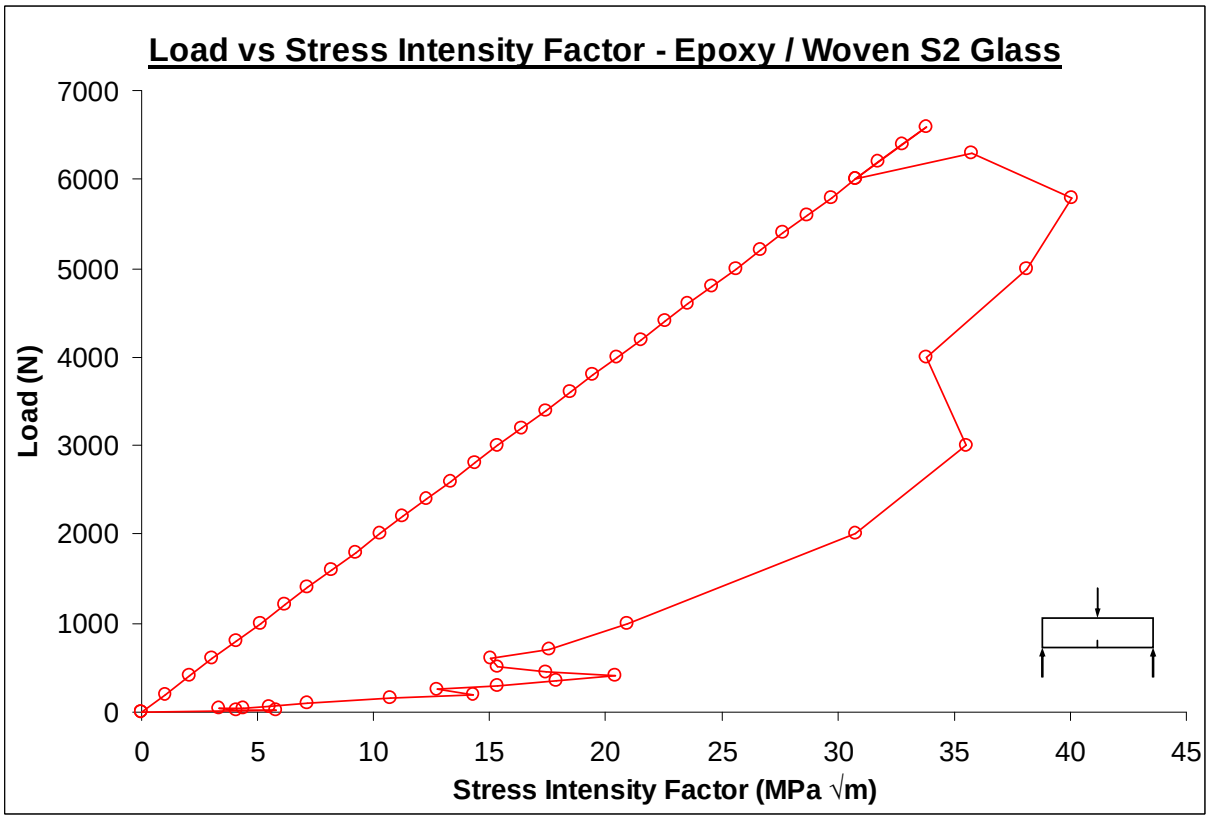

Figure 6.4: Load versus Stress Intensity Factor for Epoxy / Woven S2 Glass.

The Load – Stress Intensity Factor response for the woven fibre / epoxy specimen is shown in Figure 6.4. As in the case of the chopped fibre specimen, the initial linear portion was due to zero

crack growth. The critical stress intensity factor (K_{IC}) was 33.81 MPa$\sqrt{m}$, which was achieved at the peak load of 6600 N. This load is twice the maximum load that was carried by the chopped fibre coupon. The structured orientation of the woven fibres was able to distribute the applied load more evenly and hence the greater load carrying capability. After crack initiation, both the load and stress intensity factor decrease as expected, however, upon reaching a load of 6000 N there is an increase in both values. This suggests a temporary arrest in crack growth. Thereafter crack growth is reinitiated, and, the load and stress intensity factor decrease again. In contrast to the chopped fibre specimen, there is a gradual decrease in load because the structured fibre layout in the woven fibre specimen could contain and impede rapid crack propagation. The stress intensity factor drops to zero as the crack propagated through the width of the specimen. The latter part of the response appears erratic and this was due to momentary crack arresting. This is evident when examining the Crack Length versus Time Response.

The responses in Figure 6.5 represent the Crack Length versus Time for the Epoxy / Chopped S2 Glass and Epoxy / Woven S2 Glass. Initially both coupons experienced no crack growth and the crack length remained at the initial 5 mm. Crack growth was initiated when the critical stress intensity factor was reached at the maximum applied load. The chopped fibre specimen experienced crack initiation at t = 139 s. Crack growth was rapid at a crack propagation rate of 20.75 mm/min. This was due to the random nature of the fibres. Thereafter the crack propagation rate decreased to 2.95 mm/min.

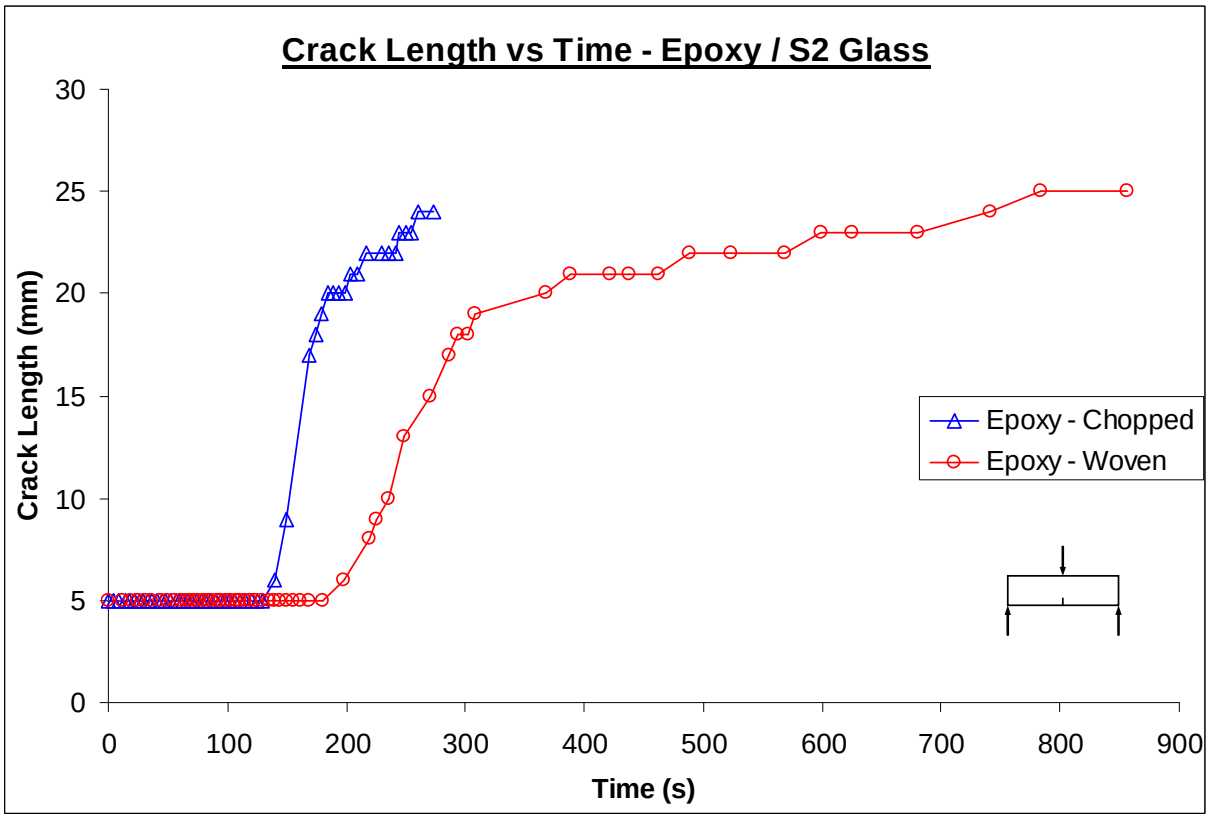

Figure 6.5: Crack Length versus Time for Epoxy / Chopped S2 Glass and Epoxy / Woven S2 Glass

In the woven fibre coupon, crack initiation was at t = 198 s, which was 42 % longer than the chopped fibre case. The woven fibre structure was able to halt crack initiation for a longer period. Thereafter the crack commenced propagating at a rate of 7.3 mm/min. This rate is 184 % less than that of the chopped fibre specimen at its commencement of crack growth. This further emphasises the better crack containment properties of the woven fibres. The crack propagation rate in the woven fibre coupon decreased to 0.62 mm/min. As mentioned earlier there were regions of crack arrest, and these are indicated in Figure 6.5 by areas of zero crack growth in the response for the woven fibre structure.

Photographs of the fracture paths of these fibre-reinforced epoxy structures are shown in Figure 6.6 and Figure 6.7.

(a) *(b)*

Figure 6.6: Fracture surfaces of Epoxy / Chopped S2 Glass SENB test coupons showing (a) front of specimen, and (b) rear of specimen.

Figure 6.6a shows the typical fracture surface of the front of the chopped fibre specimens after the SENB test. The crack path was not straight but rather a little erratic. However, the crack path at the rear of the specimen, Figure 6.6b, was much straighter. Due the random orientation of the fibres, the crack was able to assume one path on the front of the coupon and another one at the rear. It can be assumed that the intermediate layers also had different crack paths, but these paths coalesced to form a primary crack. Hence, this accounts for the erratic crack path seen in Figure 6.6a. The natural conclusion that this leads to is that the crack path in chopped fibre composite panels cannot be predicted; however the crack path in all tested specimens did not deviate more than 3 mm on either side of the centre of the coupon. This infers that the crack path can be

predicted to occur in a certain range. For example, in these chopped fibre specimens, the crack path may be predicted to occur within 5 mm on either side of the loading point.

(a) *(b)*

Figure 6.7: Fracture surfaces of Epoxy / Woven S2 Glass SENB test coupons showing (a) front of specimen, and (b) rear of specimen.

Figure 6.7 shows the typical front and rear fracture surfaces observed in the woven fibre coupons. Unlike the chopped fibre specimens, here the crack paths on the front and rear faces of the coupons were similar. These paths were initially straighter than in the chopped fibre case, and thereafter there is a deviation in the crack path from its original track. This can be seen on the front of the woven fibre specimen, Figure 6.7a, but it is more prominent on the rear face of the coupon, Figure 6.7b. The deviation in crack path occurred as a result of the "kinking" of the test coupon on the top edge. This was brought about by a localised compressive failure at the loading point.

The same phenomenon was observed with the Polypropylene / Woven S2 Glass specimens, but in that case the compression failure was more prominent. As discussed earlier, stress concentration areas were induced by the applied load at the crack front. These high stress zones increased with increasing load. When the matrix threshold was reached, crack initiation did not occur as in the chopped fibre case. The structured fibre layout was able to contain the high stress areas at the crack front and halt crack initiation. These high stresses were redirected to the loading point and resulted in the matrix being compressed by the test fixture. Upon further loading the stress concentration at the crack front increased to the point where it was large enough to initiate crack growth. This localised compression failure did not reduce the performance of the woven fibre specimen; rather it exhibited a superior load carrying capacity and stress intensity factor.

6.3. MIXED MODE BENDING (MMB) TEST

The woven fibre-reinforced epoxy structure was subjected to this test as equations (3.4) – (3.12) are valid only for directional fibres. Test coupons from the Epoxy / Woven S2 Glass panel were subjected to three mode-mix ratios. Three specimens were tested for each mode-mix ratio at a cross-head speed of 1 mm / min. Each specimen had an overall length of 200 mm, a width of 25 mm and an overall thickness of 7.5 mm, with an initial delamination length of 25 mm. The mixed mode ratios considered were G_I/G_{II} = 4, 1 and ¼. In the case where G_I/G_{II} = ¼, the value of c in equation (3.12) is small and therefore the bending stress experienced by the specimen is larger than in the case where G_I/G_{II} = 4. In order to reduce confusion, all responses pertaining to G_I/G_{II} = ¼ are in blue with unfilled circle markers. For G_I/G_{II} = 1, the responses are in red with unfilled triangle markers. And for the mode-mix ratio of G_I/G_{II} = 4, the responses are in green with unfilled square markers.

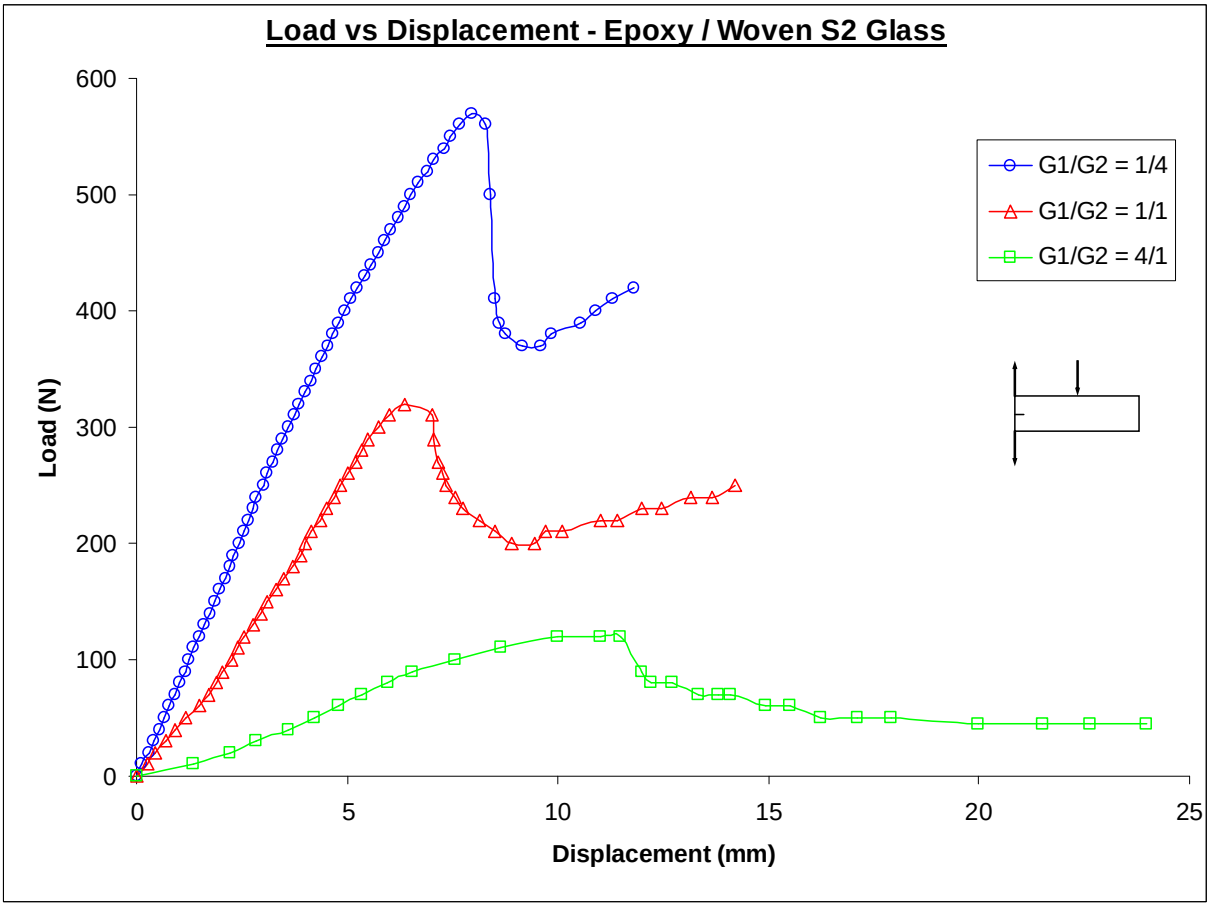

Figure 6.8: Load versus Displacement responses for Epoxy / Woven S2 Glass specimens for mode mixtures of G_I/G_{II} = 4/1, 1/1, and ¼.

The Load – Displacement responses for the Epoxy / Woven S2 Glass specimens are shown in Figure 6.8. The curves represent the typical responses achieved for the mode-mix ratios of G_I/G_{II} = 4, 1 and ¼. All tested specimens behaved similarly, resulting in similar curves as shown in the figure. The load carrying capability of the specimens increased as the mode-mix ratio decreased, which corresponded to an increase in the Mode II component. This indicates that a structure with an edge delamination that has a greater Mode II loading component will be more resistant to delamination than that of a structure with a similar defect loaded with a greater Mode I

component. The response for G_I/G_{II} = ¼ (blue curve) shows this as it was the specimen that carried the largest load before succumbing to delamination failure. This response reached a load carrying capability of 520 N before delamination growth initiated. Thereafter there was a rapid decrease in load as delamination growth was unstable. As the delamination propagation rate stabilised, the applied load decreased more steadily reaching a value of 370 N. After this point the load began to increase, as shown in Figure 6.8, and the delamination growth rate decreased. Here the delamination front approached the centred loading point, where the bending load was induced. The stresses induced by the bending load were dispersed by the woven fibres outward and away from the loading point. These dispersed stresses were more prominent around the region of the midpoint, and gradually diminished as the distance away from the midpoint increased. The delamination front induced stresses acting towards the midpoint, and these stresses were more prominent in the plane of the delamination propagation. When the stress induced by the delamination front approached the opposing stress induced by the bending load, the delamination growth rate decreased. Hence it was possible for the specimen to carry a greater load. Initially, the stress induced by the delamination front was greater than the stress induced by the bending load. Therefore the delamination front propagated albeit at a slower rate. As delamination growth proceeded, the delamination front experienced an increasing opposing stress and therefore the load bearing capacity of the specimen increased in the latter part of the test.

The curve for G_I/G_{II} = 1 (red curve), although similar to that of G_I/G_{II} = ¼, showed a less drastic variation in the load carrying capability of the specimen. Here the delamination growth rate was completely stable throughout the test, which was evident by the absence of rapid increases or decreases in the load – displacement curve. This was due to the Mode I and Mode II loading components being equal. The response achieved a maximum value of 320 N, where delamination

growth initiated, and thereafter decreased to 200 N before increasing again. The increase may be explained via the induced stresses from the bending load and delamination front. For $G_I/G_{II} = 1$, the value of *c* in equation (3.12) is greater than in the case of $G_I/G_{II} = ¼$. Hence the applied load was further away from the centred loading point, and this resulted in lower stresses being induced by the bending load. Thus the delamination front experienced a lower opposing stress than in the case where the mode-mix ratio was ¼. The load bearing capability of the specimen increased, however it was not as high as in the case of $G_I/G_{II} = ¼$.

The third curve in the figure, where $G_I/G_{II} = 4$ (green curve), exhibited poor load carrying capability. This was due to the dominance of the Mode I loading component. The maximum load achieved was 120 N and thereafter the load decreased to a final value of approximately 45 N. Unlike the other two cases, there was no increase in the load in the latter part of the test. This is because the load was applied at almost four times the distance from the midpoint than in the case of $G_I/G_{II} = ¼$. Therefore the stresses induced by the bending load were negligible. The induced stress from the delamination front experienced little or no opposing stresses. Hence, the delamination propagation rate did not decrease and therefore no increase in load occurred. There appeared to be stable delamination growth rate as there were no signs of rapid increases or decreases in the load. However, this was not the case because the scale of the graph in the figure reduced the true shape of the response due to the low load carrying capability of the specimen. Delamination growth was unstable after the initiation point and evidence of this can be seen in Figure 6.9.

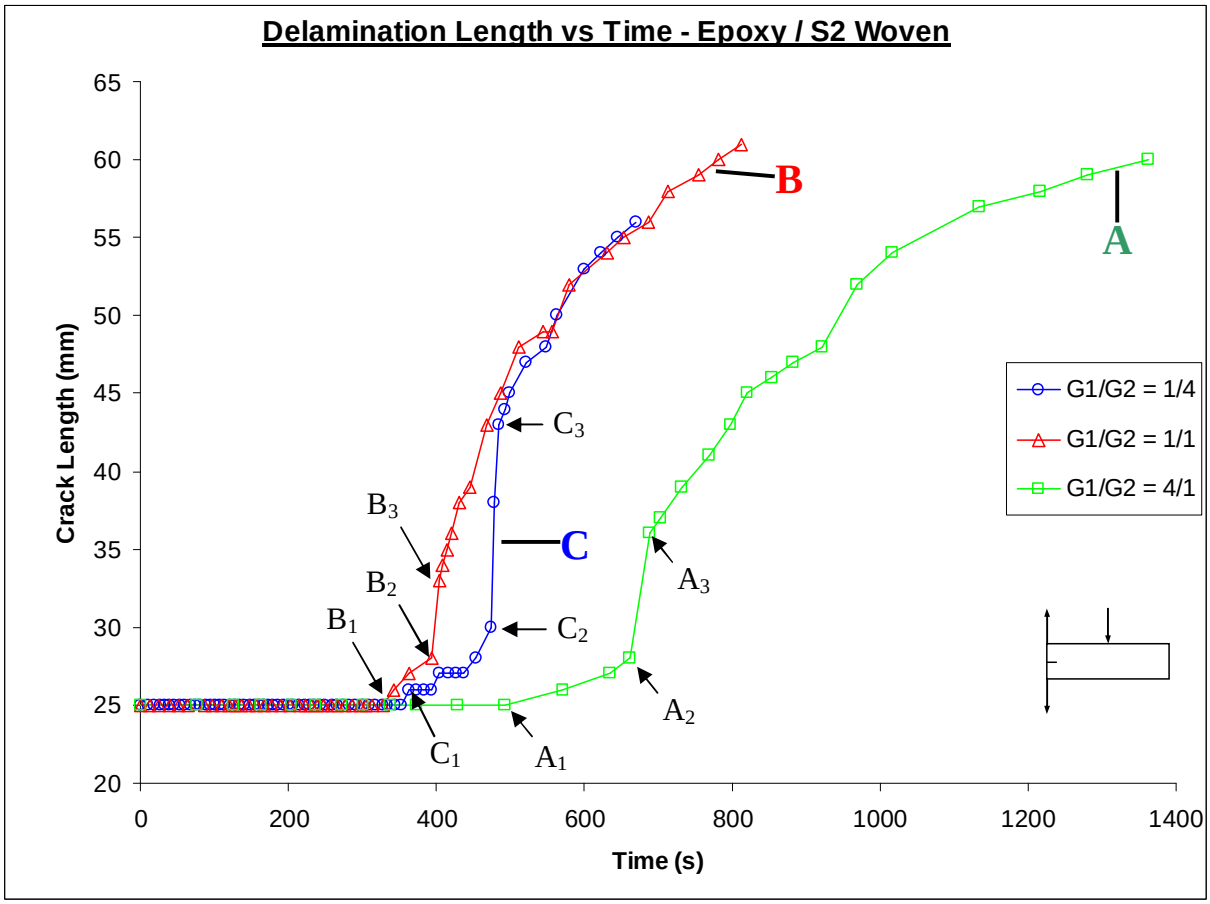

Figure 6.9: Delamination Length versus Time responses for Epoxy / Woven S2 Glass specimens for mode mixtures of G_I/G_{II} = 4/1, 1/1, and ¼.

Figure 6.9 shows the delamination propagation rate for the Epoxy / S2 Woven Glass specimens. As expected the slowest delamination rate recorded was for the mode-mix ratio of G_I/G_{II} = 4 (green). This specimen was Mode I dominant as it had a greater tearing load. This infers that structures subjected to a greater Mode I loading condition will resist delamination initiation for longer periods and delamination growth will be slow. In Curve A (green) delamination initiation occurred at Point A_1 where t = 493 s and the applied load was at its maximum value of 120 N. Delamination propagation was steady with a growth rate of 1.3 mm/min until Point A_2 was

reached. At this point there was a rapid increase in the delamination growth rate to 17.8 mm/min until Point A_3 was reached. This was the area of unstable delamination growth mentioned earlier. Thereafter delamination growth rate decreased to approximately 3.1 mm/min.

Curve B (red) had equal Mode I and Mode II components. Delamination initiation occurred at Point B_1 where t = 328 s. This is 50 % faster than the previous case (G_I/G_{II} = 4). The initial delamination growth rate, from Points B_1 to B_2, was 2.4 mm/min which is 85 % faster than the green curve. From Points B_2 to B_3 the rate increased to 25 mm/min before decreasing to 6.3 mm/min after Point B_3.

Point C_1 denotes the delamination initiation point for Curve C (blue) where the mode-mix ratio was G_I/G_{II} = ¼. This specimen was Mode II dominant and hence had a greater bending load. The delamination growth rate was 2.7 mm/min from Points C_1 to C_2, and this is 107 % and 13 % faster than the green and red curves, respectively. Thereafter the rate increased quite rapidly between Points C_2 and C_3. Here the growth rate was 70.9 mm/min and this supports that the delamination growth was unstable. Once delamination growth stability was attained after Point C_3, the delamination propagation rate decreased to 4.8 mm/min.

From all the responses, the one for the mode-mix ratio of G_I/G_{II} = ¼ (Curve C) was the quickest. This infers that delamination propagation rates are higher in Mode II dominated structures. Specimens for this mode-mix ratio experienced the fastest overall delamination propagation rates. All specimens produced identical delamination growth rates according to their respective mode-mix ratio. However, at approximately 48 mm of delamination growth, all test coupons produced an identical response.

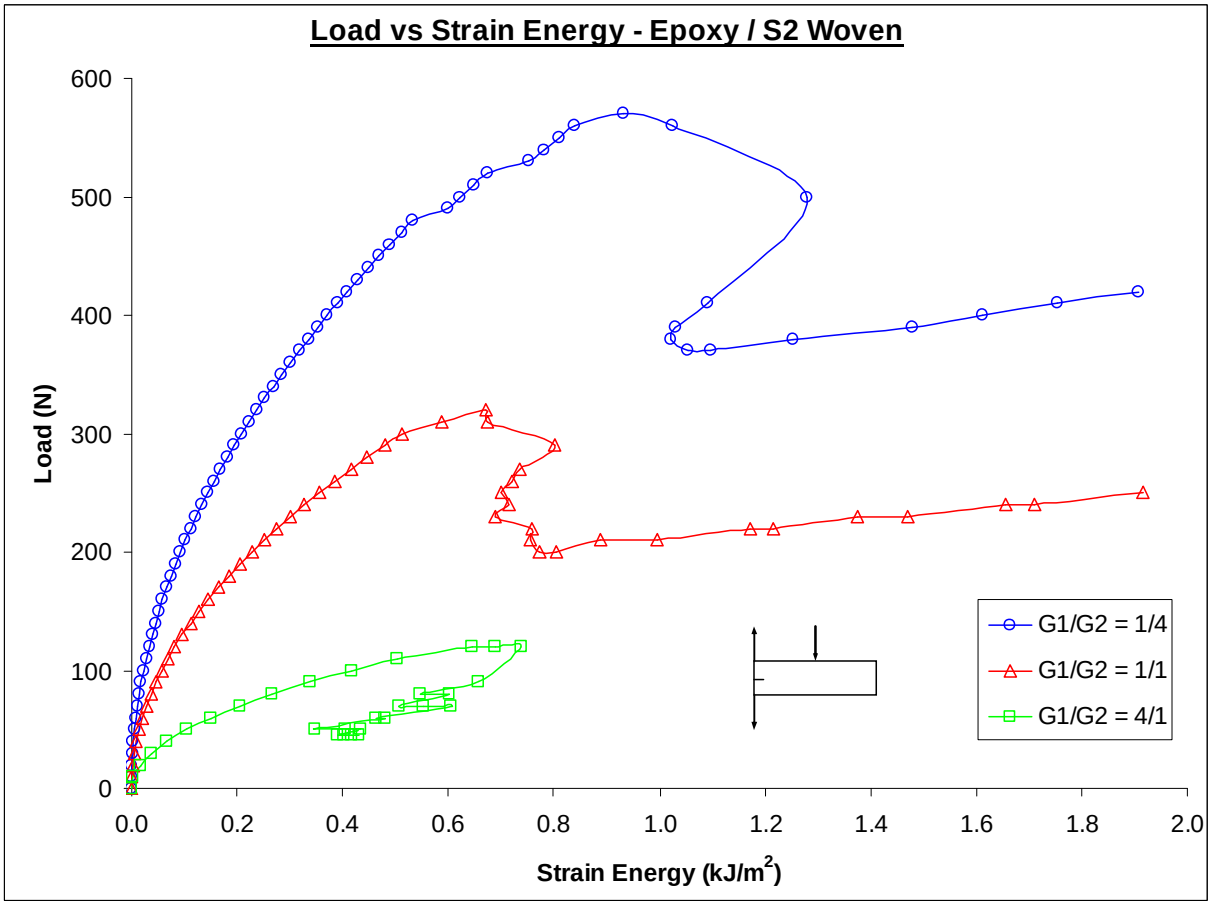

Figure 6.10: Load versus Strain Energy Release Rate responses for Epoxy / Woven S2 Glass specimens for mode mixtures of G_I/G_{II} = 4/1, 1/1, and ¼.

Figure 6.10 is the responses for the Load versus Strain Energy Release Rate for the Epoxy / Woven glass specimens. In the response for the mode-mix ratio of G_I/G_{II} = 4 (green), delamination growth initiated at the maximum applied load of 120 N, and the strain energy release rate assumed its critical value of G_C = 0.644 kJ/m^2 at this point. For the mode-mix ratio of G_I/G_{II} = 1 (red), the maximum applied load required to initiate delamination growth was 320 N and the critical strain energy release rate was G_C = 0.672 kJ/m^2. The third case, where the mode-mix ratio was G_I/G_{II} = ¼ (blue), the strain energy reached its critical value of G_C = 0.674 kJ/m^2 at

an applied load of 520 N. The values of the total critical strain energy release rates for the three cases are almost identical. This was in contrast to results obtained by Benzeggagh et al [109] and Kenane et al [110]. They reported an increase in total critical strain energy release rate with a decrease in mode-mix ratio. However, their work was based on unidirectional glass / epoxy composites. Fibre bridging is prominent with these structures, which in turn influences the strain energy release rate values. In the current study, woven glass fibres were used and no fibre bridging was observed. The delamination path was confined to the fibre – matrix interface. Photographs of the delaminated area are shown in Figure 6.11.

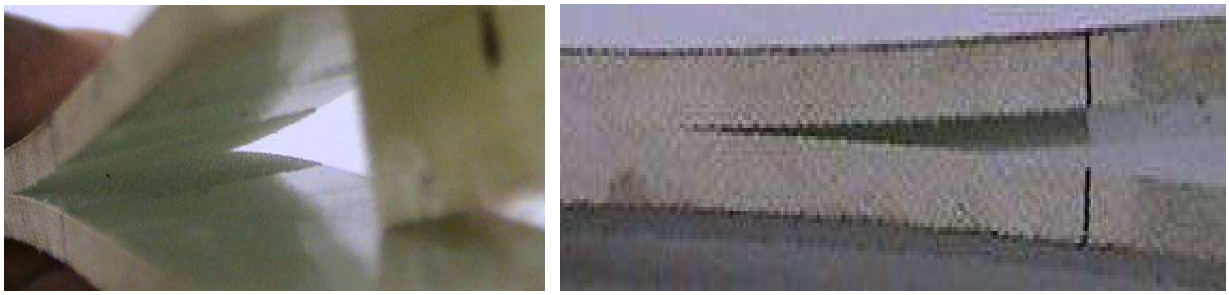

(a) *(b)*

Figure 6.11: Photographs of Epoxy / Woven S2 Glass MMB test coupon showing (a) delamination area, and (b) edge view

Delamination failure occurred at the onset of the maximum applied load and initiated at the implanted defect. The delamination propagated directly through the fibre – matrix interface in the plane of this defect. This can be seen in Figure 6.11a. The applied load was sufficient to overcome the fibre – matrix bond along this interface, but was not great enough to cause fibre breakage. Thus the delamination path did not penetrate through any of the fibre layers. Evidence of this is shown in Figure 6.11b. The structured layout of the woven fibres served to contain the

delamination front, and prohibited any propagation through the thickness of the coupon. As a result, no fibre damage was observed. These observations suggest that the delamination path in woven fibre structures may be predicted.

6.4. FAILURE ENVELOPES

The strain energy release rate values for the woven fibre structure were further analysed and a failure envelope was developed. This envelope is shown in Figure 6.12.

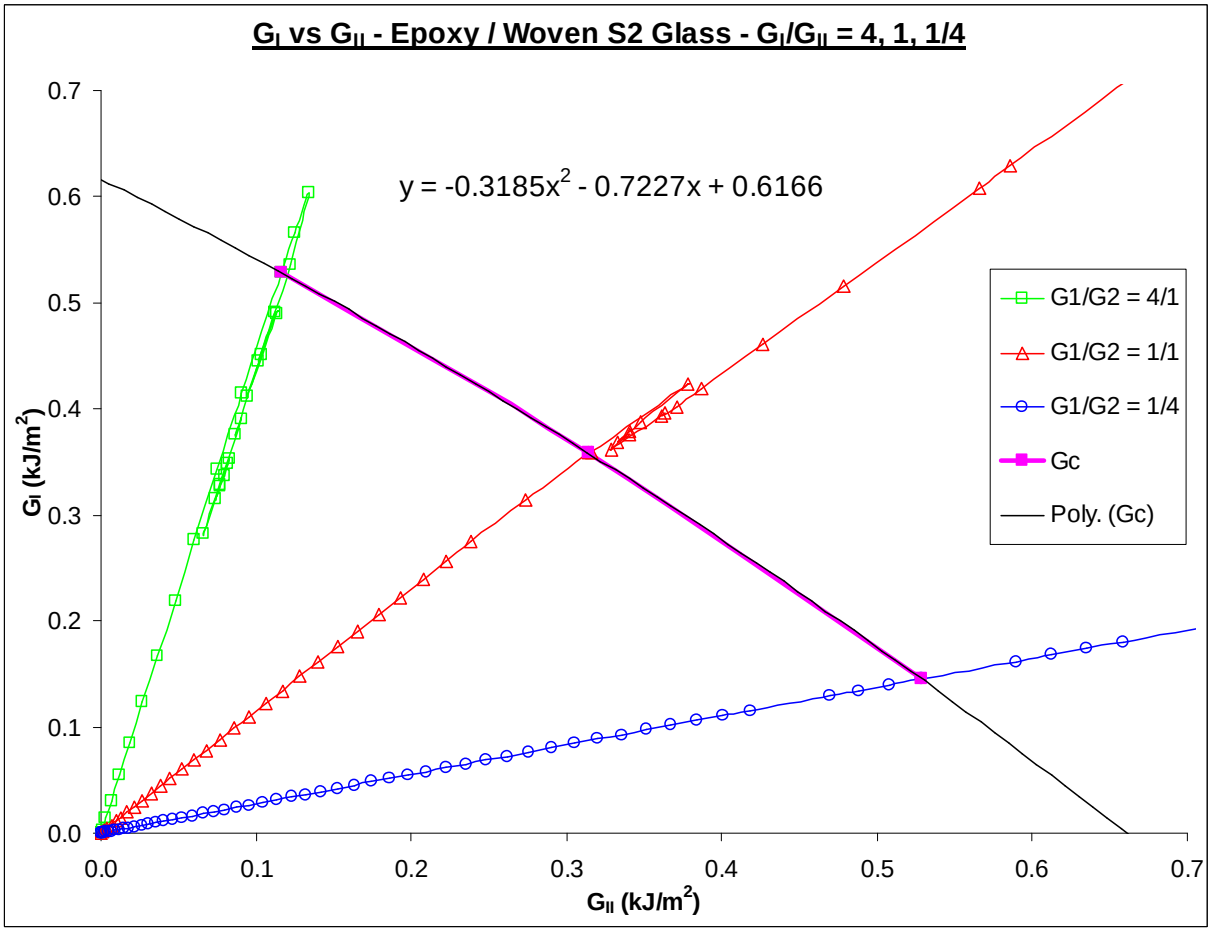

Figure 6.12: Mode I Component versus Mode II Component Epoxy / 24 layers S2 Woven Glass specimens for mode mixtures of G_I/G_{II} = 4/1, 1/1, and ¼

The green, red and blue curves in Figure 6.12 represent the Mode I component versus the Mode II component of the total strain energy release rate of the woven fibre structure. The slope of each response is equal to the mode-mix ratio concerned. For example, the green curve represents the response for the mode-mix ratio of $G_I/G_{II} = 4$, and therefore the slope of this response is equal to 4. The curve with the filled square elements (purple) represents the Mode I and Mode II components of the critical strain energy release rate (G_C) for the mode-mix ratios of $G_I/G_{II} = 4$, 1, and ¼. This curve was extended to the vertical and horizontal axes to create an envelope (black curve). The equation of this curve is:

$$G_I = -0.3185 G_{II}^{\ 2} - 0.7227 G_{II} + 0.6166 \qquad (6.1)$$

Theoretically this means that, for Epoxy / Woven S2 Glass composites, G_C can be determined for any mode-mix ratio. To do this, a straight line with the slope equal to the mode-mix ratio concerned is plotted. The intersection of this line with the envelope will determine the critical strain energy release rate for Mode I (G_{IC}) and Mode II (G_{IIC}). The total critical strain energy release rate (G_C) can be found by using equation (3.4).

This envelope needed to be validated. Therefore additional MMB tests were conducted for mode-mix ratios of $G_I/G_{II} = 2$ and ½. These new ratios were added to the above figure and the result is shown in Figure 6.13. This figure is similar to Figure 6.12. The green, red, blue and purple curves are representative of the aspects discussed earlier. The turquoise (diamond markers) and brown (X markers) curves represent the new mode-mix ratios of 2 and ½ respectively. The orange curve represents the Mode I and Mode II components of the critical strain energy release rate (G_C) for

the mode-mix ratios of G_I/G_{II} = 4, 2, 1, ½ and ¼. According to the theoretical envelope discussed earlier, the orange curve should lie on the purple curve. Clearly this is not so, however, the error between the theoretical values, calculated with equation (6.1), and the actual values are minimal. For the mode-mix ratio of 2, the percentage difference between the theoretical and actual values of G_C is 7.9 %. The percentage difference for the mode-mix ratio of ½ is 9.1 %. These values are within acceptable limits and hence the theoretical envelope is valid.

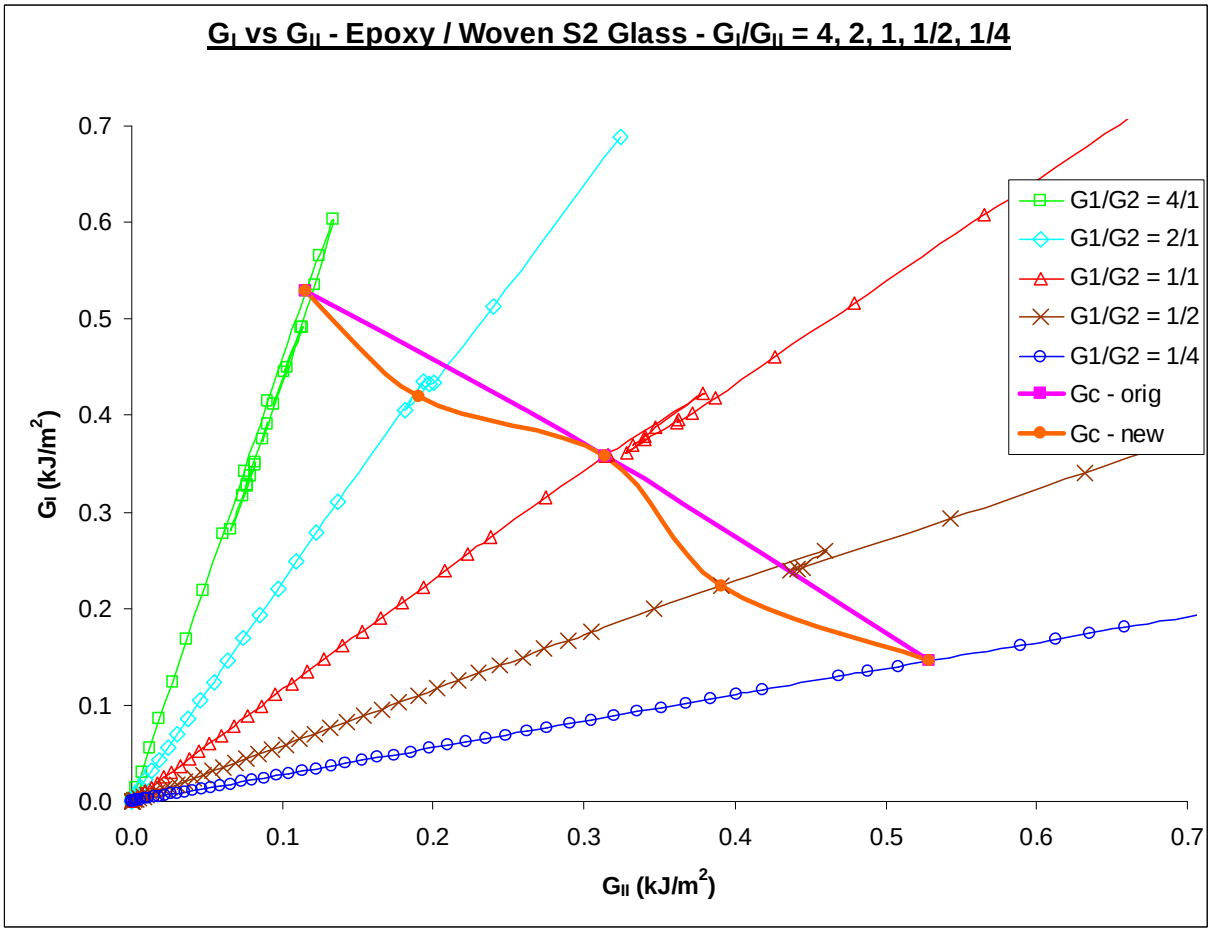

Figure 6.13: *Mode I Component versus Mode II Component Epoxy / 24 layers S2 Woven Glass specimens for mode mixtures of G_I/G_{II} = 4/1, 2/1, 1/1, ½ and ¼*

As stated earlier, in order to use this envelope the mode-mix ratio has to be known. This can be easily determined from equation (3.12) if c and L are known. These two parameters are measurable quantities and can be easily obtained from the application environment. Once the mode-mix ratio is determined, plotted on the envelope, and G_{IC} and G_{IIC} are found, then the critical load may be determined. From equations (3.5) or (3.6), P_I or P_{II} may be found and then using equation (3.7) or equation (3.8), the critical applied load may be found. This is a laborious process as there are many calculations to perform. This process may be simplified by directly plotting the mode-mix ratio versus critical load and this is shown in Figure 6.14.

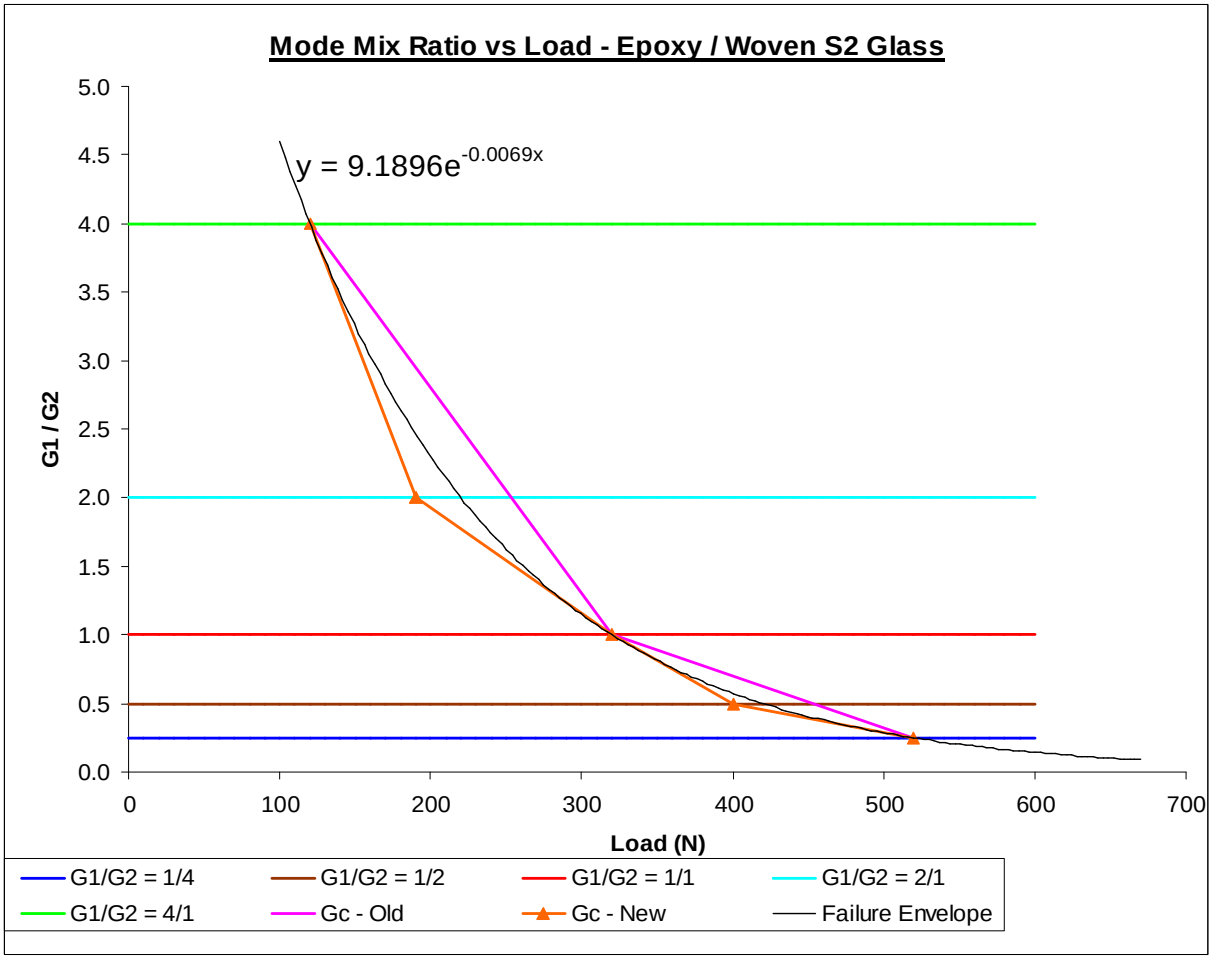

Figure 6.14: Mode-Mix Ratio versus Load for Epoxy / Woven S2 Glass

In the above figure, the different coloured horizontal lines represent the various mode-mix ratios studied. The purple curve is the plot of the critical applied load (P_C) for the original ratios, that is, for G_I/G_{II} = 4, 1 and ¼. The orange curve represents the critical applied load for all mode-mix ratios, that is, G_I/G_{II} = 4, 2, 1, ½ and ¼. The black curve is the failure envelope based on the critical applied load values. This envelope follows an exponential trend and its equation is:

$$\frac{G_I}{G_{II}} = 9.1896\, e^{-0.0069\,P} \tag{6.2}$$

The failure envelope in Figure 6.14 is much simpler to use. First the mode-mix ratio needs to be determined and Equation (3.12) may be used for this. The parameters *c* and *L* may be obtained from the application environment. Thereafter either Figure 6.14 or Equation (6.2) may be used to determine the critical applied load. If the figure is used, then a horizontal line equal to the mode-mix ratio concerned is plotted. The intersection of this line with the failure envelope will ascertain the critical applied load. In an application involving woven fibre / epoxy composites, Figure 6.14 and Equation (6.2) are essential, in that their use greatly reduces the need for time consuming testing and calculations.

6.5. SUMMARY

The woven fibre structure exhibited higher stiffness and thus greater tensile modulus. Its tensile modulus was approximately 147 % greater than the chopped fibre structure. In the SENB test, the woven fibre structure carried twice the load of the chopped fibre specimen and achieved a critical stress intensity factor of 33.81 MPa√m. The crack propagation rate in the woven fibre structure was 184 % less than the chopped fibre case. The woven fibre coupon was able to contain the

crack growth and this resulted in a straight crack path across the width of the coupon. In the MMB test, the load carrying capacity of the woven fibre coupons increased with decreasing mode-mix ratio and this corresponded to an increase in the Mode II loading component. The fastest delamination propagation rate was for G_I/G_{II} = ¼. This growth rate was 107 % faster than that of G_I/G_{II} = 4, and 13 % faster than G_I/G_{II} = 1. The critical strain energy release rate for the woven fibre structure was 0.66 kJ/m^2. The woven fibres contained delamination propagation to the fibre – matrix interface and prevented any growth through the thickness of the coupons. A failure envelope for this composite structure was developed. The critical load for any mode-mix ratio can be determined with the use of this envelope or its governing equation.

7. EXPERIMENTAL RESULTS AND DISCUSSION PART 4:

COMPARISON OF NANO AND FIBRE-REINFORCED STRUCTURES

In this chapter the nano-infused polypropylene, fibre-reinforced polypropylene, and the fibre-reinforced epoxy structures are compared with regard to their tensile properties, stress intensity factors and strain energy release rates. For each of these, the two polypropylene structures are first compared to ascertain the difference the reinforcement makes to the material properties. Thereafter the comparisons between the polypropylene and epoxy structures are made to determine which matrix material exhibits superior properties.

7.1. COMPARISON OF TENSILE PROPERTIES

The Stress – Strain responses obtained for the nano-infused polypropylene structures (Figure 4.2) are compared to that of the fibre-reinforced polypropylene structures (Figure 5.1). This comparison is shown in Figure 7.1. Although the fibre-reinforced structures show improvement over the virgin polypropylene, they performed poorly when compared to the nano-infused specimens. The 0.5, 1, 2 and 3 weight % nanocomposites show responses with higher gradients than the conventional structures. This indicates greater stiffness and hence higher elastic modulus. In the study conducted by Wu et al [94], they determined that nano-infused polyamide-6 performed better than fibre-reinforced polyamide-6. Considering these results, nano-infused polypropylene may be preferred over fibre-reinforced polypropylene in applications where higher tensile loadings are present.

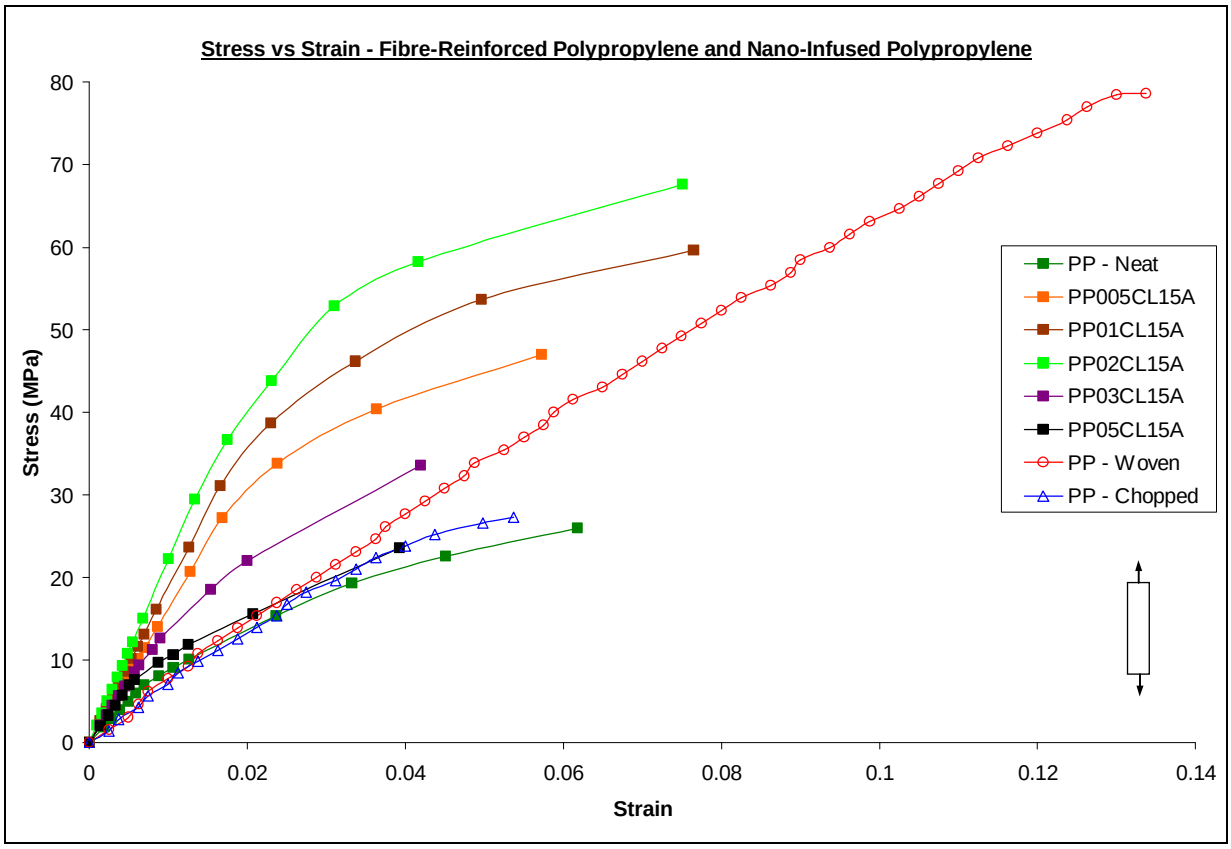

Figure 7.1: Stress versus Strain plots of nano-infused and fibre-reinforced polypropylene

In Figure 7.1, it can be seen that the 2 weight % nano-infused polypropylene exhibits the best improvement in tensile properties from all the nanocomposites. With the fibre-reinforced structures, the woven fibre specimen demonstrated superior properties to the chopped fibre case. Hence the 2 weight % nanocomposite and the woven fibre-reinforced structure were compared to the fibre-reinforced epoxy specimens.

The curves shown in Figure 7.2 represent the tensile responses of Epoxy / Chopped S2 Glass, Epoxy / Woven S2 Glass, Polypropylene / Woven S2 Glass, Polypropylene / 2 % Cloisite 15A, and virgin Polypropylene. The elastic modulus of all specimens was determined as described in

Chapter 3. The woven fibre / epoxy specimen shows superior properties to all other composite types with regard to stiffness (slope) and hence tensile modulus. It achieved a modulus of 15.76 GPa compared to 6.39 GPa for the chopped fibre / epoxy specimen, 2.9 GPa for the 2 weight % nanocomposite and 0.71 GPa for the woven fibre / polypropylene specimen. Although these materials exhibit lower modulii and load carrying capabilities than the woven fibre / epoxy specimen, they did carry more strain. This suggests that the material is becoming more ductile.

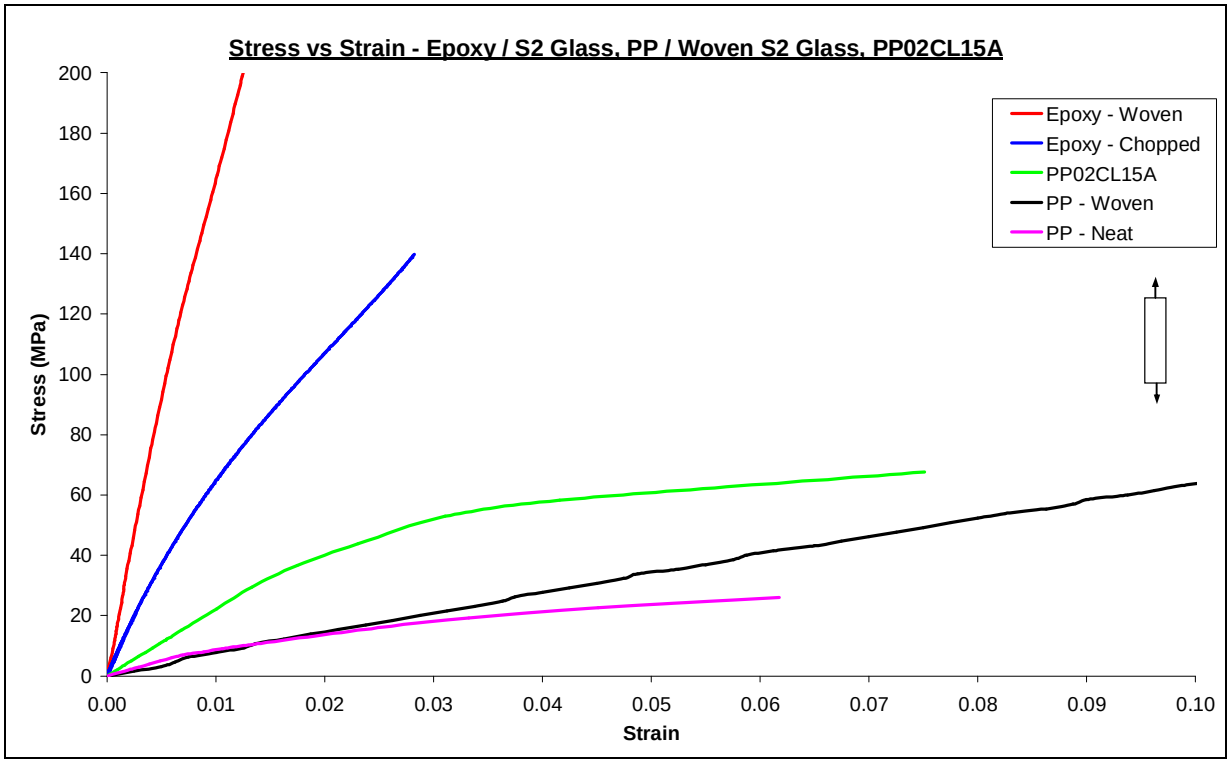

Figure 7.2: Tensile response of Epoxy / Chopped S2 Glass, Epoxy / Woven S2 Glass, PP / Woven S2 Glass, PP / 5 % Cloisite 15A, and virgin PP

The woven fibre / epoxy specimen carried the lowest strain and highest load. Therefore it exhibited the highest stiffness or rigidity. In contrast the woven fibre /polypropylene coupon carried the highest strain and lowest load. This infers that it was the most ductile of all composite

structures tested. The nanocomposite specimen showed both rigid and ductile properties. Initially the specimen showed stiffness properties, and thereafter, at approximately 30 MPa, it deviated from this stiffness response showing an increase in ductility.

7.2. COMPARISON OF STRESS INTENSITY FACTORS

From the nanocomposite structures, the 5 weight % specimen exhibited the most improvement in load carrying capability and hence stress intensity factor. In Figure 7.3, this specimen is compared to the woven fibre / polypropylene structure which showed superior crack containment properties to the chopped fibre case.

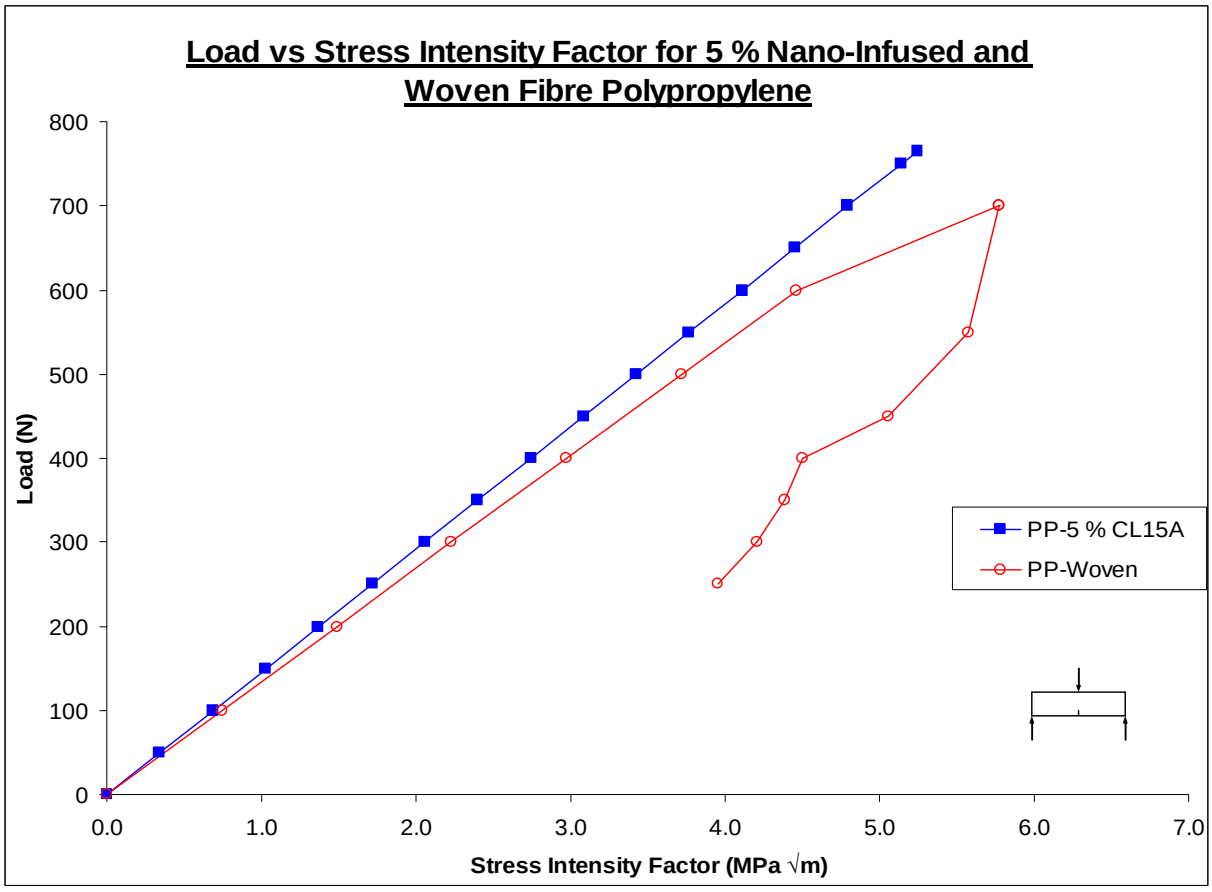

Figure 7.3: Comparison of Load versus Stress Intensity Factor for 5 % nano-infused and woven fibre-reinforced polypropylene

The most noticeable feature in Figure 7.3 is the return path demonstrated by the fibre-reinforced structure. The nano-infused specimens failed catastrophically upon reaching maximum load and hence did not have the return path. This suggests that although the nano specimens were able to resist crack initiation, they were not able to contain rapid crack growth once initiation occurred, and this resulted in the abrupt response. The fibre-reinforced structure, on the other hand, did not experience such failure. The woven fibre was able to contain the crack growth and also slow down the crack propagation rate.

Although the nano-infused polypropylene showed poor crack containment, the 5 weight % specimen exhibited higher load carrying capabilities than the woven fibre structure. This nanocomposite had a critical stress intensity factor of 5.24 MPa√m, and was 10 % less than the woven fibre case which had a critical stress intensity factor of 5.78 MPa√m. This suggests that the 5 weight % nanocomposite has a similar ability to resist crack initiation as a woven fibre structure with 6 times the reinforcement weight. This characteristic should be considered more important, because a material with a high resistance to crack initiation can sustain higher loads. Such a material may be used in applications where high tensile loading conditions are prominent.

Comparison of the nano-infused polypropylene and fibre-reinforced epoxy structures, reveal that the stress intensity factor for Epoxy / Chopped S2 Glass was approximately 4 times larger than the nanocomposite. The stress intensity factor for Epoxy / Woven S2 Glass was approximately 6.5 times larger. Similar values were obtained when comparing the fibre-reinforced polypropylene and epoxy structures. The PP structures are inferior to the epoxy structures and hence a detailed comparison is unnecessary.

7.3. COMPARISON OF STRAIN ENERGY RELEASE RATES

A comparison of the strain energy release rates for the fibre-reinforced and nano-infused polypropylene structures is possible. The nanocomposite was tested under Mode I conditions in a three point bend fixture. Therefore it should be compared with the Mode I component of the strain energy release rate for the woven fibre structure. However, the mode-mix ratio for the woven fibre specimen was 4, which corresponds to a greater tearing load than bending load. Hence a comparison would not be valid as the bending load conditions in both cases are dissimilar.

However the nano-infused polypropylene can be compared to the woven fibre-reinforced epoxy. One of the mode-mix ratios that the woven fibre / epoxy structure was subjected to is $G_I/G_{II} = ¼$. For this mixed mode ratio the bending load is greater than the tearing load. Hence, the Mode I component of the strain energy release rate for the woven fibre structure is compared to the 5 weight % nanocomposite structure. The strain energy release rate for the nanocomposite was determined using equation (3.3). This comparison is shown in Figure 7.4.

As thermoset composites are generally higher in strength than thermoplastics, it was expected that the strain energy release rate for the fibre-reinforced epoxy structure would be greater than that of the nano-infused structure. However this was not the case. In Figure 7.4, it is seen that the nano-infused polypropylene has a greater strain energy release rate and a greater load carrying capacity than the woven fibre / epoxy structure. The nanocomposite achieved a critical strain energy release rate of 9.8 kJ/m^2 at a maximum load of 765 N. The critical strain energy release rate for the epoxy structure was 0.67 kJ/m^2 at a load of 520 N. This is a remarkable improvement on the part of the nanocomposite, in that it has superior properties to a material with 13 times the

reinforcement weight. Hence it was decided to manufacture a fibre-reinforced nano-infused hybrid composite and compare it to the conventional structure.

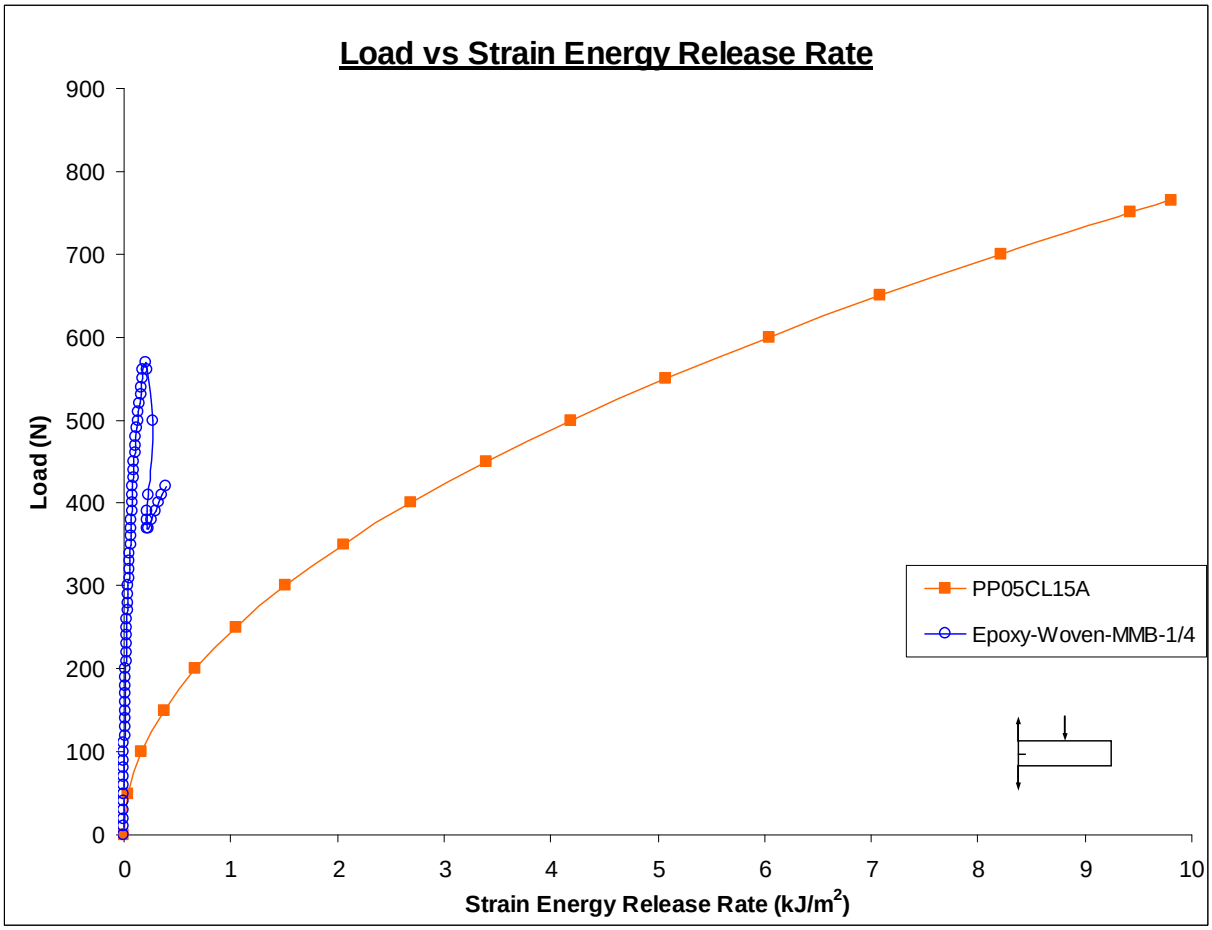

Figure 7.4: Load versus Strain Energy Release Rate for Epoxy / Woven S2 Glass and Polypropylene / 5 % Cloisite 15A

7.4. SUMMARY

The fibre-reinforced polypropylene showed poor tensile properties compared to the nanocomposites. The 2 weight % specimen exhibited the most improvement in tensile modulus. The woven fibre-reinforced epoxy structure had the highest stiffness compared to all composite

types tested. The fibre-reinforced polypropylene specimen exhibited the most ductile properties. The 5 weight % PP nanocomposite showed good crack resistant properties in that its critical stress intensity factor was 10 % less than that of the fibre-reinforced PP structure. The thermoset structures exhibited at least 4 times the critical stress intensity factor of the polypropylene structures. The 5 weight % nanocomposite achieved a higher critical strain energy release rate than the woven fibre-reinforced epoxy structure.

8. EXPERIMENTAL RESULTS AND DISCUSSION PART 5: FIBRE-REINFORCED NANO-INFUSED THERMOSET COMPOSITE (HYBRID)

This hybrid structure consisted of 24 layers of Woven S2 Glass as the fibre reinforcement embedded in an epoxy nanocomposite matrix. Cloisite 30B clay was the reinforcement in the nanocomposite. Specimens from this composite were subjected to tensile and MMB tests, as described in Chapter 3, and are directly compared to the conventional fibre-reinforced structure.

8.1. TENSILE TEST

Three specimens from the hybrid structure were tested at a cross-head speed of 1 mm / min. The length, width and thickness of the specimens were 200 mm, 13 mm and 7.5 mm, respectively. The tensile response for the hybrid fibre-reinforced composite is compared to that of the conventional fibre-reinforced structure in Figure 8.1.

In Figure 8.1, the Cloisite 30B / Epoxy / Woven S2 Glass exhibits superior tensile properties to the Epoxy / Woven S2 Glass. The elastic modulus was averaged over the three specimens and a value of 20.07 GPa was obtained. This was 27 % more than the conventional structure which has a modulus of 15.76 GPa. This improvement in properties was due to the inclusion of nanoclays into the hybrid structure.

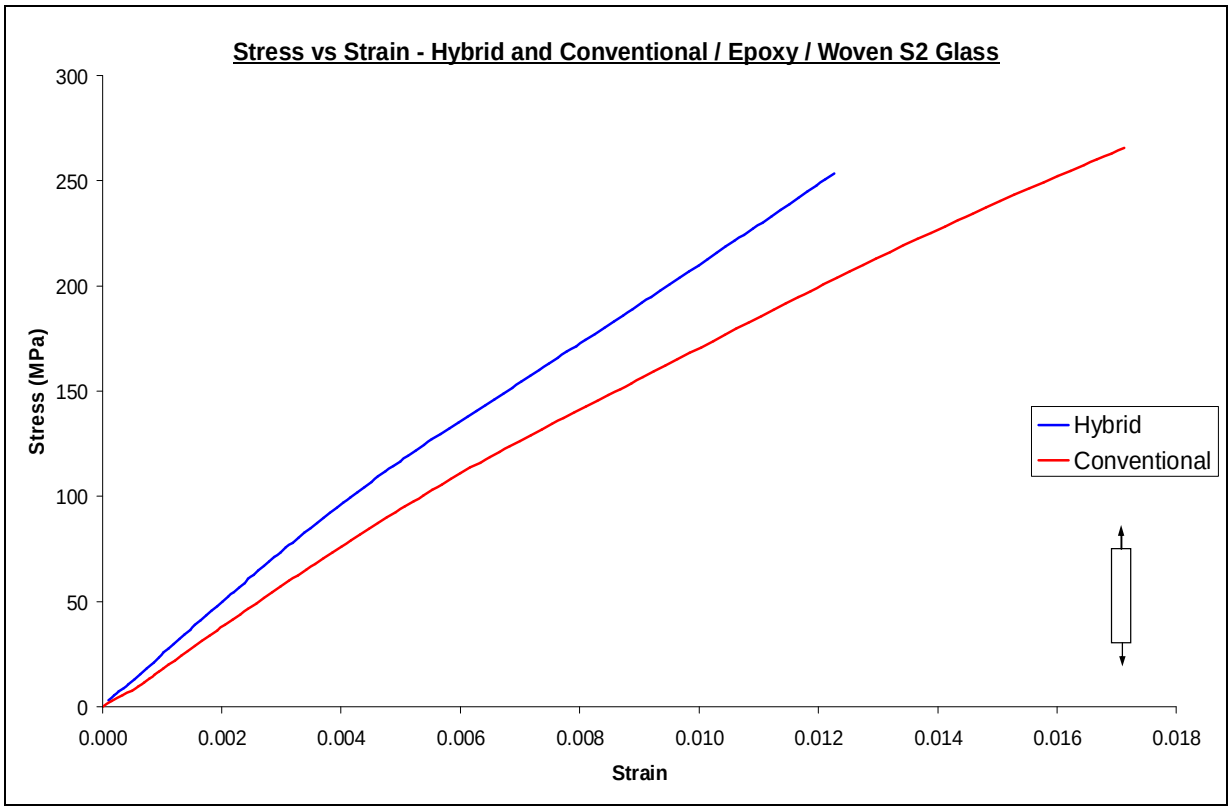

Figure 8.1: Stress versus Strain for hybrid and conventional woven fibre-reinforced epoxy composites

8.2. MIXED MODE BENDING (MMB) TEST

Specimens from the Cloisite 30B / Epoxy / Woven S2 Glass panel were subjected to the same mode-mix ratios as in the case of the conventional fibre-reinforced epoxy structure. Three specimens each were tested under the mode-mix ratios of G_I/G_{II} = 4, 1 and ¼ at a cross-head speed of 1 mm / min. Each specimen had an overall length of 200 mm, a width of 25 mm and an overall thickness of 7.5 mm, with an initial delamination length of 25 mm. Direct comparisons were made to the conventional fibre-reinforced structure. To minimise confusion, the responses for the conventional structure were plotted using the same colours and markers as before. These were blue with unfilled circle markers for G_I/G_{II} = ¼, red with unfilled triangle markers for G_I/G_{II}

= 1, and green with unfilled square markers for G_I/G_{II} = 4. The responses for the hybrid structures are plotted in similar colours but with filled markers. For example, the response for the mode-mix ration of 4 would be plotted in a shade of green but with filled square markers instead.

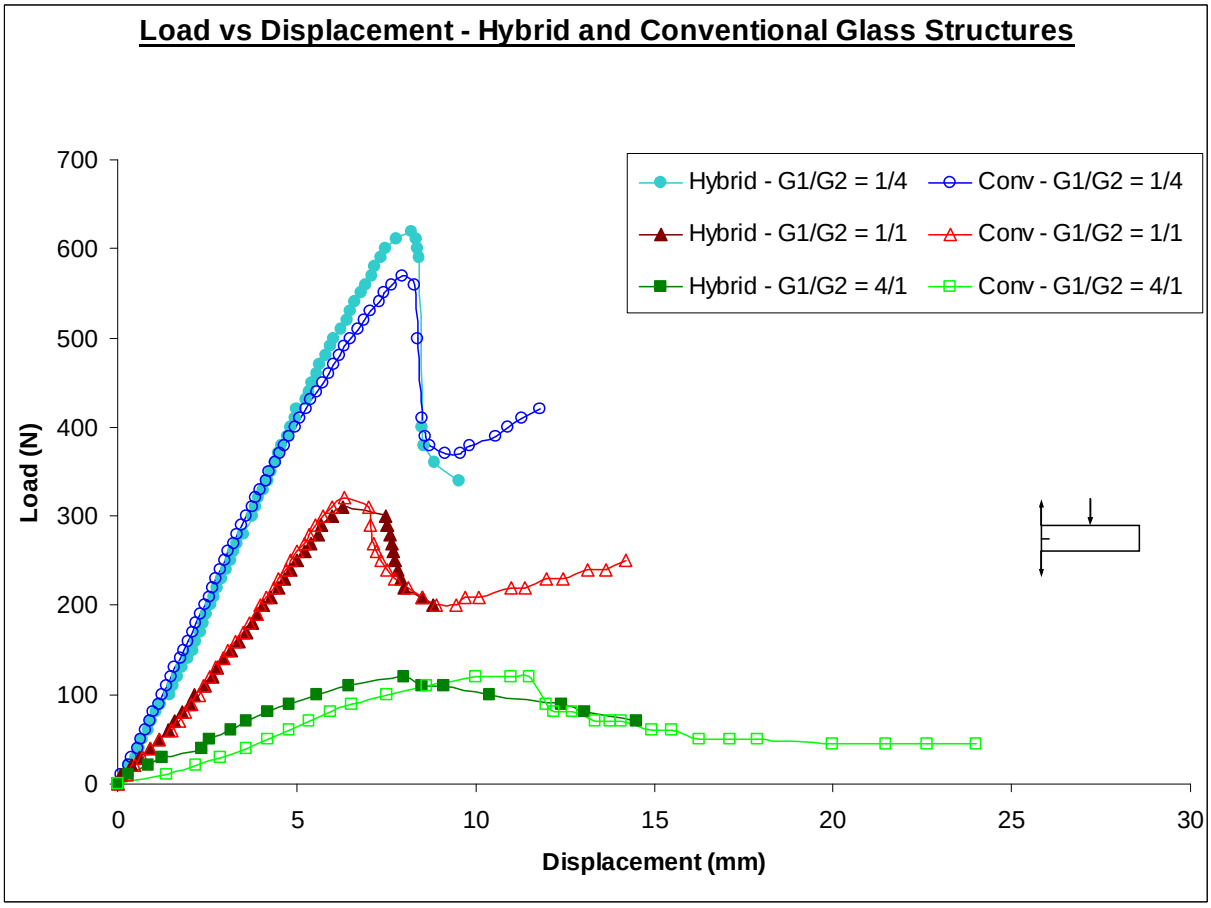

Figure 8.2: Load versus Displacement responses for mode-mix ratios of G_I/G_{II} = 4/1, 1/1, and ¼ of Epoxy / Woven S2 Glass and Cloisite 30B / Epoxy / Woven S2 Glass

In Figure 8.2, the Load – Displacement responses of the hybrid structure is compared to that of the conventional structure. The hybrid structure was expected to be superior to the conventional structure. However this was not the case. There appears to be only subtle differences. The

maximum load carrying capacity of the hybrid and conventional structures are similar for the mode-mix ratios of G_I/G_{II} = 1 and 4. In the case of the mode-mix ratio of ¼, the hybrid specimen showed a 9 % improvement in load carrying capability. This, however, is not a significant improvement. Similar features were noted in the comparison of the strain energy release rates.

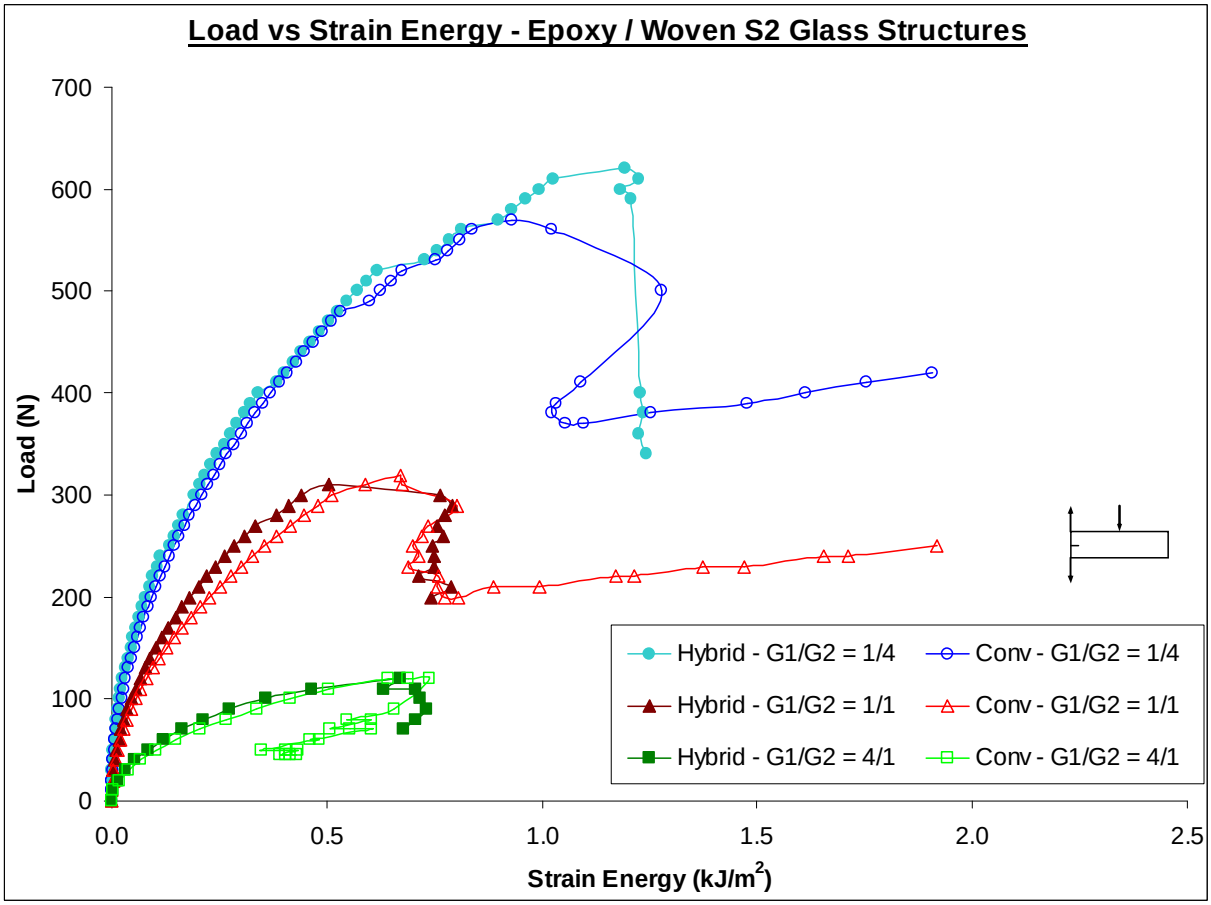

Figure 8.3: Load versus Strain Energy Release Rate for mode-mix ratios of G_I/G_{II} = 4/1, 1/1, and ¼ of Epoxy / Woven S2 Glass and Cloisite 30B / Epoxy / Woven S2 Glass

Figure 8.3 shows the comparison of the strain energy release rates of the hybrid and conventional fibre-reinforced structures. The responses appear identical and the critical strain energy release

rates were also identical. This poor performance in both load carrying capability and strain energy release rate of the hybrid structure was also experienced by Wichmann et al [96]. They conducted a study on glass fibre-reinforced structures with nanoparticle modified epoxy matrix. Their findings showed an increase in interlaminar shear strength but no significant increase in the interlaminar toughness values. They concluded that a significant increase in the fracture toughness of neat nanoparticle modified matrix could not be transferred to the FRP in a comparable manner.

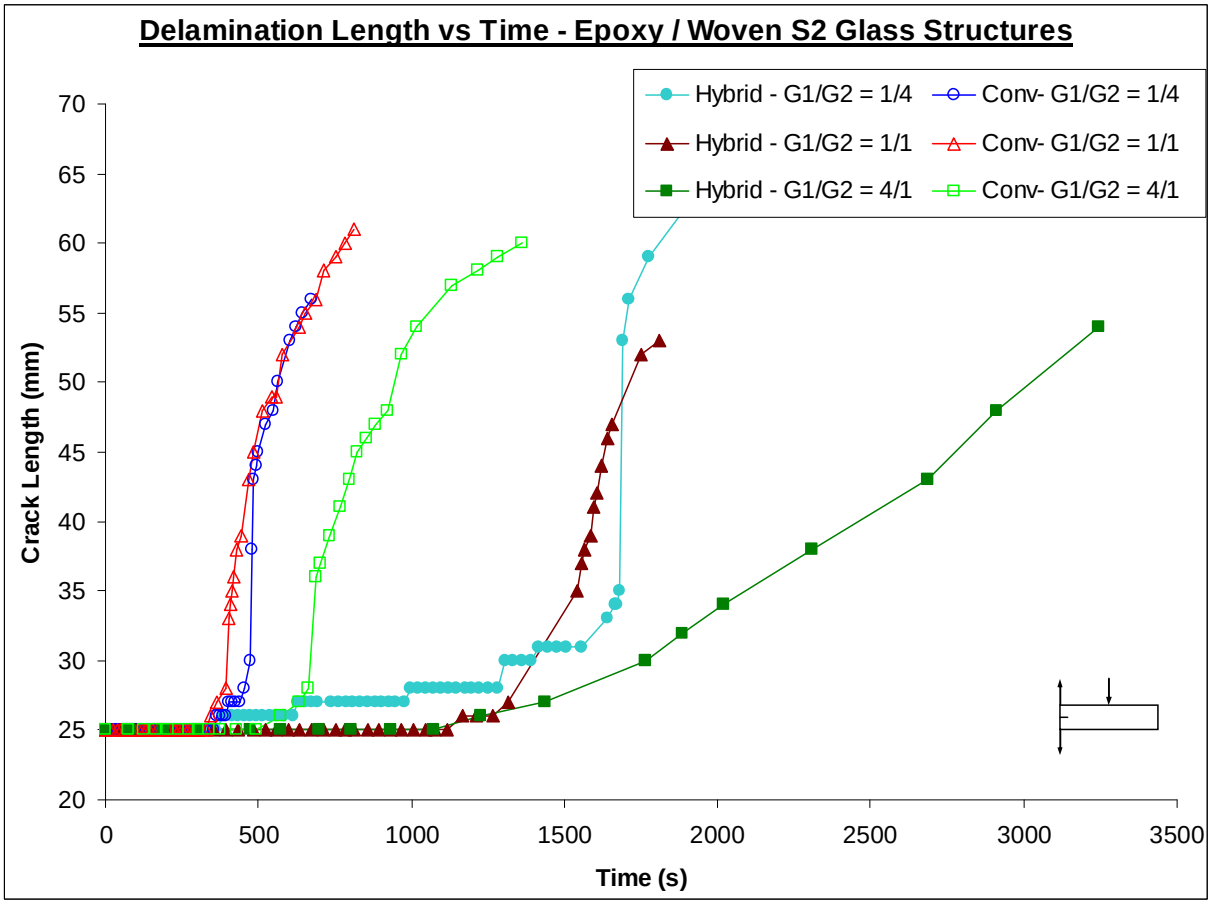

Figure 8.4: Delamination Length versus Time for mode-mix ratios of G_I/G_{II} = 4/1, 1/1, and ¼ of Epoxy / Woven S2 Glass and Cloisite 30B / Epoxy / Woven S2 Glass

In Figure 8.4, the delamination growth rates for the hybrid structure under the various mode-mix ratios are compared to that of the conventional composite. The hybrid specimens managed to slow down the delamination propagation rates. For the mode-mix ratios of 4, 1 and ¼, the delamination propagation rates were 1.2, 3.6 and 6.6 mm/min, respectively. The values obtained for the conventional structure were 17.8, 25, 70.9 mm/min for the mode-mix ratios of 4, 1 and ¼, respectively. In an application the hybrid structure would be preferred because it is more durable, in that it can resist delamination failure for a longer time.

8.3. SUMMARY

The hybrid structure had a 27 % increase in tensile modulus compared to the conventional case. This increase was attributed to the inclusion of nanoclays. Under MMB conditions, the hybrid structure exhibited similar load carrying capabilities and critical stress intensity factor as the conventional case. However, the hybrid composite was able to resist delamination initiation for a longer period. It also exhibited lower delamination propagation rates.

9. CONCLUSION

Two different material systems are considered in this study. The first system used a thermoplastic (polypropylene) matrix and the second used an epoxy matrix. The reinforcements used were chopped and woven S2 Glass, and, Cloisite 15A and Cloisite 30B nanoclays. Accordingly, the conclusions are set out as follows:

- Nano-infused Polypropylene structure
- Fibre-reinforced Polypropylene structure
- Fibre-reinforced Epoxy structure
- Comparison of nano and fibre-reinforced structures
- Hybrid Epoxy structure

The first composite analysed was the polypropylene nanocomposite with Cloisite 15A nanoclay reinforcement. Several structures were manufactured with clay loadings of 0.5, 1, 2, 3 and 5 weight %. These structures were tested under Mode I conditions using the SENB test. The specimen with the 5 weight % Cloisite 15A exhibited 161 % improvement in critical stress intensity factor (K_{IC}) over virgin polypropylene. This means that the load bearing capacity of this specimen had also increased. XRD and TEM analyses showed there was an increase in intercalated and agglomerated morphologies. The improvement in K_{IC} values may be attributed to the changing morphologies.

The second composite analysed was fibre-reinforced polypropylene. Two types of this composite structure were investigated; one used chopped fibre-reinforcement and the other used woven

fibre-reinforcement. It was found that the woven fibre structure had the following properties compared to the chopped fibre case.

- It had a greater load carrying capability and carried 100 % more load.
- It exhibited lower stress intensity factors due to localised compression failure by the test fixture.
- It exhibited superior crack containment properties. The crack propagation rate was reduced by 275 %.
- It achieved a critical strain energy release rate (G_C) of 3.47 kJ/m^2 at a maximum load of 70 N.
- The delamination propagation rate was 1.5 mm/min. This suggests that delamination growth propagates slower under Mode I dominant conditions.

The next two structures examined consisted of epoxy reinforced with chopped fibres and epoxy reinforced with woven fibres. The woven fibre structure had the following properties compared to the chopped fibre case.

- A 147 % greater tensile modulus.
- It carried twice the load under SENB conditions.
- The critical stress intensity factor (K_{IC}) was 63 % greater.
- It exhibited superior crack containment properties and reduced the crack propagation rate by 184 %. This suggests that such a structure is more durable, in that it can resist failure for a longer period of time.
- Under MMB conditions, load carrying capability for the specimens increased as the mode-mix ratio decreased. This corresponded to an increase in the Mode II component.

- Mode-mix ratio of ¼ showed the highest delamination growth rate. The delamination propagation rate is faster in Mode II dominant applications.
- The delamination growth rate for the mode-mix ratio of ¼ was 107 % faster than the ratio of 4 and 13 % faster than the ratio of 1.
- The critical strain energy release rate (G_C) achieved was 0.66 kJ/m^2.
- The delamination path was through fibre–matrix interface with no penetration of fibre layers.
- A failure envelope was developed that may be used to determine the critical applied load for any mode-mix ratio.

The nano-infused polypropylene and the fibre-reinforced polypropylene and epoxy structures were compared with regards to their tensile properties, stress intensity factors and strain energy release rates. The woven fibre-reinforced epoxy structure had the highest stiffness and thus the highest tensile modulus of all composite types tested. In comparison of the stress intensity factors, the 5 weight % nanocomposite exhibited a greater load bearing capacity than the woven fibre-reinforced polypropylene structure. The stress intensity factor of the nanocomposite was 10 % less than the woven fibre structure which had 3 times the reinforcement weight. This implies that the nanocomposite has good crack resistance. This is important because a material with a high resistance to crack initiation can sustain higher loads. The fibre-reinforced thermoset structures exhibited critical stress intensity factors that were at least 4 times greater than both the polypropylene structures. With regards to strain energy release rates, the nanocomposite was superior to the woven fibre-reinforced epoxy composite, which had 10 times the reinforcement weight.

The last composite manufactured in this study was a hybrid structure. It consisted of Woven S2 Glass fibre reinforcement in an epoxy nanocomposite matrix. The epoxy was infused with Cloisite 30B nanoclay. This structure was compared to the conventional woven fibre / epoxy composite for both tensile and MMB cases. The hybrid structure exhibited a 27 % improvement in tensile modulus compared to the conventional structure. This significant increase was due to the inclusion of the nanoclays. There was no significant increase in the load carrying capability or the strain energy release rate of the hybrid structure (MMB tests). The responses appeared identical to that of the conventional composite structure. However, the hybrid specimens were able to resist delamination initiation for a longer period. They also exhibited lower delamination propagation rates. In many applications the hybrid structure would be preferred because it is more durable and can resist delamination failure for a longer time.

Future work involves the development of failure envelopes for other material systems including nano-infused structures.

10. REFERENCES

1. Goodrich, “Why Composites?”, http://www.epp.goodrich.com/why.shtml

2. Wikipedia, “Composite Material”, *Wikipedia, the free encyclopaedia*, December 2006, http://en.wikipedia.org/wiki/Composite_material

3. Cooperative Research Centre for Advanced Composite Structures Ltd, “Putting it together – the science and technology of composite materials”, *NOVA Science in the News*, November 2000, http://www.science.org.au/nova/059/059key.htm

4. Quilter, A., “Composites in Aerospace Applications”, *ESDU International*, http://engineers.ihs.com/NR/rdonlyres/AEF9A38E-56C3-4264-980C-D8D6980A4C84/0/444.pdf

5. Crane Composites, “FRP encyclopaedia”, http://www.kemlite.com/frp_encyclopedia.cfm#top

6. Wikipedia, “Fibre-reinforced plastic”, *Wikipedia, the free encyclopaedia*, http://en.wikipedia.org/wiki/Fibre-reinforced_plastic

7. Chung. Natalie Y.L., “Fibre Reinforced Polymer (FRP) Composites”, http://gnatchung.tripod.com/FRP/

8. Mair, R.I., “Fibre Reinforced Polymers - From Aerospace to Infrastructure”, ATSE Focus No 107, May/June 1999, http://www.atse.org.au/index.php?sectionid=409

9. Structural Preservation Systems, “Fibre Reinforced Polymer (FRP) Composites”, http://www.structural.net/strengthening/frp.html

10. Wikipedia, “Airbus A320”, *Wikipedia, the free encyclopaedia*, http://en.wikipedia.org/wiki/Airbus_A320

11. Aerospace Technology, “Airbus A320 Single Aisle Medium Range Airliner, Europe”, http://www.aerospace-technology.com/projects/a320/

12. Goodrich, “Aerospace Composite Products”, http://www.deicingsystems.goodrich.com/products_acp.shtml

13. Wikipedia, “Space Shuttle Thermal Protection System”, *Answers.com*, http://www.answers.com/topic/space-shuttle-thermal-protection-system

14. Miesel, G., “Composites 2004 – The Sky’s the Limit”, *Automotive Composites Alliance*, http://www.autocomposites.org/autocomposites/pdfs/skys_the_limit_2004.pdf

15. About: Composites / Plastics, “Brunswick and TPI Display Composite Bus”, http://composite.about.com/library/PR/1999/blbrunswick5.htm

16. Nanni, A., "International Research on Advanced Composites in Construction (IRACC-96)", *Final Report to US National Science Foundation*, August 1996

17. Black, S., “How Are Composite Bridges Performing?”, *Composites Technology*, December 2003, http://www.compositesworld.com/ct/issues/2003/December/325

18. El-Salakawy, E., Kassem, C., and Benmokrane, B., “Field Application of FRP Composite Bars as Reinforcement for Bridge Decks”, *4th Structural Specialty Conference of the Canadian Society for Civil Engineering*, Montreal, Canada, June 2002, http://www.pultrall.com/pdf/PaperWottonBridge.pdf

19. Griffiths, J.R., “Plastic Highway Bridges”, *CSA*, November 2000, http://www.csa.com/discoveryguides/bridge/overview.php

20. "Composites seismic retrofit of the Arroyo Seco bridge completed successfully", *Advanced Materials & Composites News*, May 2000, 22, 9, pp 1-3

21. BRE and Trend 2000 Ltd, "Composite Swimming Pools", *Polymer Composites as Construction Materials*, http://projects.bre.co.uk/composites/pdf/AP19_Swimming%20Pools.pdf

22. Royal Plastic MFG. Inc., "Advanced Composite Products", http://www.rpm-composites.com/index_7_Products.htm

23. Fiberglass Grating Manufacturers Council, "Why specify FRP?", *American Composites Manufacturers Association*, http://www.acmanet.org/fgmc/why_specify.htm

24. Wikipedia, "Thermosetting Plastic", *Wikipedia, the free encyclopaedia*, http://en.wikipedia.org/wiki/Thermoset

25. Materials Information Service, "Thermosetting Composites – Fibres and Matrices", *Azom.com: The A to Z of Materials*, http://www.azom.com/details.asp?ArticleID=401

26. Wikipedia, "Epoxy", *Wikipedia, the free encyclopaedia*, http://en.wikipedia.org/wiki/Epoxy

27. "Epoxy Resins", http://sunilbhangale.tripod.com/epoxy.html

28. Wikipedia, "Thermoplastic", *Wikipedia, the free encyclopaedia*, http://en.wikipedia.org/wiki/Thermoplastic

29. Francis, M.M., Jr., "Polypropylene and TPO Nanocomposites", *Dekker Encyclopaedia of Nanoscience and Nanotechnology*, April 2004, 5**,** pp. 3015-3038

30. Wikipedia, “Polypropylene”, *Wikipedia, the free encyclopaedia*, http://en.wikipedia.org/wiki/Polypropylene

31. Schuh, T.G., “Renewable Materials for Automotive Applications”, *Daimler-Chrysler AG, Stuttgart*, http://www.ienica.net/fibresseminar/schuh.pdf

32. Wikipedia, “Synthetic Fiber”, *Wikipedia, the free encyclopaedia*, http://en.wikipedia.org/wiki/Synthetic_fiber

33. Warshall, P., “Inventory of Synthetic Fibers”, *Whole Earth*, 1997, 90, http://www.wholeearthmag.com/ArticleBin/113.html

34. “Composite Materials”, http://tx.technion.ac.il/~plastcom/Composite%20materials.doc

35. Wikipedia, “Carbon Fiber”, *Wikipedia, the free encyclopaedia*, http://en.wikipedia.org/wiki/Carbon_fiber

36. Wikipedia, “Aramid”, *Wikipedia, the free encyclopaedia*, http://en.wikipedia.org/wiki/Aramid

37. Wikipedia, “Fiberglass”, *Wikipedia, the free encyclopaedia*, http://en.wikipedia.org/wiki/Glass_fiber

38. Gupta, V.B., and Kothari, V.K., “Manufactured Fibre Technology”, *London: Chapman and Hall*, 1997, 544-546, ISBN 0-412-54030-4

39. Pinnavaia, T.J., and Beall, G.W., “Polymer-Clay Nanocomposites”, *John Wiley & Sons Ltd*, New York, 2002

40. Okada, A., Kawasumi, M., Usuki, A., Kojima, Y., Kurauchi, T., and Kamigaito, O., "Synthesis and properties of nylon-6/clay hybrids. Polymer based molecular composites", *MRS Symposium Proceedings*, 1999, 171, pp 45–50

41. Vaia, R.A., Ishii, H., and Giannelis, E.P., "Synthesis and properties of two-dimensional nanostructures by direct intercalation of polymer melts in layered silicates", *Chemistry of Materials*, 1993, 5, pp 1694–1696

42. Biswas, M., and Sinha, R. S., "Recent progress in synthesis and evaluation of polymer–montmorillonite nanocomposites", *Advances in Polymer Science*, 2001, 155, pp 167–221

43. Giannelis, E.P., "Polymer layered silicate nanocomposites", *Advanced Materials*, 1996, 8, pp 29–35

44. Giannelis, E.P., Krishnamoorti, R., and Manias, E., "Polymer-silicate nanocomposites: model systems for confined polymers and polymer brushes" *Advances in Polymer Science*, 1999, 138, pp 107–147

45. Lebaron, P.C., Wang, Z., and Pinnavaia, T. J., "Polymer-layered silicate nanocomposites: an overview", *Applied Clay Science*, 1999, 15, pp 11–29

46. Vaia, R.A., Price, G., Ruth, P.N., Nguyen, H.T., and Lichtenhan, J., "Polymer/layered silicate nanocomposites as high performance ablative materials", *Applied Clay Science*, 1999, 15, pp 67–92

47. Giannelis, E.P., "Polymer-layered silicate nanocomposites: synthesis, properties and applications", *Applied Organomettalic Chemistry*, 1998, 12, pp 675–680

48. Xu, R., Manias, E., Snyder, A.J., and Runt, J., "New biomedical poly (urethane urea)-layered silicate nanocomposites", *Macromolecules*, 2001, 34, pp. 337–339

49. Bharadwaj, R. K., “Modeling the barrier properties of polymer layered silicate nanocomposites”, *Macromolecules*, 2001, 34, pp 1989–1992

50. Messersmith, P. B., and Giannelis, E. P., “Synthesis and barrier properties of poly (1-caprolactone)-layered silicate nanocomposites”, *Journal of Polymer Science, Part A: Polymer Chemistry*, 1995, 33, pp 1047–1057

51. Yano, K., Usuki, A., Okada, A., Kurauchi, T., and Kamigaito, O., “Synthesis and properties of polyimide–clay hybrid”, *Journal of Polymer Science, Part A: Polymer Chemistry*, 1993, 31, pp 2493–2498

52. Kojima, Y., Usuki A., Kawasumi, M., Fukushima, Y., Okada, A., Kurauchi, T., and Kamigaito O., “Synthesis of nylon 6–clay hybrid”, *Journal of Materials Research*, 1993, 8, pp 1179–1184

53. Gilman, J.W., Kashiwagi, T., and. Lichtenhan, J.D., “Flammability studies of polymer-layered silicate nanocomposites”, *SAMPE Journal*, 1997, 33, pp 40–45

54. Gilman, J.W., “Flammability and thermal stability studies of polymer-layered silicate (clay) nanocomposites”, *Applied Clay Science*, 1999, 15, pp 31–49

55. Gilman, J.W., Jackson, C.L., Morgan, A.B., Harris J.R., Manias, E., Giannelis, E.P., Wuthenow, M., Hilton, D., and Phillips S.H., “Flammability properties of polymer-layered silicate nanocomposites. Propylene and polystyrene nanocomposites”, *Chemistry of Materials*, 2000, 12, pp 1866–1873

56. Dabrowski, F., Bras, M.L., Bourbigot, S., Gilman, J.W., and Kashiwagi, T., “PA-6 montmorillonite nanocomposite in intumescent fire retarded EVA”, *Proceedings of Eurofillers 99*, France, September 1999, pp 6-9

57. Bourbigot, S., Lebras, M., Dabrowski, F., Gilman, J.W., and Kashiwagi, T., "PA-6 clay nanocomposite hybrid as char forming agent in intumescent formulations", *Fire and Materials*, 2000, 24, pp 201–208

58. Moodley, V.K., and Kanny, K., "Characterisation of Polypropylene Nanocomposite Structures", *Journal of Engineering Materials and Technology*, 2007, 40, pp 1 – 8

59. Kojima, Y., Usiki, A., Kawasumi, M., Okada, A., Fukushima, Y., Karauchi, T., and Kamigaito, O., "Mechanical Properties of Nylon-6 Clay Hybrids", *Journal of Material Research*, 1993, 6, pp 1185-1189

60. Kato, M., Y., Usiki, A., and Okada, A., "Synthesis of Polypropylene Oligomer-Clay Intercalation Compounds", *Journal of Applied Polymer Science*, 1997, 66, pp 1781-1785

61. Kawasumi, M., Hasegawa, N., Kato, M., Y., Usiki, A., Okada, A., Karauchi, T., and Kamigaito, O., "Preparation and Mechanical Properties of Polypropylene-Clay Hybrids", *Macromolecules*, 1997, 30, pp 6333-6338

62. Chow W. S., Bakar, A. A., et al, "Effect Of Maleic Anhydride-Grafted Ethylene–Propylene Rubber On The Mechanical, Rheological And Morphological Properties Of Organoclay Reinforced Polyamide6/Polypropylene Nanocomposites", *European Polymer Journal*, 2005, 41, pp 687-696

63. Sinha, R.S, K. Okamoto, M. Okamoto, (2003), "Structure–property relationship in biodegradable poly (butylenes succinate)/layered silicate nanocomposites" Macromolecules, 36, pp. 2355–2367

64. Hay, J.N., "A Review of Nanocomposites 2000", 2000, http://www.azom.com/details.asp?ArticleID=921

65. Nanocompositech.com, “Clay polymer nanocomposites: Brief outline”, http://www.nanocompositech.com/review-nanocomposite.htm

66. Demetrakakes, P., “Nanocomposites raise barriers, but also face them: Clay-based additives increase the barrier qualities of plastics, but obstacles to commercialization must be overcome”, *Nanocomposite Materials*, 2002, http://www.findarticles.com/p/articles/mi_m0UQX/is_12_66/ai_96123509

67. Julio F. Davalos, “Characterisation of bonded interfaces for wood-fibre reinforced polymer composites”, 3rd International Conference on Advanced Engineered Wood Composites, Bar Harbour, ME, USA, July 2005, http://www.aewc.umaine.edu/research/ABSTRACT%20pdfs/Davalos.pdf

68. C. Au, J. Shim, V. Barzov, I. Jacobi, and A. Reyes, “Durability Behaviour of FRP/epoxy/concrete Multilayer Systems and Constituent Material Characterization and Moisture Diffusion Simulation”, *MPC, Advancing Materials Research*, http://mpc-web.mit.edu/about_mpc/ar2005/buyukozturk05.php

69. Vaidya, U.K., Samalot, F., Pillay, S., Janowski, G.M., Husman, G., and Gleich, K., “Design and Manufacture of Woven Reinforced Glass/Polypropylene Composites for Mass Transit Floor Structure”, *Journal of Composite Materials*, 2004, 38, 1949, http://jcm.sagepub.com/cgi/reprint/38/21/1949

70. Crews, J.H., and Reeder, J.H., “Nonlinear Analysis and Redesign of the Mixed-Mode Bending Delamination Test”, *NASA Technical Memorandum 102777*, January 1991

71. O’ Brien, T.K., “Characterisation, Analysis and Prediction of Delamination in Composites Using Fracture Mechanics”, *NASA Langley Research Centre ICF100942OR*, 2001

72. Szekrényes, A., and Uj, J., “Comparison of Some Improved Solutions for Mixed-Mode Composite Delamination Coupons”, *Composite Structures*, 72, 2006, pp. 321 – 329

73. Jensen, H.M., and Sheinman, I., “Straight-sided, buckling-driven delamination of thin films at high stress levels”, *International Journal of Fracture*, 2001, 110 (4), pp 371 – 385

74. Glaessgen, E.H., Raju, I.S., and Poe, C.C., “Analytical and experimental studies of the debonding of stitched and unstitched composite joints”, *Journal of Composite Materials*, 2002, 36 (23), pp 2599 – 2622

75. Robinson, P., and Hodgkinson, J.M., “Interlaminar fracture toughness”, *Mechanical Testing of Advanced Fibre Composites*, (ed.) Hodgkinson, J.M., Woodhead Publishing, Cambridge (UK), 2000, pp 170 – 210

76. Davies, P., “Protocols for interlaminar fracture testing of composites”, *Polymer and Composites Task Group*, European Structural Integrity Society, 1992, Plouzané (France)

77. ASTM D 5528-01, “Standard test method for Mode I interlaminar fracture toughness of unidirectional fibre-reinforced polymer matrix composites”, *Annual Book of ASTM Standards*, 2003, 15.03, Philadelphia (USA)

78. Carlsson, L.A., Gillespie, J.W., and Pipes, R.B., “On the analysis and design of the end notched flexure (ENF) specimen for mode-II testing”, *Journal of Composite Materials*, 1986, 20 (6), pp 594 – 604

79. Crews, J.H., and Reeder, J.R., “A Mixed-Mode Bending Apparatus for Delamination Testing”, *NASA Technical Memorandum 100662*, August 1988

80. Crews, J.H., and Reeder, J.H., “Mixed-Mode Bending Method for Delamination Testing”, *AIAA Journal*, Vol. 28, No. 7, July 1990, pp. 1270 – 1276

81. Crews, J.H., and Reeder, J.H., "Redesign of the Mixed-Mode Bending Test for Delamination Toughness", *Composites Design, Manufacture, and Application*, ICCM / 8 Conference Proceedings, SAMPE, July 1991, pp. 36-B-1 – 36-B-10

82. ASTM D 6671 / D 6671M – 04, "Standard Test Method for Mixed Mode I – Mode II Interlaminar Fracture Toughness of Unidirectional Fiber Reinforced Polymer Matrix Composites", *Annual Book of ASTM Standards*, 15.03, 2004

83. Alif, N., Carlsson, L.A., and Boogh, L., "The effect of weave pattern and crack propagation direction on mode I delamination resistance of woven glass and carbon composites", *Composites Part B*, 29B, 1998, pp 603-611

84. Suppakul, P., and Bandyopadhyay, S., "The effect of weave pattern on the mode-I interlaminar fracture energy of E-glass/vinyl ester composites", *Composites Science and Technology*, 62, 2002, pp 709-717

85. El-Hajjar, R., and Haj-Ali, R., "Mode-I fracture toughness testing of thick section FRP composites using the ESE(T) specimen", *Engineering Fracture Mechanics*, 72, 2005, pp 631-643

86. Compston, P., and Jar, P.Y.B., "Comparison of Interlaminar Fracture Toughness in Unidirectional and Woven Roving Marine Composites", *Applied Composite Materials*, 5, 1998, pp 189-206

87. Hibbs, M. F., Tse, M. K., and Bradley, W. L., 'Interlaminar Fracture Toughness and Real-Time Fracture Mechanism of Some Toughened Graphite/Epoxy Composites', *Toughened Composites*, ASTM STP 937, 1987, 115–130

88. Hunston, D. L., 'Composite Interlaminar Fracture: Effect of matrix energy', *Composites Technology Review*, 6, 1984, 176–180

89. Madhukar, M. S. and Drzal, L. T., 'Fiber-Matrix Adhesion and Its Effects on Composite Mechanical Properties: IV. Mode I and Mode II Fracture Toughness of Graphite/Epoxy Composites', *Journal of Composite Materials*, 26(7), 1992, 936–968

90. Albertsen, H., Ivens, J., Peters, P., Wevers, M. and Verpoest, I., 'Interlaminar Fracture Toughness of CFRP Influenced by Fibre Surface Treatment: Part I. Experimental Studies', *Composites Science and Technology*, 54, 1995, 133–145

91. Prombut, P., Michel, L., Lachaud, F., and Barrau, J.J., "Delamination of multidirectional composite laminates at 0°/θ° ply interfaces", *Engineering Fracture Mechanics*, 73, 2006, pp 2427-2442

92. Rikards, R., Buchholz, F.G., Wang, H., Bledzki, A.K., Korjakin, A., and Richard, H.A., "Investigation of mixed mode I/II interlaminar fracture toughness of laminated composites by using a CTS type specimen", *Engineering Fracture Mechanics*, 61, 1998, pp 325-342

93. Kim, B.W., and Mayer, A.H., "Influence of fibre direction and mixed-mode ratio on delamination fracture toughness of carbon/epoxy laminates", *Composites Science and Technology*, 63, 2003, pp 695-713

94. Wu, S.-H., Wang, F.-Y., Ma, C.-C.M., Chang, W.-C., Kuo, C.-T., Kuan, H.-C., and Chen, W.-J., "Mechanical, thermal and morphological properties of glass fiber and carbon fiber reinforced polyamide-6 and polyamide-6 / clay nanocomposites", *Materials Letters*, 49, 2001, pp 327-333

95. Vlasveld, D.P.N., Daud, W., Bersee, H.E.N., and Picken, S.J., "Continuous fibre composites with a nanocomposite matrix: Improvement of flexural and compressive strength at elevated temperatures", *Composites Part A*, 38, 2007, pp 730-738

96. Wichmann, M.H.G., Sumfleth, J., Gojny, F.H., Quaresimin, M., Fiedler, B., and Schulte, K., "Glass-fibre-reinforced composites with enhanced mechanical and electrical properties

– Benefits and limitations of a nanoparticle modified matrix", *Engineering Fracture Mechanics*, 73, 2006, pp 2346-2359

97. Pavan Kumar, D.V.T.G., "Interlaminar Fracture Toughness Of Composites - Higher Order Shear Deformation Beam Theories, *J. Indian Inst. Sci.*, "81, May - June 2001, pp 365-369

98. Bower, A.F., "Advanced Mechanics of Solids", *Division of Engineering, Brown University*, http://www.engin.brown.edu/courses/en175/Notes/Failure_mechanisms/Failure_mechanisms.htm

99. Estevez, R., Tijssens, M.G.A., and Van der Giessen, E., "Modeling of the competition between shear yielding and crazing in glassy polymers", *Journal of the Mechanics and Physics of Solids*, 2000, 48, pp 2585–2617

100. Haward, R.N., *The Physics of Glassy Polymers*, Applied Science Publishers, London, 1973

101. Kambour, R.P., "A review of crazing and fracture in thermoplastics", *Journal of Polymer Science*, Macromolecular Reviews 7, 1973, pp 1-154

102. "Chapter 16. Polymers. Characteristics, Applications and Processing", http://www.virginia.edu/bohr/mse209/chapter16.htm

103. Mazumdar, S.K., *Composite Manufacturing: Materials, Product, and Process Engineering*, CRC Press LLC, 2002

104. ASTM D 3039 / D 3039M – 93, "Standard Test Method for Tensile Properties of Polymer Matrix Composite Materials", *Annual Book of ASTM Standards*, 08, 1993

105. ASTM D 5045 – 93, "Test Methods for Plane-Strain, Fracture Toughness and Strain Energy Release Rate of Plastic Materials", *Annual Book of ASTM Standards*, 08.03, 1995

106. Adams, D.F., Carlsson, L.A., and Pipes, R.B., *Experimental Characterization of Advanced Composite Materials*, Third Edition, CRC Press LLC, 2003

107. Ding, C., Jia, D., Hui, H., Guo, B., and Hong, H., "How Organo-Montmorillonite Truly Affects the Structure and Properties of Polypropylene", *Polymer Testing*, 2004, 20, pp 1-7

108. Bharadwaj, R.K., "Structure-Property Relationships in Cross-Linked Polyester-Clay Nanocomposites", *Polymer Journal*, 2002, 43, pp 3699-3705

109. Benzeggagh, M.L., and Kenane, M., "Measurement of Mixed-Mode Delamination Fracture Toughness of Unidirectional Glass/Epoxy Composites with Mixed-Mode Bending Apparatus", *Composites Science and Technology*, 1996, 56, pp 439-449

110. Kenane, M., and Benzeggagh, M.L., "Mixed-Mode Delamination Fracture Toughness of Unidirectional Glass/Epoxy Composites under Fatigue Loading", *Composites Science and Technology*, 1997, 57, pp 597-605

LIST OF JOURNAL AND CONFERENCE PAPERS

JOURNAL PAPERS

1. Ramsaroop, A., and Kanny, K., "Fracture Toughness of Nano-infused and Fibre-reinforced Polypropylene Composites", *Engineering Fracture Mechanics*, Submitted

CONFERENCE PAPERS

1. Ramsaroop, A., and Kanny, K., "Analysis of Crack Propagation in Polymeric Structures", *ICCM 15*, Polymeric Composites Institute of South Africa (PCISA), ICC, Durban, South Africa, June 2005

2. Kanny, K., Pillay, S., Moodley, V.K., Ramsaroop, A., Li, Y., and Dilsani, P., "On A Hybrid Composite Pedestrian Bridge", *Research Day 2005*, Durban Institute of Technology, Durban, South Africa, September 2005

3. Ramsaroop, A., and Kanny, K., "Crack Behaviour in Glass Reinforced Polymeric Structures", *Research Day 2006*, Durban University of Technology, Durban, South Africa, September 2006

4. Ramsaroop, A., and Kanny, K., "Smart Manufacturing Methods to Increase Delamination Resistance in GFRP Structures", *20th SAIIE Annual Conference*, South African Institute for Industrial Engineering (SAIIE), Elangeni Hotel, Durban, South Africa, October 2006

5. Ramsaroop, A., and Kanny, K., "A Study of Crack Behaviour in Laminated Glass Reinforced Polymeric Structures", *Second Annual Ledger Conference Agenda 2006,* The Council of Scientific and Industrial Research (CSIR) and Denel Aerospace Systems (DAS), Cape Town, South Africa, December 2005

6. Ramsaroop, A., and Kanny, K., "Experimental and Finite Element Analysis of Crack Propagation in Random and Woven Glass Composite Structures", *Sixth International Conference on Composite Science and Technology (ICCST 6)*, Elangeni Hotel, Durban, South Africa, January 2007

7. Ramsaroop, A., and Kanny, K., "Investigation of Crack Behaviour in Glass Polymeric Structures", *Second International Conference on Recent Advances in Composite Materials (ICRACM 2)*, New Delhi, India, February 2007

NB: Two technical papers are currently in preparation for submission to journals. These are:

1. Failure Envelopes for Epoxy / Woven S2 Glass Structures
2. Manufacturing Techniques for Complex-shaped Parts